OPTIMISATION OF FILTERS FOR OPTICAL CORRELATION OF NOISY IMAGES

BY
LIN SHANG ©

DEPARTMENT OF MECHANICAL ENGINEERING
THE UNIVERSITY OF GLASGOW

SUBMITTED
TO
THE UNIVERSITY OF GLASGOW
FOR THE DEGREE
OF
DOCTOR OF PHILOSOPHY

OCT 1999

Contents

Synopsis

The capacity of an optical correlator to identify, recognise and locate a target object in a cluttered scene depends greatly upon the qualities of the spatial filter it uses to represent the reference image. Noise in the input scene degrades the discriminative powers of correlators in the several optical configurations that have been proposed and realised. That this loss might be ameliorated in the design of the spatial filter by trading-off the noise tolerance of the classical matched filter with the high spatial resolution yielded by the phase alone filter is examined herein. Spatial discriminant function filters so designed are evaluated by simulations of their performance that account for distortions of the target object, the discrimination of the target from a nearly similar object and noise corrupting the input scene. Criteria are established for the purposes of this evaluation, including measures of the signal to noise ratio, the spatial discrimination of the correlation peak in the correlation plane and the ease of its detection. A cosine-wave joint transform correlator is proposed, an alternate to the binary joint transform correlator, and is evaluated by simulations of its performance when presented at its input with multiple objects contained in noisy scenes.

The design strategy seeks an optimisation that values the sharp spatial discrimination contributed by the high spatial frequency components and the tolerance to noise imparted by the low frequency components of the spatial filter. Chapter 3 examines the trade-off between these characteristics by applying a filter composed with two difference of Gaussian, band-pass filters – one passing in a high frequency band the other passing in a low frequency band – to a matched filter. An optimisation of the spatial discrimination of the correlation peak that accounts for noise in the input scene is found by systematically varying the two pairs of parameters that define the composite filter. The primary effect of the optimal filter is to cut the low frequency spectrum of the matched filter in a sharply defined band centred on its zero order. The high frequency spectrum is little affected. This is a significant result, for the optimisation across four parameters is complex and computationally slow. The design of the more demanding spatial discriminant function (SDF) filters might then proceed by variation of a single parameter in a function that attenuates the low frequency end of the spectra of the training set of images.

A single parameter function is adopted in the optimisation of SDFs reported in Chapter 4, which introduces the weighted amplitude SDF. This design balances the sharpness of the correlation peak against the filter's capacity to distinguish between similar target objects as the signal to noise ratio deteriorates. Though the location of the correlation peak produced by the optimal filter is never left in doubt, in light of the results of Chapter 3 the chosen weighting function is considered to be less effective than a sharp, low cut filter might have been.

Notwithstanding the sensitivity to noise of phase encoded filters, a SDF filter synthesised from phase-encoded images and correlating phase-encoded images is examined in Chapter 5 because this scheme can be realised in real time, using current phase modulating spatial light modulators. The general case for this form of phase-phase correlation is not proved by the results of the simulations performed, but value is to be found in this scheme whenever the optical efficiency is at a premium.

Although the design goal is unchanged, the design objective in the case of the joint transform correlator is to extract information directly from the joint power spectrum rather than to modify the spectrum of the reference image. A scheme is devised that is similar to even function correlation of the phase information in the spatial frequency spectra of the input and reference images. When an object in the input scene coincides with the reference image the inversion of the cosine-wave term extracted from the JPS generates a pair of delta functions in the output plane, being spaced apart by a distance corresponding to the relative displacement of the object and the reference images. The performance of the cosine-wave JTC is superior to that of the binary JTC and more especially so when multiple targets are presented in a low contrast, noisy scene. However, the thresholding function JTC is entirely comparable with the cosine-wave scheme. It remains for future work to examine the relative sensitivity to noise of these competing systems.

In prospect a JTC is capable of real time correlation that accommodates distortion of the input object and the depredations of noise through the use of cosine-wave extracting SDF filters.

Acknowledgements

Firstly, I wish to thank my supervisor, Professor B.F.Scott. He gave me overwhelming support during the research, in writing the thesis and in personal matters. Secondly, I would like to thank Professor C.R.Chatwin and my colleague Dr R.K.Wang, who introduced me to this exciting research field. My thanks are also due to Dr J.H.Sharp for his interest throughout the research.

I thank Professor J.W. Hancock, Head of the Mechanical Engineering Department, for the use of departmental facilities.

I am very indebted to my family and especially so to my wife for her support and encouragement throughout the research.

Finally, I wish to acknowledge the award of an Overseas Research Studentship (ORS) by the CVCP and a Postgraduate Studentship given by the University of Glasgow.

Nomenclature

$*$	complex conjugate function
Θ	convolution
$\otimes$	correlation
δ	delta function
η	Horner efficiency
ψ	damping coefficient
ζ_i	components of synthesising vector
κ	Constant
κ'	Constant
λ	wavelength
σ	standard deviation
Ω_1	images from class 1
C_1	constant
C_2	constant
$comb$	comb function
$\boldsymbol{A}$	weighting parameter
B	region outside the correlation peak area contained within its half-peak intensity profile
C_{max}	intensity of the highest secondary correlation peak
$\boldsymbol{E}$	ensemble average
$\boldsymbol{F}$	Fourier transform
$\boldsymbol{F}^{-1}$	inverse Fourier transform
f	focal length of the lens
$H(u,v)$	filter function
$\boldsymbol{M}$	phase extraction
$\boldsymbol{N}$	is weighting function
N'	total number of pixels inside R
P_{min}	intensity of the lowest correlation peak

P_t	intensity of the correlation peak for target inputs
P_{nt}	maximum intensity of correlation peak for non-target input
P_{noise}	intensity of the noise impressed on the image
P_{object}	intensity in the pixels representing the image
$P_n(u,v)$	power spectral density
R	region of the correlation peak contained within its half peak intensity profile
$rect$	rectangle function
$sinc$	sinc function
t	scaling factor
u	spatial frequency in x direction
v	spatial frequency in y direction
var	variance
W_u	cut-off frequencies of the spectrum
W_v	cut-off frequencies of the spectrum
(x, y)	space domain co-ordinates
(x_0, y_0)	central co-ordinates in the space domain
(x_f, y_f)	frequency domain co-ordinates

Acronyms

APC	armoured personnel carrier
BJTC	binary joint transform correlator
CCD	charge coupled device
CMF	classical matched filter
COM	composite filter
$\mathrm{COM}_{\mathrm{optim}}$	optimum composite filter
CPI	intensity of the correlation peak
$\mathrm{CPI}_{\mathrm{in-class}}^{\max}$	intensity of the maximum correlation peak with in-class images
$\mathrm{CPI}_{\mathrm{in-class}}^{\min}$	intensity of the minimum correlation peak with in-class images
CWJTC	cosine-wave, joint transform correlator
DC	discrimination capability
dog	difference of Gaussian function in the space domain
DOG	difference of Gaussian function in the frequency domain
$\mathrm{DOG}_{\mathrm{high}}$	high band-pass DOG filter
$\mathrm{DOG}_{\mathrm{low}}$	low band-pass DOG filter
DR	discrimination ratio
FWHM	full-width of the correlation peak defined at its half-maximum intensity.
GV	greatest variation
JPS	joint power spectrum
JTC	joint transform correlator
MSI	maximum in the output plane of the side-lobe peak intensities
MACE	minimum average correlation energy filter
PAC	phase-amplitude correlation
PAIR	ratio of the intensity of the correlation peak to the average intensity evaluated across the entire correlation plane

PI	number of pixels inside the full-width of the correlation peak defined at its half maximum intensity
PIC	maximum intensity of the correlation peak
PNR	ratio of the intensity of the correlation peak to the average intensity of the noise evaluated across the entire output plane
POF	phase-encoded filter
PPC	phase-phase correlation
PRMSR	ratio of the intensity of the correlation peak to the root mean square of the intensity in the correlation plane, evaluated outside the region of the peak
PSR	ratio of the intensity of the correlation peak to that of the highest secondary peak detected.
PSR_w	worst PSR in the case of a SDF filter
SDF	synthetic discriminant function
SLM	spatial light modulator
SNR	signal to noise ratio
SNR_I	input signal to noise ratio
SNRo	output signal to noise ratio
SNR_{max}	maximum signal to noise ratio

List of Figures

Chapter 2

Chapter 3

Chapter 4

Chapter 5

Chapter 6

List of Tables

Chapter 3

Chapter 4

Chapter 6

CHAPTER 1

Introduction

Pattern recognition employing optical correlation of target and object images is investigated. The research is of filter design, seeking an optimisation between the capacities of filters to recognise and locate target objects and tolerate noise. The application of the design ethos is demonstrated in the construction of synthetic discriminant function filters. Consideration is also given to the design of joint transform correlators suitable for operation in real-time.

Vander Lugt's construction of a matched filter[1] to record a hologram containing the complex conjugate of the frequency spectrum of the object was a signal result for optical pattern recognition. This work was the catalyst for current research of optical signal processing.

The matched filter provides the best signal to noise ratio when the input signal is corrupted by noise impressed on the image or generated in the optical system. In many real images the amplitude of the Fourier spectrum is greatest at lower spatial frequencies and smallest at higher frequencies. Therefore, the Vander Lugt filter blocks much of the light incident upon it. The transmittance of a filter[2] is a maximum when it is entirely phase-encoded (Horner and Gianino; 1984). However, though "phase only" filters may generate a sharp correlation peak, they are greatly sensitive to noise in the input image[3]. This is so because the weighting in the Fourier plane inherent to filters constructed on complex representations of the spatial frequency spectra discriminates against noise; an entirely phase-encoded filter passes all frequencies equally well.

The design of a filter[4] composed of two Gaussian form, band-pass filters is considered in Chapter 3. The aim is to study the optimisation of filters accounting for the sharpness of the correlation peak generated by the filter and its tolerance of noise that might be impressed on the input image. The method adopted balances the tolerance of noise imparted by the low-pass filter and the finesse of the correlation peak generated by the high-pass filter. The performance criteria were the accuracy with which the position of the target object might be located and the extent of the deterioration caused by noise.

A challenge for the matched filter is its great sensitivity to distortion of the input image[5] with respect to the reference image. Changes in scale and of angular orientation in the field of the object constitute distortion. The synthetic discriminant function (SDF) introduced by Hester and Casasent[6] is a powerful tool, having the capacity to resolve and detect distorted images. The SDF filter is a composite formed from a linear combination of reference images having pre-determined distortions and constituting a training set. A cross-correlation of such a filter with a distorted version of the target object detects the object and may quantify its distortion. The training set images are so weighted that identical outputs are formed by all auto-correlations with images that are members of the training set. The filter's capacity to discriminate in-class from out-of-class objects and its optical efficiency are enhanced when it is composed from phase-encoded images[7] However, a penalty is exacted in the sensitivity that this form of filter exhibits to noise in the image.

A compromise is sought in Chapter 4 between the capacity of an SDF to recognise and locate the object and its tolerance of noise. A design method[8] is described that optimises the filter's performance by applying an appropriate weighting to the amplitude components of the spatial frequency spectra of the training set of images. The relaxation algorithm proposed by Jared and Ennis[9] is adopted to determine the weighting of training set images so that an equality of the heights of auto-correlation peaks is achieved. The optimisation criteria are the quality of recognition of in-class and rejection of out-of-class images and the optical efficiency and tolerance of noise.

In Chapter 5 an entirely phase-encoded SDF filter is designed by the methods of Chapter 4. A simulation demonstrates the finesse with which this scheme recognises target objects when the range of distortion is restricted. However, the susceptibility of phase-encoded filters to noise is, once more, made evident.

Weaver and Goodman[10] demonstrated the first joint transform correlator. In the absence of suitable interface devices, the JTC was left fallow until 1984, when Yu and Lu[11] reported a real-time, programmable JTC. Whilst the JTC is an attractive alternative to the frequency plane correlator, a strong zero-order peak in the output plane, being the sum of the auto-correlations of the reference and input images, overlaps the desired correlation signal.

A cosine-wave, joint transform correlator[12] is proposed in Chapter 6, which removes the zero-order term. Simulations undertaken demonstrate the capacity of this correlator to discriminate target objects from other objects contained in complex scenes that are corrupted by noise.

REFERENCES

---

[1] A. Vander Lugt, "Signal detection by complex spatial filtering," *IEEE Trans. Inform. Theory,* **IT-10**, 139-145 (1964).

[2] J. L. Horner and P. D. Gianino, "Phase-only matched filtering," *Appl.Opt.* **23**, (812-816) 1984.

[3] F. M. Dickey, K. T. Stalker and J. J. Mason, "Bandwidth considerations for binary phase only filters," *Appl.Opt.* **27**, (3811-3818) 1988.

[4] L. Shang, R. K. Wang and C. R. Chatwin, "Frequency Multiplexed DOG filter," *Optics and Lasers in Engineering.* **27**, (161-177) 1997.

[5] D. Casasent and A. Furman, "Sources of correlation degradation," *Appl.Opt.* **16**, (1652-1661) 1977.

[6] C. F. Hester and D. Casasent, "Multivariant technique for multi-class pattern recognition," *Appl.Opt.* **23**, (1758-1761) 1980.

[7] J. L. Horner, "Optical signal processing," Academic Press, 1987.

[8] L. Shang, B. F. Scott and J. H. Sharp, "Design of Synthetic Discriminate Functions for use in a Hybrid Optical-Digital Correlator," (3073-02). *AeroSense'97*, Florida, USA, 20-25 April. 1997.

[9] D. Jared and D. Ennis, "Inclusion of filter modulation in synthetic discrimination function construction," *Appl.Opt.* **28**, (232-239) 1989.

[10] C. S. Weaver and J. W. Goodman, "A technique for optically convolving two functions," *Appl.Opt.* **5**, (1248-1249) 1966.

[11] F. T. S. Yu and X. J. Lu, "A real time programmable joint transform correlator," *Opt.Commun.* **52**, (10-16) 1984.

[12] R. K. Wang, L. Shang, I. A.Watson and C. R. Chatwin, "Cosine Wave Encoded Joint Transform Correlation," *Opt.Eng.* **35**, 1901-1910 (1996).

CHAPTER 2

Design of Optical Filters and Correlators for Image Recognition

Those several definitions and theorems that are employed throughout the thesis are established here to avoid the need for their repetition.

2.1 THE SAMPLING THEOREM

The representation of analogue optical signals at discrete intervals occurs whenever the signal is detected by a finite photo-detector array or else is encoded in a spatial light modulator. A band-limited, continuous function $g(x, y)$ has a Fourier transform $G(u,v)$, that is zero for spatial frequencies $|u| > W_u$ and $|v| > W_v$. W_u and W_v are the cut-off frequencies of the spectrum. The one-dimensional sampling function is defined by

$$comb(x) = \sum_{n=-\infty}^{\infty} \delta(x-n) \tag{2.1}$$

with n an integer.

The sampled version of a continuous function $g(x, y)$ is

$$g_s(x, y) = g(x, y) comb\left(\frac{x}{a}\right) comb\left(\frac{y}{b}\right), \tag{2.2}$$

when the sampling is at intervals a and b in the x and y directions respectively. Remembering that the Fourier transform of the sampling function is

$$F\{comb(x)\} = comb(u)\,, \tag{2.3}$$

the Fourier transform of Equation 2.2 is found to be

$$G_s(u,v) = G(u,v)\Theta ab \cdot comb(au)comb(bv)\,, \tag{2.4}$$

in which Θ indicates the convolution operation, and $G_s(u,v)$ and $G(u,v)$ are the Fourier transform of $g_s(x,y)$ and $g(x,y)$, respectively. $G_s(u,v)$ is plotted in Figure 2.1.

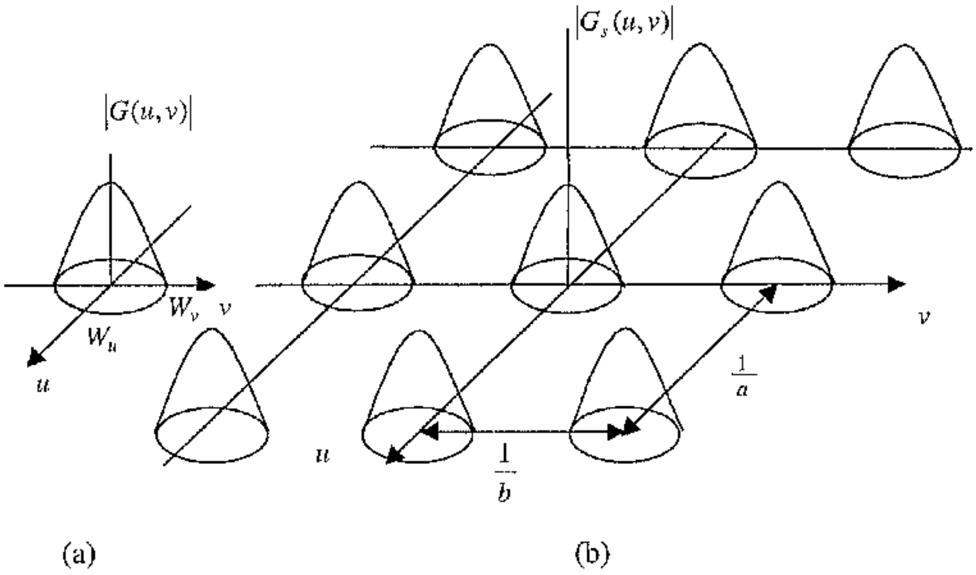

Figure 2.1. The Fourier spectra of (a) a continuous band-limited function and (b) the same function sampled at intervals a and b in the x and y directions. Replicas (aliases) do not overlap when $a \le \frac{1}{2W_u}$ and $b \le \frac{1}{2W_v}$.

Thus, sampling with the *comb* function replicates the original Fourier distribution $G(u,v)$ around points spaced at intervals $\frac{1}{a}$ and $\frac{1}{b}$ in the u and v directions, respectively. These replications of the original distribution are called aliases. It is evident from Figure 2.1(b) that aliases do not overlap when

$$a \leq \frac{1}{2W_u} \; and \; b \leq \frac{1}{2W_v}. \tag{2.5}$$

Therefore, the sampling interval must be sufficiently fine that the highest frequency component occurring in the spectrum is sampled at least twice. (In this work, the word "pixel" is adopted to represent a sampling interval with dimensions a and b in two-space.) Equation 2.5 expresses the Nyquist criterion. When this criterion is satisfied, the original continuous function $g(x, y)$ can be recovered by applying a low-pass filter to the sampled function $g_s(x, y)$. The spectrum is recovered as

$$G(u,v) = G_s(u,v) rect\left(\frac{u}{2W_u}\right) rect\left(\frac{v}{2W_v}\right), \tag{2.6}$$

in which the low-pass filter is represented by

$$rect\left(\frac{u}{2W_u}\right) = \begin{cases} 1, & \left|\frac{u}{2W_u}\right| \leq \frac{1}{2} \\ 0, & otherwise. \end{cases} \tag{2.7}$$

The mathematical operation on the sampled function $g_s(x, y)$ is a convolution

$$g(x, y) = g_s(x, y) \Theta [4W_u W_v sinc(2W_u x) sinc(2W_v y)], \tag{2.8}$$

with

$$sinc(x) = [\sin(\pi x)]/\pi x. \tag{2.9}$$

Equation 2.8 expresses the Whittaker-Shannon sampling theorem.

2.2 ROTATION AND SCALE CHANGE AFFECTING CORRELATION

The capacity of an optical correlator to detect patterns independently of their spatial position is a direct consequence of the shift invariance property of the Fourier transform (Appendix). However, correlation is sensitive to other variations of the input pattern; specifically, it is severely affected by rotations and scale changes[9]. The correlation of a pattern function $h(x, y)$ of size $2L \times 2L$ and a scaled version of this pattern $h(tx, ty)$ is

$$\begin{aligned} & h(x, y) \otimes h^*(tx, ty) \\ & = \int_{-\infty}^{\infty}\int_{-\infty}^{\infty} h(x', y') rect\left(\frac{x'}{2L}\right) rect\left(\frac{y'}{2L}\right) h^*(tx' - x, ty' - y) \times rect\left(\frac{tx'}{2L} - x\right) rect\left(\frac{ty'}{2L} - y\right) dx'dy' \end{aligned} \tag{2.10}$$

Consider first of all the effect of scaling on a single, two-dimensional complex spatial frequency component of amplitude $A(u, v)$ and size 2L $\times 2L$, viz.

$$h(x, y) = A(u, v) rect\left(\frac{x}{2L}\right) rect\left(\frac{y}{2L}\right) \exp(-i2\pi ux) \exp(-i2\pi vy). \tag{2.11}$$

The scaled version of Equation 2.11 is

$$h(tx, ty) = A(u, v) rect\left(\frac{tx}{2L}\right) rect\left(\frac{ty}{2L}\right) \times \exp(-i2\pi utx) \exp(-i2\pi vty), \tag{2.12}$$

with t the scaling factor. The resulting detection statistic is the cross-correlation evaluated at the origin, viz.

$$\begin{aligned} G(u, v) &= \{h(x, y) \otimes h^*(tx, ty)\}_{x=0} \\ &= \int_{-\infty}^{\infty}\int_{-\infty}^{\infty} |A(u, v)|^2 rect\left(\frac{x'}{2L}\right) rect\left(\frac{y'}{2L}\right) \\ & \times \exp[-i2\pi u(1 - t)x'] \exp[-i2\pi v(1 - t)y'] dx'dy' \end{aligned} \tag{2.13}$$

Equation 2.13 is the Fourier transform of the two-dimensional rectangle function with transform variables $u(1-t)$ and $v(1-t)$. Therefore,

$$G(u,v) = \left|A(u,v)\right|^2 4L^2 sinc\left[2u(1-t)L\right] sinc\left[2v(1-t)L\right]. \tag{2.14}$$

Secondly, consider the case of a real image composed of many spatial frequency components. Changes of scale do not cause one spatial frequency component to impinge on a neighbour when the various spatial frequency components remain uncorrelated. In this case, the total detection statistic is given by

$$\begin{aligned} G = \int_{-\infty}^{\infty}\int_{-\infty}^{\infty} G(u,v)dudv = 4L^2 \int_{-\infty}^{\infty}\int_{-\infty}^{\infty} \left|A(u,v)\right|^2 \\ \times sinc[2u(1-t)L]\, sinc[2v(1-t)L]dudv \end{aligned}, \tag{2.15}$$

in which $\left|A(u,v)\right|^2$ is the power spectrum of the original function. The whole of the spectrum contributes to the detection statistic when the scaling is exact (t=1), for the *sinc* function is then reduced to unity. In the presence of a scaling error the original spectrum is rolled-off by a *sinc* function and G is attenuated. The severity of this degradation is determined by the power spectrum $\left|A(u,v)\right|^2$ of the image, the degree of scale change (1-t) and the image size L. Higher spatial frequencies are more affected by scale changes than are lower frequencies. Therefore, images that have spectra rich in high frequencies will be especially sensitive to scaling errors. This result is significant for the application of phase-encoded filters.

Rotational error has an effect similar to that described above.

The synthetic discrimination function, introduced in section 2.3.3, has been devised to accommodate errors of scaling and rotation.

2.3 OPTICAL FILTERS

An optical filter is a transmission mask that controls the complex transmittance of the lens-pupil function in an optical processor. The filter defines the optical transfer function of the processor, which, in turn, controls the frequency distribution of the information that is imaged from the input to the output of the processor.

2.3.1 Matched Filter

The matched filter [1] maximises the ratio of the intensity of the correlation peak to the mean square intensity of the noise when the input signal contains additive, stationary-random noise. The input to a linear filter system may be regarded as being the superposition of the signal $s(x,y)$ and the stationary-random noise $n(x,y)$:

$$f(x,y) = s(x,y) + n(x,y). \tag{2.16}$$

The signal to noise ratio (SNR_o) at the output peak, centred on $(x=0, y=0)$, is

$$SNR_o = \frac{|E\{c(0,0)|^2}{var\{c(0,0)\}}, \tag{2.17}$$

where E, var and c are the ensemble average, the variance and correlation output function respectively, i.e.

$$E\{c(0,0)\} = \int_{-\infty}^{\infty}\int_{-\infty}^{\infty} S(u,v)H(u,v)dudv \text{ and} \tag{2.18}$$

$$var\{c(0,0)\} = \int_{-\infty}^{\infty}\int_{-\infty}^{\infty} P_n(u,v)\,|\,H(u,v)\,|^2\,dudv, \tag{2.19}$$

in which $P_n(u,v)$ and $H(u,v)$ are the power spectral density and filter function respectively.

To find that function $H(u,v)$ which maximises the SNR_o, the Schwartz inequality[10] is applied to Equation 2.17

$$SNR_o = \frac{\left|\int\limits_{-\infty}^{\infty}\int\limits_{-\infty}^{\infty}\left[\frac{S(u,v)}{\sqrt{P_n(u,v)}}\right]\left[\sqrt{P_n(u,v)}H(u,v)\right]dudv\right|^2}{\int\limits_{-\infty}^{\infty}\int\limits_{-\infty}^{\infty}P_n(u,v)\left|H(u,v)\right|^2 dudv} \leq \frac{\int\limits_{-\infty}^{\infty}\int\limits_{-\infty}^{\infty}\frac{\left|S(u,v)\right|^2}{P_n(u,v)}dudv\int\limits_{-\infty}^{\infty}P_n(u,v)\left|H(u,v)\right|^2 dudv}{\int\limits_{-\infty}^{\infty}\int\limits_{-\infty}^{\infty}P_n(u,v)\left|H(u,v)\right|^2 dudv}$$

$$= \int\limits_{-\infty}^{\infty}\int\limits_{-\infty}^{\infty}\frac{\left|S(u,v)\right|^2}{P_n(u,v)}dudv = SNR_{\max}\,, \tag{2.20}$$

with the equality holding if and only if

$$\sqrt{P_n(u,v)}H(u,v) = \kappa\frac{S^*(u,v)}{\sqrt{P_n(u,v)}}\,, \tag{2.21}$$

with κ a constant. Thus the highest possible SNR_o (i.e., $SNR_{\max}$) is obtained when the filter function is

$$H(u,v) = \kappa\frac{S^*(u,v)}{P_n(u,v)}\,. \tag{2.22}$$

In the case of white noise the power spectral density $P_n(u,v)$ is constant and the optimal filter is:

$$H(u,v) = \kappa' S^*(u,v)\,. \tag{2.23}$$

2.3.2 Phase-Encoded Filter

While the matched filter discussed above is optimal from an SNR_o standpoint, it is highly sensitivity to distortions in the image and has a low Horner efficiency. Horner and Gianino [2] have suggested that the "phase only" filter will mitigate the latter because

$$H_{POF}(u,v)=\frac{S^*(u,v)}{|S(u,v)|} \tag{2.24}$$

and, leaving aside the effect of the medium on which the filter is recorded, the filter plane does not absorb light. As is demonstrated in Chapters 3 and 5, a phase-encoded filter yields a sharper correlation peak than does the matched filter, but is very sensitive to noise.

2.3.3 Synthetic Discriminant Function Filters

The synthetic discriminant function (SDF)[5] represents one approach to the design of distortion invariant filters.

A SDF is constructed on a training set of n images, being deliberate distortions of the reference image and chosen to represent the range of distortions expected in the input images. A composite image $h(x,y)$ is formed by a superposition of the training images, as follows:

$$h(x,y)=\zeta_1 s_1(x,y)+\zeta_2 s_2(x,y)+\ldots+\zeta_n s_n(x,y)=\sum_{i=1}^{n}\zeta_i s_i(x,y)\,. \tag{2.25}$$

The coefficients ζ_i are selected so that when $h(x,y)$ is cross-correlated with $s_i(x,y)$, the value of the output at the origin

$$\int_{-\infty}^{\infty}\int_{-\infty}^{\infty} h(x,y)s_i(x,y)dxdy=c_i\,, \tag{2.26}$$

is the same constant value for all n images. The output c_i may be made unity when the input images are members of the training set. If the training set contains two separate classes of images, the c_i may be set to unity for in-class images and to zero for out-of-class images. In this case, the aim is to achieve the widest possible separation of the correlations formed with members of the two classes.

The n unknowns of Equation 2.25 are determined by the n linear equations of Equation 2.20. The substitution of Equation 2.25 into Equation 2.26 yields:

$$\sum_{i=1}^{n} \zeta_i R_{ij} = c_i \qquad \text{for } j=1,2,\ldots,n. \tag{2.27}$$

With the coefficients $\zeta_1, \ldots \zeta_n$ determined in this way, the synthetic discriminant function filter can be constructed.

2.4 OPTICAL CORRELATORS

The correlation in two-space of an input image $f(x,y)$ and reference image $r(x,y)$ is

$$c(x,y) = \int_{-\infty}^{\infty}\int_{-\infty}^{\infty} f(\alpha,\beta) r(\alpha - x, \beta - y) d\alpha d\beta\,. \tag{2.28}$$

Using the correlation properties established in Appendix, Equation 2.28 may be written as

$$c(x,y) = \boldsymbol{F}^{-1}[F(u,v)R^{*}(u,v)\}, \tag{2.29}$$

in which $u = (\frac{x_f}{f\lambda})$, and $v = (\frac{y_f}{f\lambda})$ are the spatial frequencies of the input.

2.4.1 Vander Lugt Correlator

A Vander Lugt correlator is shown in Figure 2.2. P_1, P_2 and P_3 denote the input, spatial frequency and output planes respectively.

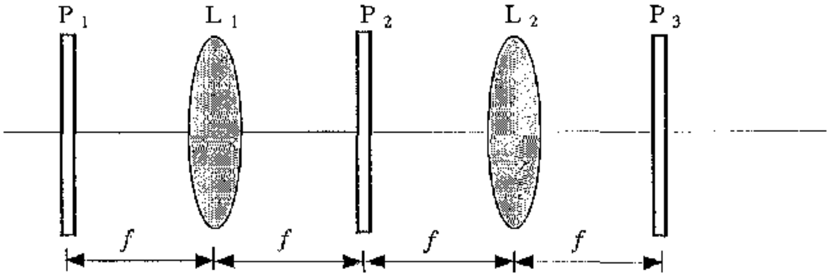

Figure 2.2. A Vander Lugt Correlator.

The light distribution at P_2 is the Fourier transform of the input illumination $f(x,y)$ in P_1

$$F(u,v) = \mathcal{F}[f(x,y)]. \tag{2.30}$$

If a spatial filter $H(u,v)$ is inserted in the Fourier plane P_2, the light distribution leaving this plane is the product of $F(u,v)$ and $H(u,v)$. In this case $H(u,v) = R^*(u,v)$ and the second lens L_2 generates the inverse two-dimensional Fourier transform of $F(u,v)R^*(u,v)$ in plane P_3. From Equation 2.29, the output in plane P_3 is the correlation of the input image $f(x,y)$ with the reference image $r(x,y)$. This scheme has been dubbed the 4f correlator.

2.4.2 Joint Transform Correlator

A joint transform correlator (JTC) is illustrated in Figure 2.3.

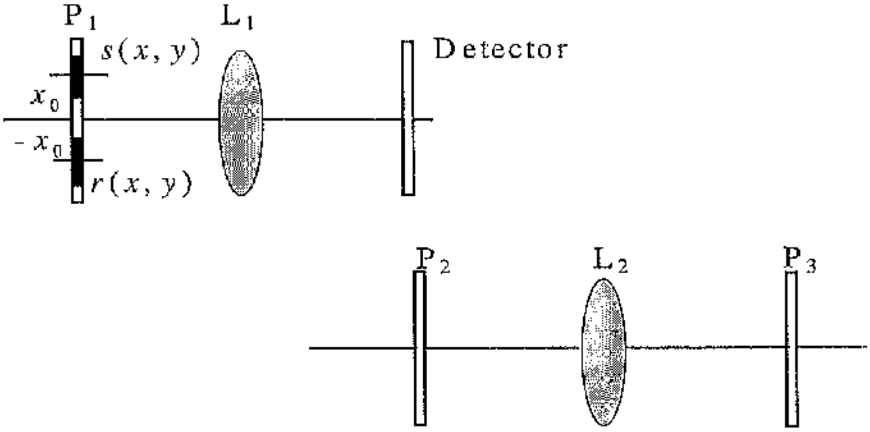

Figure 2.3. A Joint Transform Correlator.

The input image $s(x, y)$ and reference image $r(x, y)$ are placed simultaneously in the input plane P$_1$, but are spaced by distances $x = x_0$ and $x = -x_0$ from the origin. The joint image in P$_1$ is:

$$f(x, y) = r(x + x_0, y) + s(x - x_0, y). \tag{2.31}$$

Lens L$_1$ produces the Fourier transform of the joint image $f(x, y)$ in plane P$_2$, in which the intensity of the Fourier transform of the joint image can be detected by e.g. a CCD camera to yield:

$$\begin{aligned} |F(u,v)|^2 &= |R(u,v)\exp(j2\pi ux_0) + S(u,v)\exp(-j2\pi ux_0)|^2 \\ &= |R(u,v)|^2 + |S(u,v)|^2 + R(u,v)S^*(u,v)\exp(j4\pi ux_0) + R^*(u,v)S(u,v)\exp(-j4\pi ux_0). \end{aligned} \tag{2.32}$$

Alternatively, lens L_2 may be employed to produce the inverse Fourier transform of the intensity in the output plane P_3. A central spot on the optical axis is undesired, but two spots displaced from the origin on the x axis represent the correlation.

2.4.3 Comparison of the Vander Lugt Correlator and Joint Transform Correlator

The matched filter in the Vander Lugt correlator is recorded in the correlator and must be returned precisely to the position in which it was recorded. No constraints are placed on the accuracy with which the filter is placed in the joint transform correlator and, indeed, the reference image may be changed in real-time.

2.5 PERFORMANCE CRITERIA

The following criteria have been applied in the assessment of the performance of correlation filters.

2.5.1 Signal to Noise Ratio (*SNR*)

- Output Signal to Noise Ratio (SNR_o)

The Signal to Noise Ratio (SNR_o)[3] of a filter is defined by

$$SNR_o = \frac{|E\{c(x_0, y_0)\}|^2}{var\{c(x_0, y_0)\}}, \tag{2.33}$$

where *E*, *var*, and *c* denote the ensemble average, the variance and the correlation output function respectively; the correlation peak is located at x_0, y_0. A filter with a high SNR_o, being tolerant of noise, will achieve error free detection with a high probability.

The evaluation of the SNR_o requires that correlations be performed with many images, variously corrupted by noise.

- Input Signal to Noise Ratio (SNR_I)

The relative level of noise impressed on a single input image is defined by:

$$SNR_I = \frac{\sum \left| P_{object} \right|^2}{\sum \left| P_{noise} \right|^2}, \tag{2.34}$$

where the sum in $\sum \left| P_{object} \right|^2$ is formed over the entire image and the P_{object} are the intensities in the pixels representing the image. P_{noise} is the intensity of the noise impressed on the image.

2.5.2 Ratio of the Intensity of the Correlation Peak to that of the Worst Secondary Peak Detected (*PSR*)

The degree of side-lobe suppression that has been achieved is assessed from the ratio of the intensity of the primary correlation peak to that of the maximum secondary peak detected (PSR)[3], which is defined by

$$PSR = \frac{\text{Correlation peak intensity}}{\text{Secondary peak intensity}} = \frac{| c(x_0, y_0) |^2}{Max_B \{ | c(x_0, y_0) |^2 \}}, \tag{2.35}$$

where Max_B denotes the maximum of the output function in the area of B which is constrained to $x - x_0 > 3$ pixels, and $y - y_0 > 3$ pixels. Side-lobes and other undesired peaks in the correlation plane are frequently consequences of noise impressed on the input scene

2.5.3 Peak to Noise Ratio for JTC (*PNR*)

The Peak to Noise Ratio[7] is defined as the ratio of the intensity of the correlation peak to the average value of the noise intensity, measured across the output plane:

$$PNR = \frac{CPI}{\sum_{(i,j) \in R} | n(x_i, y_i) |^2 / N}. \tag{2.36}$$

The sum in the denominator is evaluated across the output plane, but excluding that region R of the correlation peak contained within its half peak intensity profile; N' is the total number of pixels inside R and $|n(x_i, y_i)|^2$ is the background intensity of noise recorded in the pixels.

2.5.4 Horner Efficiency (η)

It is important that the correlator should transmit a high proportion of the light incident upon it, for the power dissipation of a correlator, and therefore its size, are determined by its optical efficiency and the sensitivity and *SNR* of the detector employed to scan the output. Horner[6] introduced the following measure of optical efficiency:

$$\eta = \frac{\textit{total light power in output}}{\textit{total light power in input}} = \frac{\int_{-\infty}^{\infty}\int_{-\infty}^{\infty} |c(x,y)|^2 \, dxdy}{\int_{-\infty}^{\infty}\int_{-\infty}^{\infty} |s(x,y)|^2 \, dxdy}. \tag{2.37}$$

The Horner efficiency of a phase-encoded filter is close to 100%, depending upon losses in the optical medium employed e.g. as in a phase-encoding SLM.

Caulfield[8] suggested defining the "Horner efficiency" as

$$\eta_{caulfield} = \frac{CPI}{\textit{total light power in input}} = \frac{|c(x_0, y_0)|^2}{\int_{-\infty}^{\infty}\int_{-\infty}^{\infty} |s(x,y)|^2 \, dxdy} \tag{2.38}$$

It determines how much of the input energy actually does useful information processing in the correlation peak. At the same time this measure also says something about the sharpness of the correlation peak.

2.5.5 Ratio of the Intensity of the Correlation Peak to the Root Mean Square Intensity (*PRMSR*)

The sharpness of the correlation peak is characterised by the ratio of the intensity of correlation peak to the root mean square intensity of the region ($PRMSR$)[3] B outside the correlation peak area contained within its half-peak intensity profile.

$$PRMSR = \frac{|c(x_o, y_0)|^2}{\frac{1}{N_B}\sum_B |c(x_o, y_0)|^2}. \tag{2.39}$$

In this, N_B is the number of pixels contributing to the rms value. Although the identification of the N_B is analytically straightforward, the calculation of the denominator remains operationally cumbersome. The *PAIR* is a more readily calculated measure of the distinctiveness of the correlation peak in the output field.

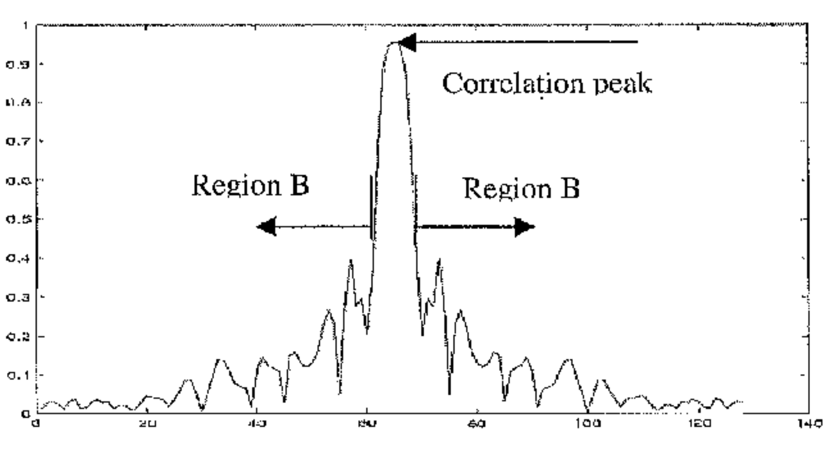

2.5.6 Ratio of the Intensity of the Correlation Peak to the Average Intensity in the Correlation Output Plane (*PAIR*)

This measure of the sharpness of the correlation peak is defined by the following ratio:

$$PAIR = \frac{|c(x_0, y_0)|^2}{[1/N_1 N_2]\sum_{i=1}^{N_1}\sum_{j=1}^{N_2}|c(x_i, y_j)|^2}, \tag{2.40}$$

in which $|c(x_0, y_0)|^2$ denotes the intensity of the correlation peak and the denominator is the average intensity taken across the entire correlation plane. When the correlation peak is sharply defined, the intensity of the correlation peak will substantially exceed the average intensity in the correlation output.

2.5.7 Discrimination Capability (*DC*)

The discrimination capability (*DC*)[4] of a filter is defined as

$$DC = \frac{P_t}{P_{nt}}, \tag{2.41}$$

where P_t is the intensity of the correlation peak corresponding to the target image and P_{nt} is the maximum signal intensity for a non-target input image.

2.5.8 Ratio of the Intensity of the Correlation Peak to that of the Secondary Peak Detected with a SDF Filter, in the Worst Case (*PSR$_w$*)

The performance can be quantified in terms of the ratio of the intensity of the correlation peak to that of the secondary peak in the worst cases that are detected. The (PSR_W) is

$$PSR_w = \frac{P_{\min}}{C_{\max}}. \tag{2.42}$$

$P_{\min}$ is the intensity of the lowest correlation peak and $C_{\max}$ is the intensity of the highest secondary correlation peak amongst the peaks that are detected across the range of distortion. $P_{\min}$ and $C_{\max}$ may not coincide within the distortion range and frequently do not do so. A secondary peak may be due to a correlation with an out-of-class member of the training set.

2.5.9 Discrimination Ratio (*DR*)

This quantifies the rotation invariance of an SDF; it is a measure of the distortion defined by:

$$DR = \frac{CPI_{in-class}^{\min}}{CPI_{out-of-class}^{\max}} = \frac{\min_{i\in\Omega_1}|c_i(x_0, y_0)|}{\max_{i\in\Omega_2}|c_i(x_0, y_0)|}, \tag{2.43}$$

where Ω_1 denotes the set of all possible images from class 1 and Ω_2 denotes the set of all possible images from class 2. $|c_i(x_0, y_0)|$ is the intensity of the correlation peak at the origin when the input is the *i*th member of the set. If DR>1 the correlation peak may be extracted from the clutter unambiguously over the entire range of distortion.

2.5.10 Greatest Variation for SDF Filters (*GV*)

The greatest variation measures the extent to which the minimum correlation peak falls below the maximum correlation peak within the range of rotation. It is defined by:

$$GV = \frac{CPI_{in-class}^{\max} - CPI_{in-class}^{\min}}{CPI_{in-class}^{\max}}. \tag{2.44}$$

$CPI_{in-class}^{\max}$ and $CPI_{in-class}^{\min}$ are the intensities of the maximum and minimum correlation peaks detected in the output plane, corresponding to in-class input images.

2.6 DISCRETE FOURIER TRANSFORM

In the foregoing, the sampling interval has been denoted by the word pixel. In the various simulations reported below 128×128 pixel versions of originally 512×512 pixel images were used in order to limit the computational effort. To aid the comparison of performances, all images, including noisy images, were centred and normalised to transmit unit power.

The sampling theorem provides a convenient way to characterize the complexity of an analog signal, such as an image, in terms of the required number of samples. Optical images, in contrast to time signals, do not have a fixed underlying metric. For example, images can be magnified or demagnified, thereby, changing their areas and their spatial frequency bandwidths but the number of samples remains the same.

Real-time optical correlators currently employ pixellated SLMs in the input and filter planes and a pixellated detector in the output plane. Pixellation in the input plane generates multiple-order optical Fourier transforms in the filter plane of the correlator and, for the same reason, multiple-order correlations appear in the output plane. These replications can be suppressed by choosing the focal length of the input Fourier transform lens so that that the area covered by the zero-order matches the active area of the SLM. It is conventional to assume that the replicated correlation results in the output plane will be spaced so that their boundaries are coincident as long as the input and the filter plane SLMs have the same number of pixels in both the horizontal and vertical directions. This assumption implies that the correlation and input images are identical in size.

2.7 REFERENCES

[1] A. Vander Lugt, "Signal detection by complex spatial filtering," *IEEE. Trans. Inform. Theory,* **IT-10**, 139-145 (1964).

[2] J. L. Horner and P. D. Gianino, "Phase-only matched filtering," *Appl.Opt.* **23,** (812-816) 1984.

[3] B. V. K. Vijaya Kuma and L. Hassebrook, "Performance measures for correlation filters," *Appl.Opt*, **29**. 2997-3006 (1990).

[4] L. Shang, R. K. Wang and C. R. Chatwin, "Frequency Multiplexed DOG filter," *Optics and Lasers in Engineering,* **27**. (161-177) 1997.

[5] C. F. Hester and D. Casasent, "Multivariant technique for multi-class pattern recognition," *Appl.Opt.* **23**, (1758-1761) 1980.

[6] J.L.Horner, "Light utilization in optical correlators," *Appl.Opt*, **21**. 4511-4514 (1982).

[7] J. L. Horner, "Metrics for assessing pattern recognition performance," *Appl.Opt.* **31**, 165-166 (1992).

[8] H. J.Caulfield, "Role of the Horner efficiency in the optimization of spatial filters for optical pattern recognition," *Appl.Opt*, **21**. 4391-4392 (1984).

[9] H. Stark, "Applications of Optical Fourier Transforms," *Academic Press.* 1982.

[10] C. R. Rao, "Linear Statistical Inference and Its Applications," *Jone Wiley and Sons.* 1973.

[11] Reference, "Linear Statistical Inference and Its Applications," *Jone Wiley and Sons.* 1973.

CHAPTER 3

Filter Composed from High Band-Pass and Low Band-Pass Difference of Gaussian Filters

A filter constructed from two difference of Gaussian profiles is designed and is evaluated against two primary performance criteria, being the accuracy with which the position of the target object can be resolved and the extent of the deterioration in this resolution that noise in the input signal will cause. The design strategy seeks an optimisation that values the sharp spatial discrimination yielded by the high band-pass and the noise tolerance imparted by the low band-pass elements from which this filter is composed.

3.1 INTRODUCTION

Kumar[1] introduced the prospect that a trade-off between the noise tolerance of the classical matched filter and spatial discrimination of the phase-encoded filter might yield a filter superior to either of these extremes. Refregier[2] proposed and evaluated an optimal trade-off filter accounting for the criteria of tolerance of noise, sharpness of the correlation peak and Horner efficiency. It is proposed here that an effective filter may be formed by the superposition of two difference of Gaussian (DOG) band-pass filters. A filter[3] has been designed which incorporates two DOG filters, one passing in a band at a lower central frequency, the other passing in a band at a higher central frequency. Thereby, the balance between the tolerance of noise and the sharpness of the correlation peak may be adjusted. An aim has been to assess the attenuation caused by these band-pass filters in an optimum case and so aid the direction of later work, including the design of SDF filters.

3.2 COMPOSITE DIFFERENCE OF GAUSSIAN FILTER

The difference of Gaussian function is formed by the subtraction of two Gaussian functions $g_i(x,y)$; i=1,2. The Gaussian function is

$$g_i(x,y) = \frac{1}{2\pi\sigma_i^2}\exp(-\frac{x^2+y^2}{2\pi\sigma_i^2}), \tag{3.1}$$

in which the σ_i are the defining standard deviations. The DOG function is

$$dog(x,y) = g_1(x,y) - g_2(x,y), \tag{3.2}$$

the corresponding result in the spatial frequency domain being

$$\begin{aligned} DOG(u,v) &= G_1(u,v) - G_2(u,v) \\ &= \exp[-2\pi^3\sigma_1^2(u^2+v^2)] - \exp[-2\pi^3\sigma_2^2(u^2+v^2)]. \end{aligned} \tag{3.3}$$

Appendix 3.6 develops the Fourier transform of $g(x,y)$.

When applied in the frequency domain, the difference of Gaussian function constitutes a band-pass filter of which the width of the passing band and the central frequency can be varied. The function is characterised by the standard deviations σ_1 and σ_2; smaller values of the σ bias the passing band towards higher spatial frequencies. The composite filter is the superposition of two such filters and is expressed in the frequency domain by

$$\begin{aligned} COM(u,v) &= DOG_{high}(u,v) + DOG_{low}(u,v) \\ &= \{\exp[-2\pi^3\sigma_1^2(u^2+v^2)] - \exp[-2\pi^3\sigma_2^2(u^2+v^2)]\} \\ &\quad + \{\exp[-2\pi^3\sigma_3^2(u^2+v^2)] - \exp[-2\pi^3\sigma_4^2(u^2+v^2)]\}. \end{aligned} \tag{3.4}$$

Figures 3.1(a) and (b) show cross-sections taken through DOG functions in the frequency domain with [σ_1=0.04 and σ_2=0.064] and [σ_3=1 and σ_4=1.6] respectively. Figure 3.1(c) shows a cross-section through the composite function, being the superposition of these DOG functions.

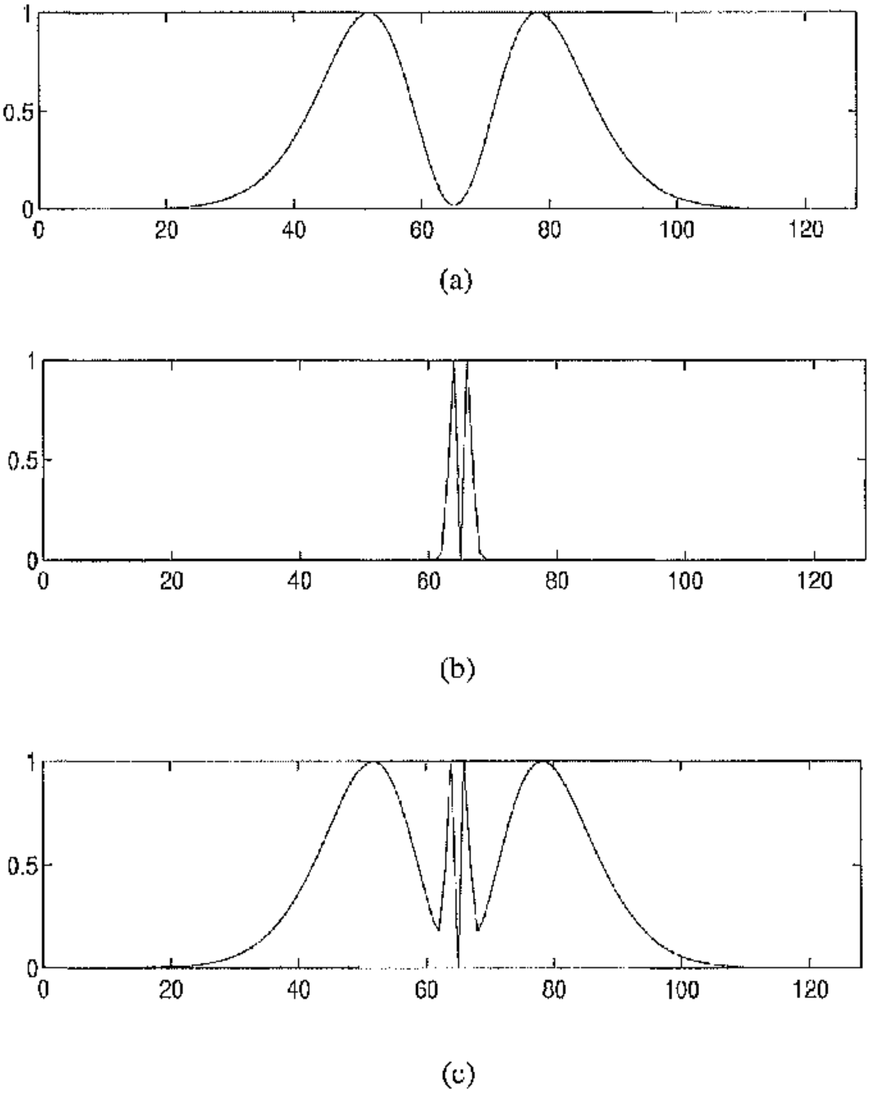

Figure 3.1. Cross-sections taken through the frequency domain of (a) a DOG_{high} function with σ_1=0.04, σ_2=0.064, (b) a DOG_{low} function with σ_1=1, σ_2=1.6 and (c) the composite function, being the superposition of (a) and (b).

3.3 SYNTHESIS OF THE COMPOSITE FILTER

The criteria applied in the optimisation of the filter are the ratio of the central intensity of the primary correlation peak to that of the maximum secondary peak detected (*PSR,* article 2.5.1) and the ratio of the intensity of the correlation peak to the root mean square of the intensity. (*PRMSR,* article 2.5.2)

The filter's performance is tuned by variation of the defining standard deviations σ_i: the application of the high band-pass element sharpens the correlation peak; the robustness of the filter in the presence of noise is enhanced by application of the low band-pass element. The optimisation finds a balance between the sharpness of the correlation peak and the tolerance of noise and is dependent upon the characteristics of the input image.

A scheme devised to discover the optimum is illustrated in Figure 3.2. The cross-correlation is of a reference image and a noise corrupted version of the reference. The procedure is outlined below:

1. Arbitrarily choose four values of the standard deviations sufficient to define an initial filter.
2. Construct the filter according to Equation 3.4.
3. Form the cross-correlation of the reference with the filtered version of the noisy input image.
4. Calculate the ratio of the central intensities of the primary and secondary peaks detected in the correlation plane.
5. Adjust the standard deviations and repeat process 2, to 4, so as to maximise the value of the *PSR*.
6. Fine-tune the four standard deviations within the neighbourhood of the previously obtained value and repeat process 2 and 3.
7. Calculate the *PRMSR*.
8. With the standard deviations so determined, repeat process 2, 3 and 7, until the *PRMSR* is maximised.

The values of the standard deviations found in this way are optimal for the defined image and the structure of the noise imposed upon it.

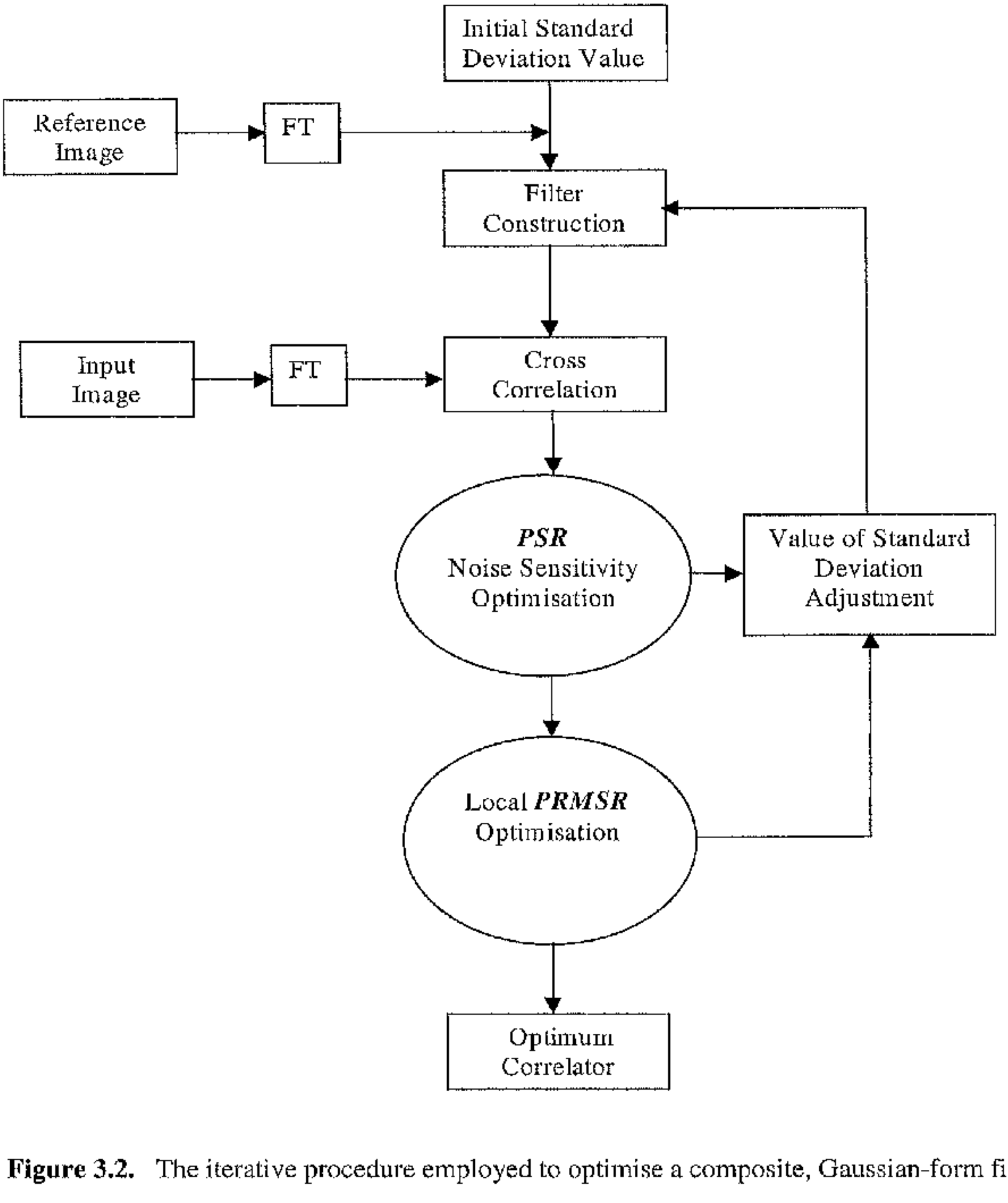

Figure 3.2. The iterative procedure employed to optimise a composite, Gaussian-form filter.

The maximised value of the *PSR* varied little during the application of step 7 and could, therefore, be regarded as constant during the subsequent search for the maximum *PRMSR*.

The image chosen in conducting the optimisation was that of a Bradley APC. The reference image, Figure 3.3(a), was left free of noise; the input was this same image corrupted to a variable depth by Gaussian white noise. Corruption to an SNR_I of 0.5 was regarded as being representative of a severely degraded image, Figure 3.3(b). All images, including their backgrounds, were encoded with a resolution of 128x128 pixels and represented over 256 grey levels.

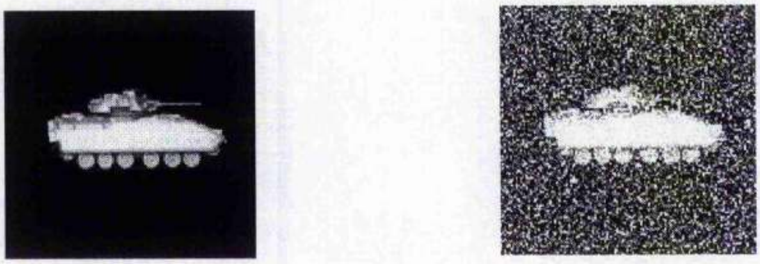

(a) (b)

Figure 3.3. Images of the Bradley APC resolved in 128×128 pixels: (a) noise free image and (b) image corrupted by noise to an SNR_I of 0.5.

Table 3.1. Standard deviations defining the optimum COM function for the case of the Bradley APC and two arbitrary COM functions.

	σ_1	σ_2	σ_3	σ_4
COM_{optim}	0.02	0.06	0.08	1.4
COM_1	0.009	0.04	0.12	2.5
COM_2	0.01	0.1	0.2	2.0

Cross-sections taken through the several composite filters defined in table 3.1 are plotted in the spatial frequency plane in Figure 3.4. The results of correlations employing them, represented in Figure 3.5, demonstrate the robustness of the optimum filter. Table 3.3 lists the values of *PSR* and *PRMSR* obtained with this optimum filter.

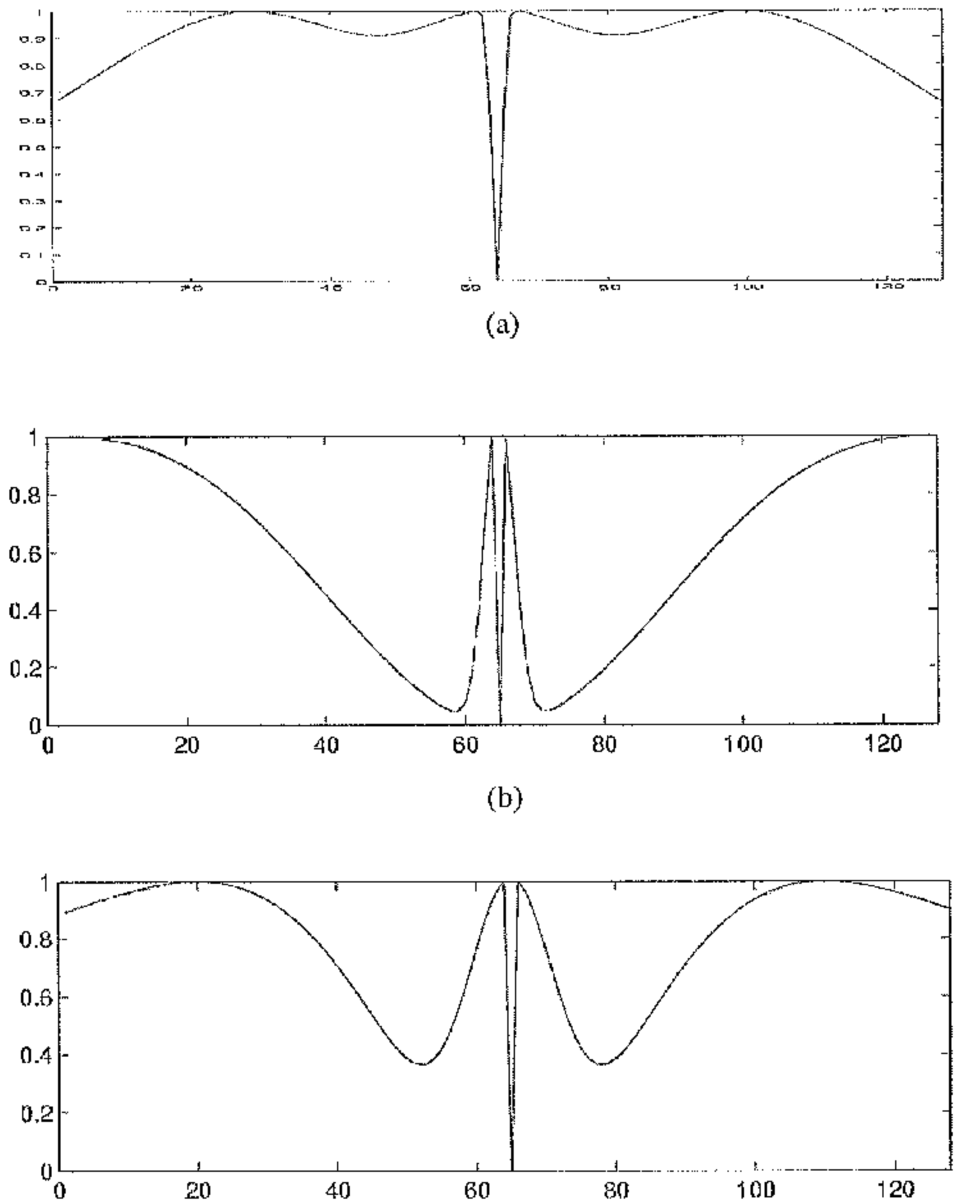

(a)

(b)

(c)

Figure 3.4. Cross-sections taken through the frequency domain of the (a) COM_{optim}, (b) COM_1 and (c) COM_2 filters.

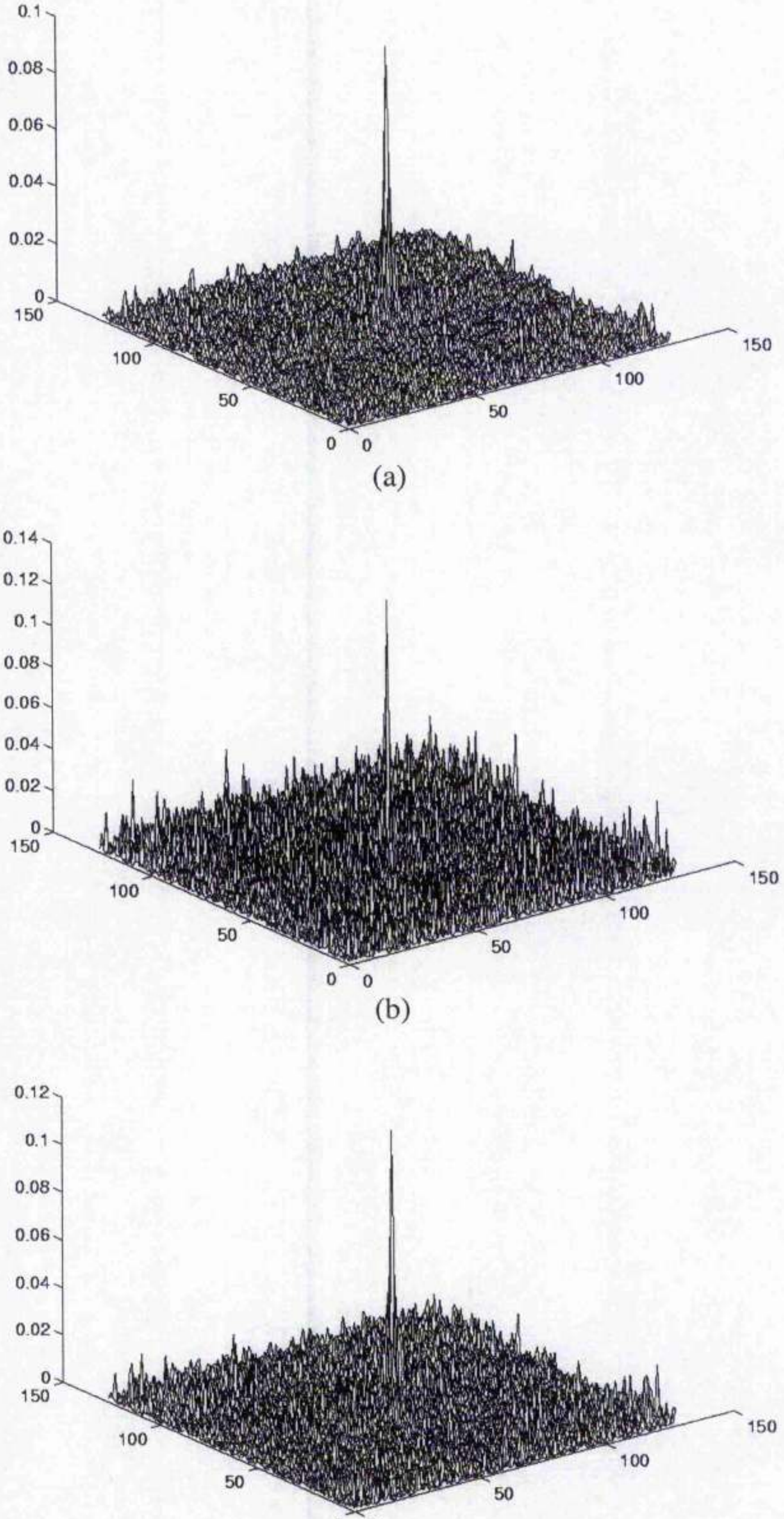

(a)

(b)

(c)

Figure 3.5. Cross-correlations for the case of the Bradley APC, obtained with the (a) $\mathrm{COM}_{\mathrm{optim}}$, (b) COM_1 and (c) COM_2 filters.

3.4 ASSESSMENT OF FILTER PERFORMANCE

The images of the Bradley APC shown in Figures 3.3(a) and 3.3(b) were used in this comparison of performances. The cross-correlation with the noise free image and the cross-correlation with the noisy image were assessed.

3.4.1 Performance of the Composite Filter and of its Component Filters

These simulations were made to demonstrate the effect on performance of the superposition of the characteristics of high and low band-pass filters in a single optimum filter. Table 3.2 describes the component and optimum filters in terms of the standard deviations that define them.

Table 3.2. Values of the standard deviations of the DOG_{high}, DOG_{low}, and COM_{optim} filters.

	σ_1	σ_2	σ_3	σ_4
DOG_{high}	0.02	0.06		
DOG_{low}			0.08	1.4
COM_{optim}	0.02	0.06	0.08	1.4

Figure 3.6 illustrates the auto-correlations obtained and demonstrates the truth of assertions made earlier concerning the effects of band-pass filters on the form of the correlation output. The optimum filter retains the spatial discrimination of a high band-pass filter.

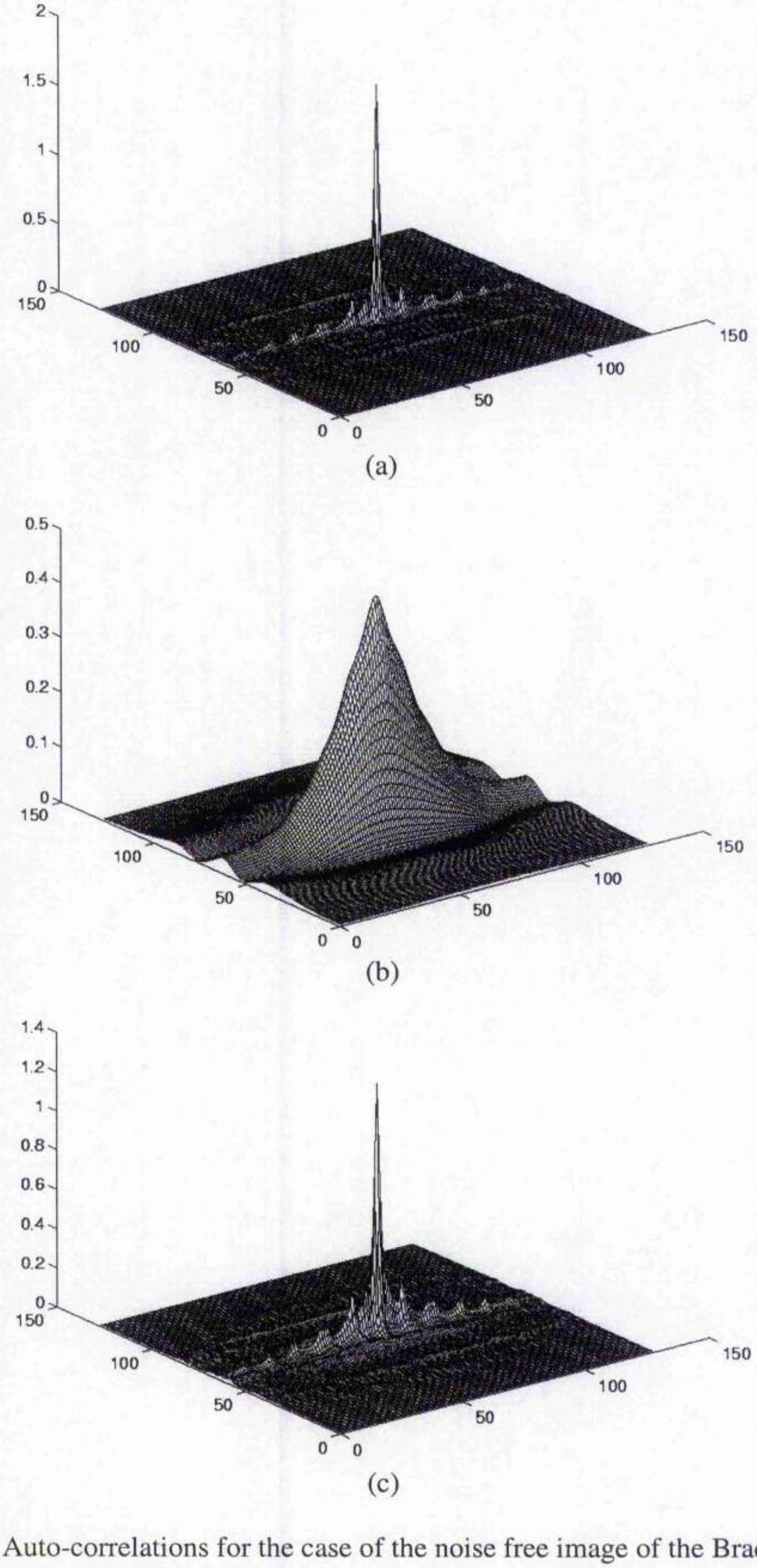

(a)

(b)

(c)

Figure 3.6. Auto-correlations for the case of the noise free image of the Bradley APC obtained with the (a) $\mathrm{DOG}_{\mathrm{high}}$, (b) $\mathrm{DOG}_{\mathrm{low}}$ and (c) $\mathrm{COM}_{\mathrm{optim}}$ filters.

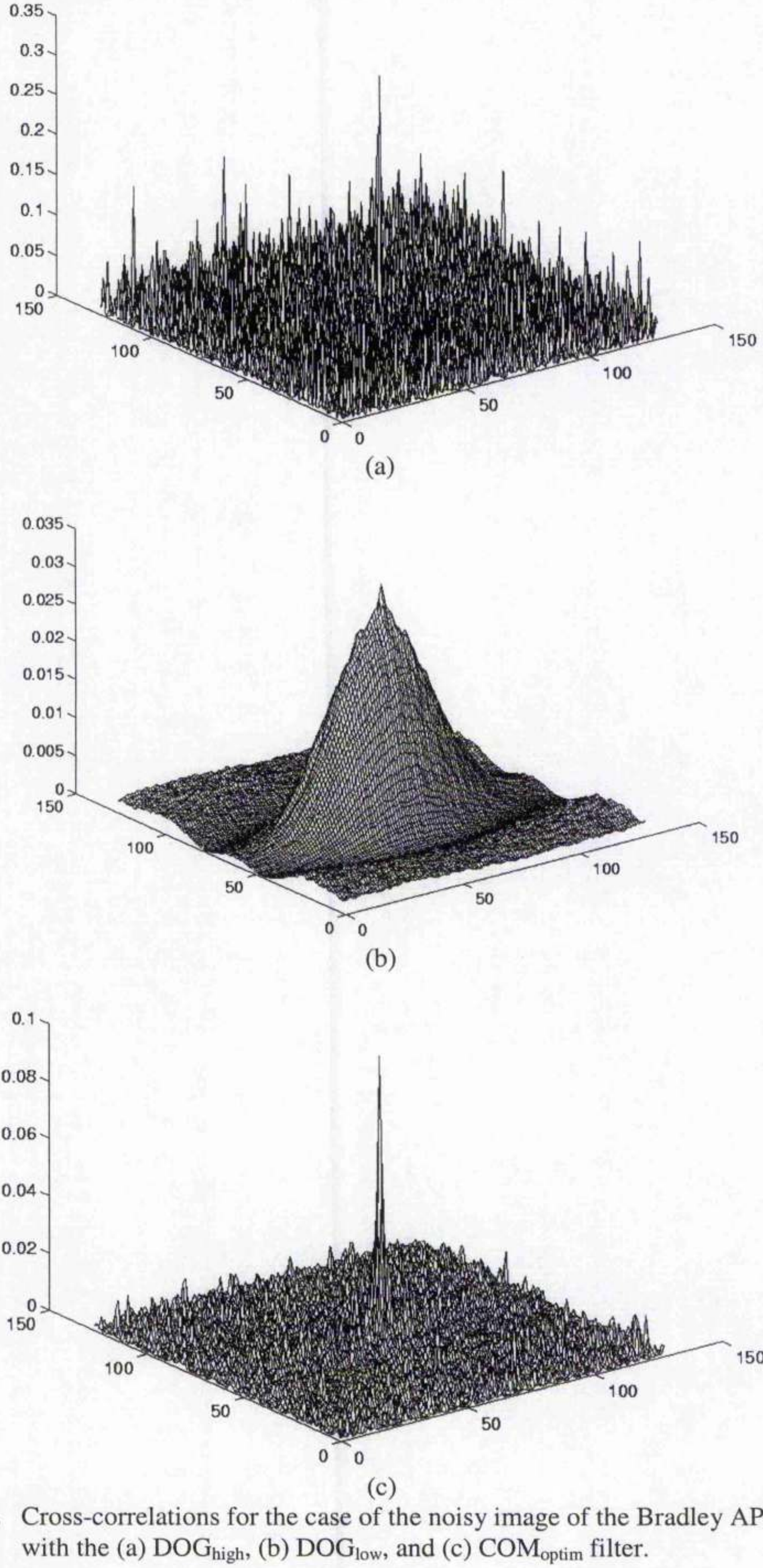

(a)

(b)

(c)

Figure 3.7. Cross-correlations for the case of the noisy image of the Bradley APC obtained with the (a) $\mathrm{DOG}_{\mathrm{high}}$, (b) $\mathrm{DOG}_{\mathrm{low}}$, and (c) $\mathrm{COM}_{\mathrm{optim}}$ filter.

Cross-correlations represented in Figure 3.7 demonstrate the sensitivity of the high band-pass filter to noise and the relatively poor spatial discrimination of the low band-pass filter. The contrast is with the superposition of these filters in the composite filter, which latter retains a sharply defined correlation peak and achieves a significant compression of the spurious spikes that noise in the image creates. In considering these results it must be recalled that the component DOG filters are not optimised filters; the optimisation is of their superposition. Nothing may be concluded here concerning the relative merits of filters that are composed on single and multiple band-pass filters.

3.4.2 Comparison of the Optimum Composite Filter with a Classical Matched Filter and a Phase-Encoded Filter

A comparison of these filters must account for their capacity to accommodate noise in the input scene, whilst maintaining a satisfactory degree of discrimination. This capacity can be characterised in terms of three measures, being the SNR_o, the *PRMSR* and the *PSR* (see article 2.5). Table 3.3 lists the results of simulations employing the image of the Bradley APC in the manner described previously. The component DOG filters on which the composite filter is formed are included in this table for no reason other than completeness; being not optimised, they are excluded from the comparison.

Table 3.3 Comparison of the performance of filters.

	PRMSR	*PSR*	*PI*	SNR_o	*CPI*
$\text{COM}_{\text{optim}}$	5.38	4.27	5	8.27	0.096
DOG_{high}	6.44	1.33	2	3.15	0.17
DOG_{low}	4.36	1.45	793	13.36	0.035
POF	8.58	1.01	3	3.46	0.46
CMF	2.36	1.27	1075	16.89	0.021

The SNR_o was evaluated from simulations using 24 variously corrupted images. In the table, *CPI* denotes the correlation peak intensity and *PI* is the number of pixels falling inside the correlation peak at its full-width, half height value. The characteristics of the three filters being compared are demonstrated in the three-dimensional representations of the outputs of cross-correlations employing them given in Figures 3.8 (a), (b) and (c).

The phase alone filter generates a sharply defined, high-intensity and optically efficient central peak having a *PI* of only three. However, the field contains many such peaks, being the consequences of noise, that are poorly differentiated (a *PSR* as low as 1.01). The risk of ambiguity in detection is high indeed and, therefore, the filter must be adjudged unsatisfactory.

Being little affected by noise the matched filter achieves a SNR_o of 16.89, the highest value recorded with any of the filters. The central intensity is low (*CPI* = 0.021) and the peak, being very broad, is poorly discriminated in the output field (*PI*=1015 and *PSR*=1.27). Nonetheless, the peak might be located with an acceptable spatial resolution by the application of a suitable algorithm to the output of a CCD camera viewing the correlation plane. Both *PSR* and SNR_o being used to measure the noise level in the output plane, SNR_o gives more accurate measurement than *PSR* because it uses many correlation operations. The *PSR* just represents one correlation experiment from the noise process corrupt from the input signal.

Because of the low frequency cut inherent in its design, the composite filter returns a much reduced peak intensity (*CPI* = 0.096) when compared with the phase-encoded filter. The correlation peak is, however, defined without an attendant loss in sharpness. Furthermore, this filter strongly suppressed the degradation caused by noise: the SNR_o is 8.27:1 whilst the *PSR* of 4.27:1 is the highest achieved amongst the filters. Overall, the composite filter performs significantly better than do the competitor phase-encoded and matched filters. The need to optimise four parameters against two primary criteria is a disadvantage in design. Certainly, the optimisation of a SDF filter constructed on a set of composite filters, such as this, would be made complex.

Returning to Figure 3.4(a), which plots the form of the optimum filter in the frequency domain, it is evident that the primary action of the optimised filter is to cut a narrow frequency band centred on the zero order. The profiles of the constituent band-pass filters merge outside this band and leave the spectrum of the image little changed. A filter with this characteristic can, of course, be constructed on a single parameter. This is a signal result for filter design and the basis for a simplification in the development of SDF filters introduced in Chapter 4.

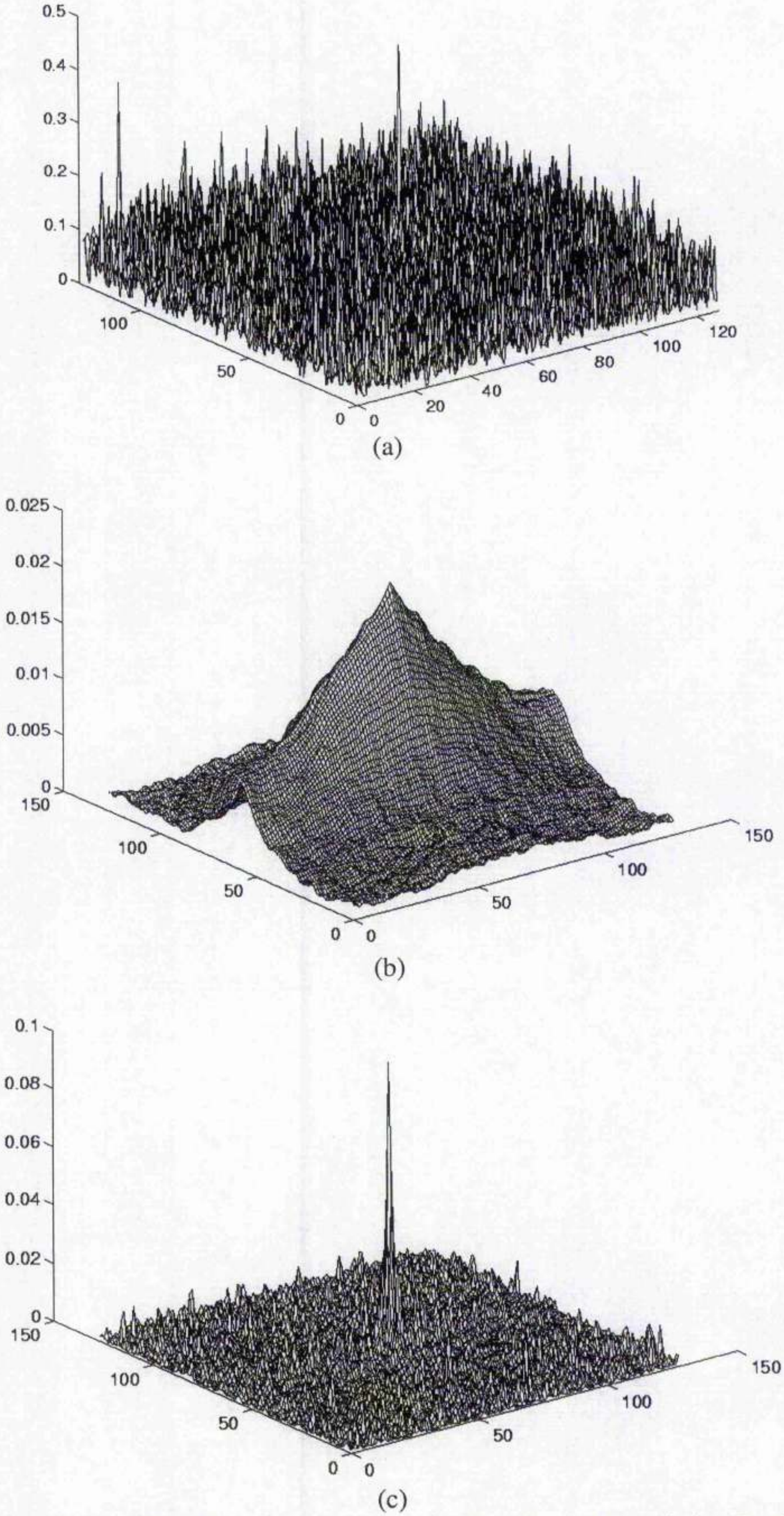

(a)

(b)

(c)

Figure 3.8. Cross-correlations for the case of the noisy image of the Bradley APC obtained with the (a) phase-encoded filter, (b) classical matched filter and (c) optimum composite filter.

The discrimination by the filters between target and non-target images of similar size and shape was also assessed. An M1 tank, Figure 3.9(b), was the chosen non-target (out-of-class) object.

Two simulations were performed with each filter: the first cross-correlated noise free images of the Bradley APC and M1 tank; the second cross-correlated the same images corrupted by noise to a SNR_I of 0.5, Figure 3.10(b). The assessment was of the discrimination capability defined in article 2.5.4.

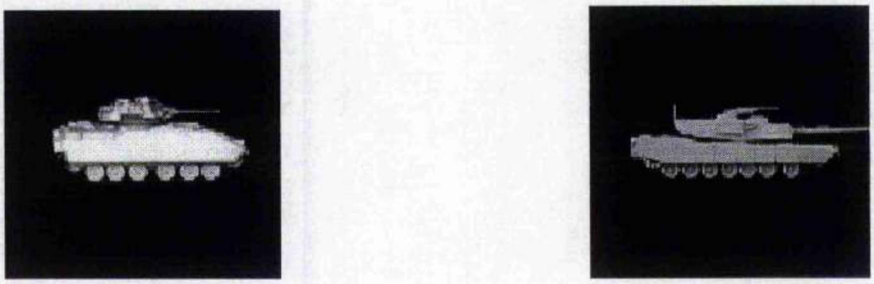

(a) (b)

Figure 3.9. Noise free images resolved in 128×128 pixels: (a) Bradley APC and (b) M1 tank.

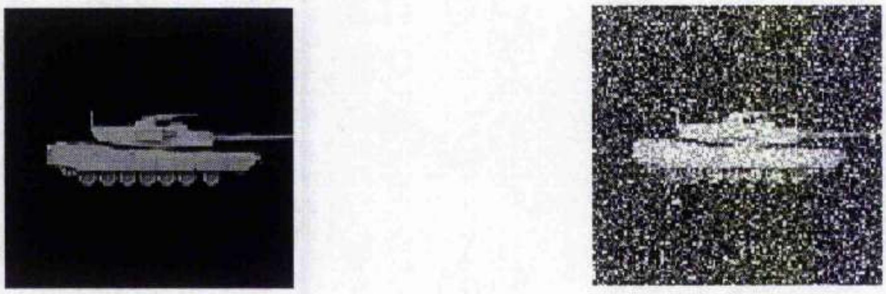

(a) (b)

Figure 3.10. M1 tank resolved in 128×128 pixels: (a) noise free and (b) corrupted by noise to an image SNR_I of 0.5.

Table 3.4 collects the results of these simulations. Whilst the phase-encoded filter is superior when presented with noise free images, its performance is seriously compromised by noise. The composite filter distinguishes the images unequivocally, in the noisy and as noise free cases.

Table 3.4. Comparison of Capacities for Discrimination.

		COM_{optim}	CMF	POF
Noise free case	DC	7.49	1.45	13.69
Noisy case	DC	1.26	0.73	0.59

The widely available photorefractive material, Bismuth silicon oxide (BSO), which is used as a tuneable holographic filter[4] is an effective optical technique with which the performance of optical correlators can be improved. This approach was physically implemented as part of a matched filter by Young[5] [6]. It exploits selective erasure of spatial frequencies at the Fourier plane in the photorefractive material BSO.

3.5 CONCLUSIONS

A filter has been constructed on a superposition of Gaussian form high band-pass and low band-pass component filters, to serve as an experimental tool with which the susceptibility of an optical correlator to noise impressed on the input image might be examined. The classical matched filter and phase encoded filters were the chosen benchmarks. By variation of four parameters - the standard deviations defining the Gaussian forms - the characteristic of the composite filter could be made intermediate between these extremes.

Optical correlations of noisy and noise free images made with these filters have been simulated. The measures of performance adopted were the ratio of the intensity of the correlation peak to the root mean square intensity (*PRMSR*), the ratio of the central intensities of the primary and secondary peaks detected (*PSR*), the intensity of the correlation peak and its width and the signal to noise ratio. All of these were evaluated in the output field of the correlator. An optimisation scheme was devised so that the *PSR* and *PRMSR* might be maximised simultaneously, for a given target, by variation of the parameters defining the composite filter.

The filter so optimised performed significantly better than did the benchmark filters when presented with a noisy image. Its capacity to discriminate between a target object and a similar non-target object also exceeded that of the benchmark filters. The composite filter generated a sharply defined central correlation peak, such as might be obtained with phase-encoded filters, and strongly attenuated spurious peaks consequent upon noise in the image.

The primary effect of the optimised composite filter was to cut a narrow band of frequencies centred on the zero-order. The filter's spectral characteristic was virtually flat elsewhere in the frequency domain. This is a signal result for filter design, for a low-cut filter can be optimised by variation of a single parameter. The optimisation of an SDF filter by variation of four parameters would, in comparison, constitute a formidable design task.

An investigation of the influence of the characteristics of the image upon the optimisation of frequency plane filters is required, but is left for future work.

3.6 APPENDIX

The Fourier Transform of the Gaussian function, Equation 3.1, is developed herein.

$$
\begin{aligned}
G(u,v) &= \int_{-\infty}^{\infty}\int_{-\infty}^{\infty} g(x,y)\exp[-j2\pi(ux+vy)]dxdy \\
&= \int_{-\infty}^{\infty}\int_{-\infty}^{\infty} \frac{1}{2\pi\sigma^2}\exp\left(-\frac{x^2+y^2}{2\pi\sigma^2}\right)\exp[-j2\pi(ux+vy)]dxdy \\
&= \frac{1}{2\pi\sigma^2}\int_{-\infty}^{\infty}\int_{-\infty}^{\infty}\exp\left(-\frac{x^2}{2\pi\sigma^2}\right)\exp(-j2\pi ux)\exp\left(-\frac{y^2}{2\pi\sigma^2}\right)\exp(-j2\pi vy)dxdy \\
&= \frac{1}{2\pi\sigma^2}\int_{-\infty}^{\infty}\int_{-\infty}^{\infty}\exp\left[-\left(\frac{x^2}{2\pi\sigma^2}+j2\pi ux\right)\right]dx\exp\left(-\frac{y^2}{2\pi\sigma^2}\right)\exp(-j2\pi vy)dy \\
&= \frac{1}{2\pi\sigma^2}\int_{-\infty}^{\infty}\int_{-\infty}^{\infty}\exp\left[-\left(\frac{x}{\sigma\sqrt{2\pi}}+j\pi u\sigma\sqrt{2\pi}\right)^2-2\pi^3u^2\sigma^2\right]dx\exp\left(-\frac{y^2}{2\pi\sigma^2}\right)\exp(-j2\pi vy)dy \\
&= \frac{1}{2\pi\sigma^2}\int_{-\infty}^{\infty}\int_{-\infty}^{\infty}\exp\left[-\left(\frac{x}{\sigma\sqrt{2\pi}}+j\pi u\sigma\sqrt{2\pi}\right)^2\right]\exp(-2\pi^3u^2\sigma^2)dx\exp\left(-\frac{y^2}{2\pi\sigma^2}\right)\exp(-j2\pi vy)dy \\
&= \frac{\exp(-2\pi^3u^2\sigma^2)}{2\pi\sigma^2}\int_{-\infty}^{\infty}\int_{-\infty}^{\infty}\exp\left[-\left(\frac{x}{\sigma\sqrt{2\pi}}+j\pi u\sigma\sqrt{2\pi}\right)^2\right]dx\exp\left(-\frac{y^2}{2\pi\sigma^2}\right)\exp(-j2\pi vy)dy \\
&= \frac{\exp(-2\pi^3u^2\sigma^2)}{2\pi\sigma^2}\int_{\infty}^{\infty}\int_{-\infty}^{\infty}\exp\left[-\left(\frac{x}{\sigma\sqrt{2\pi}}+j\pi u\sigma\sqrt{2\pi}\right)^2\right](\sigma\sqrt{2\pi})d\left(\frac{x}{\sigma\sqrt{2\pi}}+j\pi u\sigma\sqrt{2\pi}\right)\exp\left(-\frac{y^2}{2\pi\sigma^2}\right)\exp(-j2\pi vy)dy \\
&= \frac{\exp(-2\pi^3u^2\sigma^2)}{2\pi\sigma^2}(\sigma\sqrt{2\pi})\int_{-\infty}^{\infty}\int_{-\infty}^{\infty}\exp\left[-\left(\frac{x}{\sigma\sqrt{2\pi}}+j\pi u\sigma\sqrt{2\pi}\right)^2\right]d\left(\frac{x}{\sigma\sqrt{2\pi}}+j\pi u\sigma\sqrt{2\pi}\right)\exp\left(-\frac{y^2}{2\pi\sigma^2}\right)\exp(-j2\pi vy)dy \\
&= \frac{\exp(-2\pi^3u^2\sigma^2)}{2\pi\sigma^2}(\sigma\sqrt{2\pi})\int_{-\infty}^{\infty}\exp\left(-\frac{y^2}{2\pi\sigma^2}\right)\exp(-j2\pi vy)dy \\
&= \frac{1}{2\pi\sigma^2}\exp(-2\pi^3u^2\sigma^2)(\sigma\sqrt{2\pi})\exp(-2\pi^3v^2\sigma^2)(\sigma\sqrt{2\pi}) \\
&= \exp[-2\pi^3\sigma^2(u^2+v^2)]
\end{aligned}
$$

3.7 REFERENCES

---

[1] B. V. K. Vijaya Kumar and Zouhir Bahri, "Phase-only filters with improved signal to noise ratio," *Appl.Opt.* **28**, 250-257 (1989).

[2] P. Refregier, "Optimal trade-off filters for noise robustness, sharpness of the correlation peak and Horner efficiency," *Opt. Lett.* **16**, 829-831 (1991).

[3] L. Shang, R. K. Wang and C. R. Chatwin, "Frequency Multiplexed DOG filter," *Optics and Lasers in Engineering,* **27**. 161-177 (1997).

[4] I. Cooper, M. Nicholson, M and C. Petts, "Dynamic frequency plane correlator," *Proc. IEEE.* **133**, 70-76 (1986).

[5] R. C. D. Young, C. R. Chatwin, "Design and simulation of a synthetic discriminant function filter in an updateable photorefractive correlator," *Optical Pattern Rcognition III. SPIE.* **1701**, 239-253 (1992).

[6] R. C. D. Young, C. R. Chatwin, "Experimental assessment of a photorefractive bandpass joint transform correlator," *Opt. Eng.* **36**, 2754-2774 (1997).

CHAPTER 4

Weighted Amplitude Synthetic Discriminant Function Filter

A method for the design of synthetic discriminant function (SDF) filters is developed that maximises the filters' discrimination between the classes of objects represented in a training set of images when presented with a noisy image in an optical correlator. The optimisation depends upon the variation of a parameter A and a vector ζ. The parameter is applied to the member images of the training set in a pre-processing stage that draws on the results of Chapter 3. The amplitude components of the spatial frequency spectrum of these images are differentially weighted so that the contribution from lower spatial frequencies is attenuated. The objective is to sharpen the correlation peak, but yet to avoid the deleterious effects of noise. The vector operates on the group of pre-processed images that constitutes the training set; its components are determined so that the SDF filter responds equally well to all in-class members and discriminates strongly against the out-of-class members of the training set.

A SDF filter is constructed on a training set of entirely phase-encoded images to serve as a basis for a comparison with the performance of the weighted amplitude filter.

4.1 INTRODUCTION

A method suggested by Awwal *et al*[1] was used to achieve the desired weighting of the spatial frequency spectrum of the member images of the training set. If $S(u,v)$ is the Fourier spectrum of a member image $s(x,y)$, the weighted version $S'(u,v)$ is

$$S'(u,v) = \frac{|S(u,v)|}{|S(u,v)| + \mathrm{A}} \exp[i\theta(u,v)]. \qquad (4.1)$$

The spectral distribution of the weighting is determined by the choice made of the parameter A; the filter modulation is by phase alone in the limit that A approaches zero. In illustration of the influence of this parameter, the application of Equation 4.1 to the Fourier spectrum of the Bradley APC (Figure 4.2(a)) is represented in Figure 4.1.

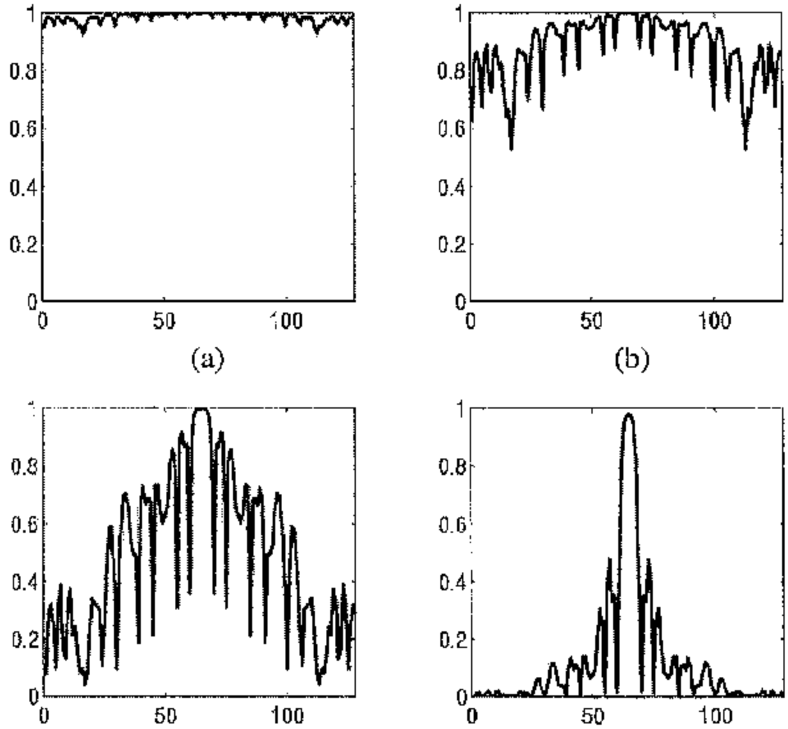

(a) (b)

(c) (d)

Figure 4.1. Cross-section in the spatial frequency domain of the normalised Fourier spectrum of the Bradley APC with A = (a) 0.001,(b) 0.01, (c) 0.1 and (d) 1.0, respectively.

An iterative procedure due to Schils and Sweeney[2] was used to determine the components of the vector ζ that resolves the member images of the training set into the plane of SDF. The condition applied is that the SDF filter shall generate a unit response when presented with an in-class image having the orientation of a member of the training-set and strongly reject[3] out-of-class images.

4.2 DESIGN

The design of the SDF[4] starts with a set of training images $t_n(x, y)$ that spans the range of distortions over which the target object is to be detected and recognised. The superposition of $h(x,y)$ is found in:

$$h(x,y) = \sum_{n=0}^{k} \zeta_n t_n(x,y) . \tag{4.2}$$

The modulation of $h(x, y)$ according to Equation 4.1 is

$$h^{'}(x,y) = \boldsymbol{F}^{-1} \boldsymbol{NF}[h(x, y)] \ , \tag{4.3}$$

where $\boldsymbol{N}$ is the weighting function. The requirement that the correlator shall respond equally to every in-class member of the training set and reject out-of-class members is the condition determining the ζ_n elements of the vector ζ. The output of the correlator is

$$\iint t_n(x,y) h'^{*}(x,y) dx dy \ = \ t_n(x,y) \otimes h^{'}(x,y) \ = \ c_n \, , \tag{4.4}$$

and the c_n are set to unity for in-class images and to zero for out-of-class images of the $t_n(x, y)$.

The iterative procedure[2] adopted to solve Equation (4.4) for the ζ_n relies on the Newton-Raphson method:

$$\zeta_n^{i+1} = \zeta_n^i + \psi [|c_n| - |c_0|(|c_n^i| / |c_0^i|)], \tag{4.5}$$

in which ψ is a damping coefficient and ζ_n^i is the ith iteration of the nth element of ζ.

A range of values on A, (and correspondingly on the ζ_{n},), was explored in a simulation of the filter in an optical correlator. The ratio of the intensity of the correlation peak to the average intensity in the output field, the optical efficiency, the signal-to-noise ratio and the discrimination achieved between classes of images were the optimisation criteria.

4.3 THE SIMULATION

The training set was constituted from images of the in-class Bradley APC and the near, out-of-class M1 tank, which are described in Chapter 3. The simulation was of the SDF employed in an optical correlator to detect in-plane rotations, being the chosen mode of "distortion" of the images (article 2.2). Sixty-one images of these vehicles were recorded at 1^0 increments of rotation in the interval from 0^0 to 60^0, as is illustrated in Figure 4.2. Ten noisy versions of this same set of images were recorded, so that the susceptibility of the SDF to noise in the input image (Figure 4.3) might be assessed.

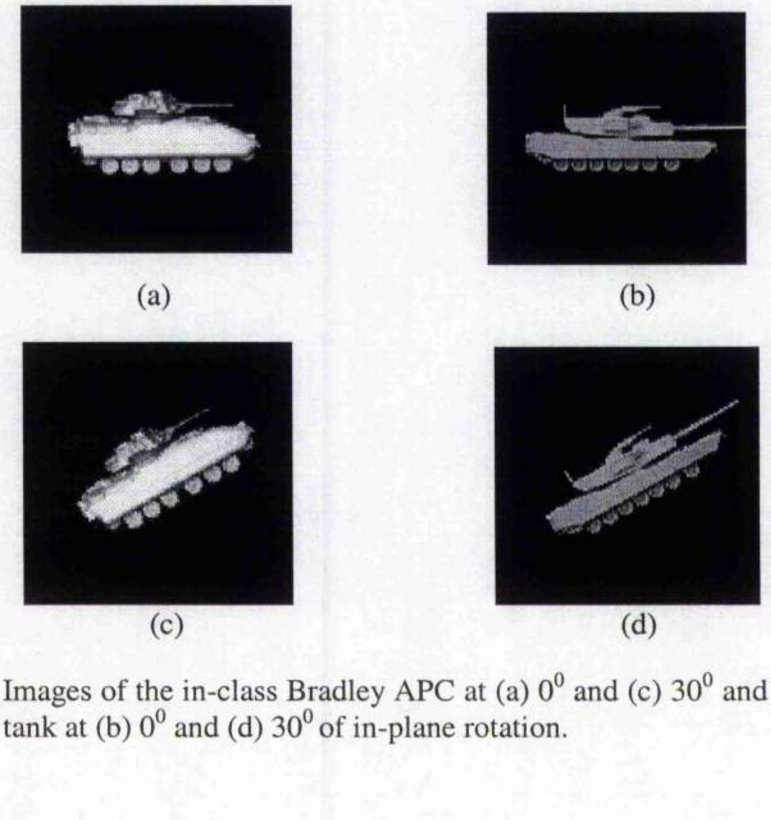

(a) (b)

(c) (d)

Figure 4.2. Images of the in-class Bradley APC at (a) 0^0 and (c) 30^0 and the out-of-class M1 tank at (b) 0^0 and (d) 30^0 of in-plane rotation.

(a)

(b)

Figure 4.3. Images of the (a) Bradley APC and (b) M1 tank corrupted by Gaussian distributed white noise with an SNR_I of 0.5.

4.3.1 Angular Spacing of the Training Set of Images

As a preliminary, the sensitivity of the correlation output to the chosen angular spacing of the images forming the training set was evaluated. The purpose was to reduce the volume of information encoded in the SDF, whilst maintaining a sufficient separation of its responses to in-class and out-of-class images. This simulation employed noise free images.

SDF filters constructed with training images spaced at 5^0 and 10^0 intervals of in-plane rotation were compared. Two cases of amplitude weighting were evaluated. In the first of these the training images were entirely phase-encoded (A =0.001, Figure 4.1(a)). Figure 4.4 plots the variation of the intensities of the primary correlation peak and of secondary peaks detected in the output plane when in-class images were presented to the correlator. With A set equal to 0.1 the contribution to the correlation from lower frequencies in the spectrum of the member images is significant (Figure 4.1(c)). Figure 4.5 illustrates the performance achieved in this, the second case simulated.

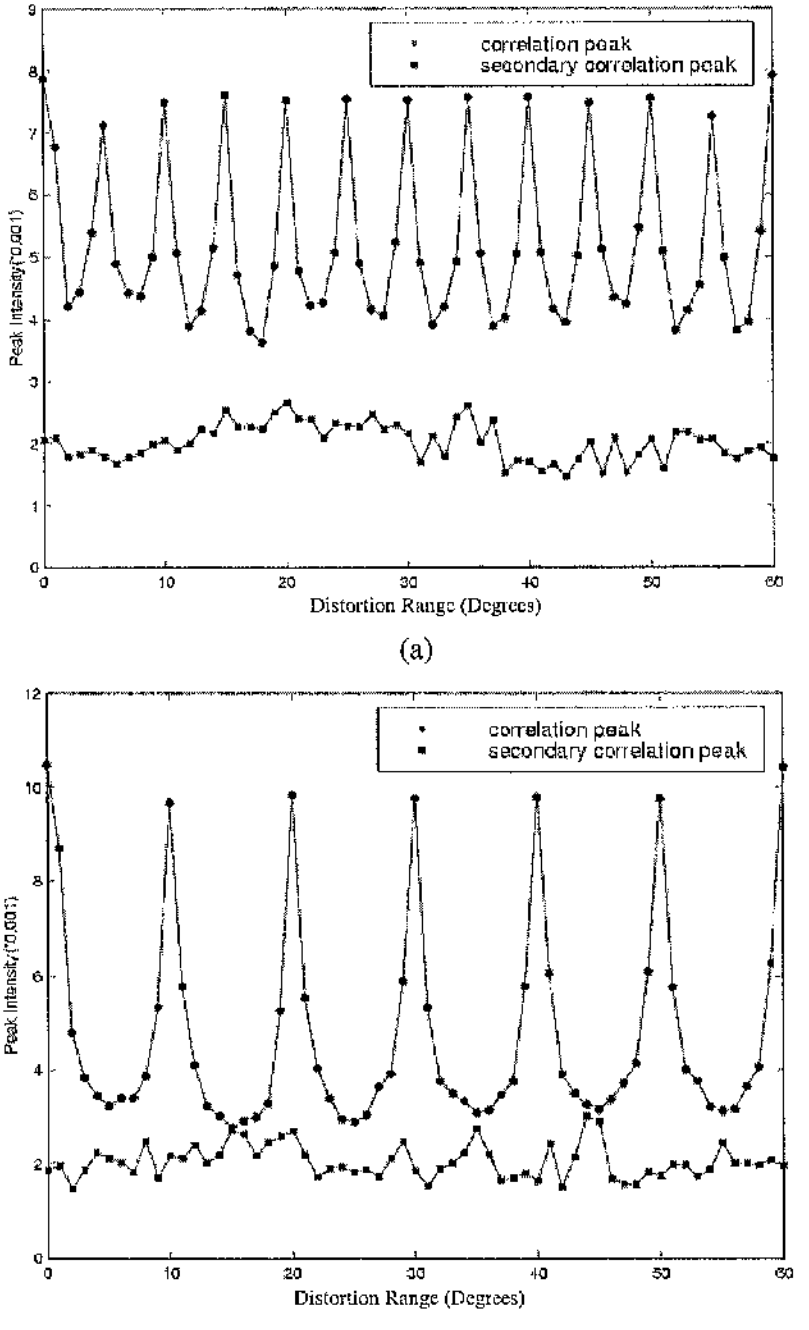

(a)

(b)

Figure 4.4. Correlations obtained for the case $A = 0.001$, with the input images rotated over a range of 60^0 and the training images spaced by (a) 5^0 and (b) 10^0 of rotation.

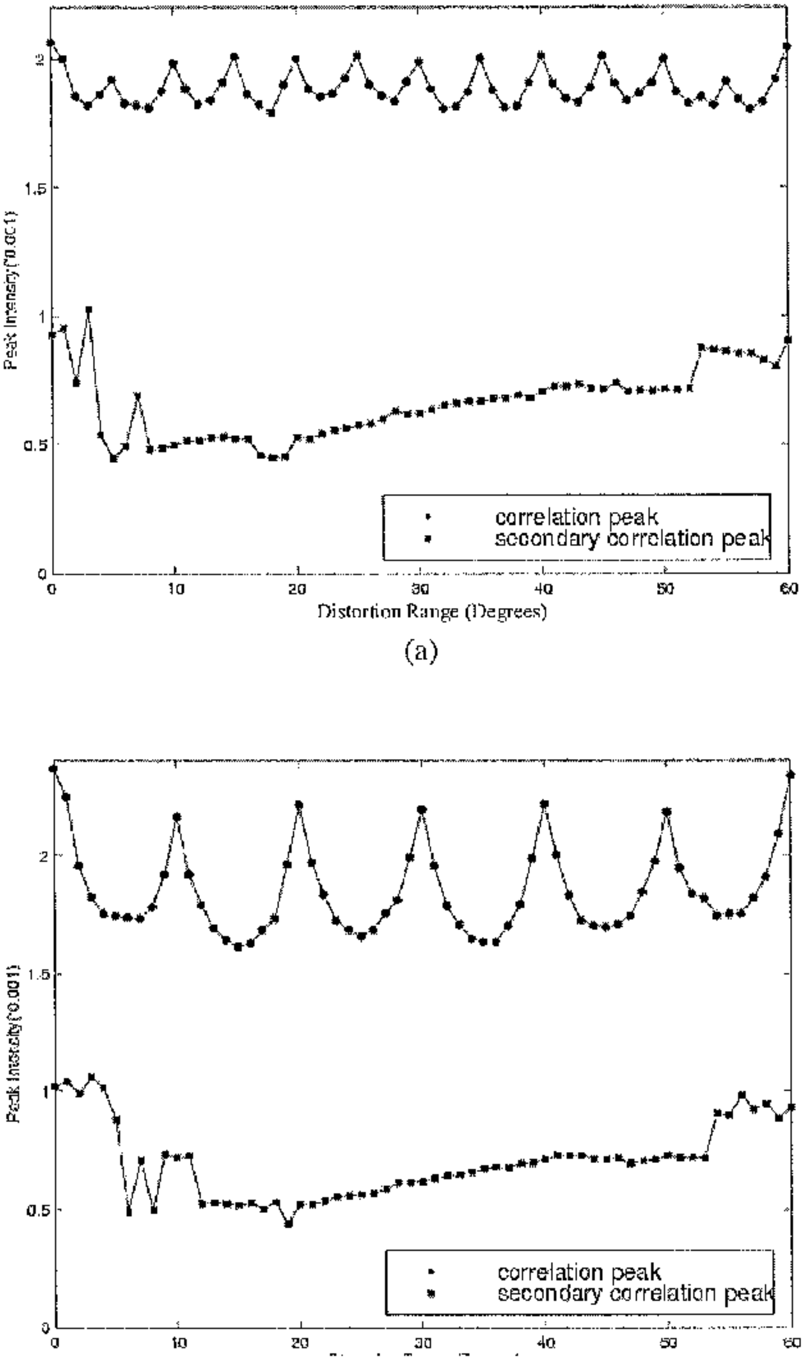

(a)

(b)

Figure 4.5. Correlations obtained for the case $A = 0.1$, with the input images rotated over a range of 60^0 and the training images spaced by (a) 5^0 and (b) 10^0 of rotation.

The phase-encoded SDF is the more sensitive to the angular spacing of the training set because of the sensitivity of the high frequencies in the spectrum to rotation of the input image. (article 2.2) When the interval is 10^0, the minima on the primary correlation profile intersect the maxima on the profile of the secondary peaks. The discrimination is, however, made satisfactory when the interval is halved to 5^0. In contrast, the weighted amplitude SDF is not so affected; the discrimination between classes is little changed when the interval is increased to 10^0 from 5^0. An advantage is won by increasing the angular resolution, for thereby the variation in the intensity of the correlation peaks caused by rotation of the input image is reduced.

4.3.2 Performance of the Filters

In light of the result concerning the angular resolution of the training set images obtained in the preceding section, the assessments reported herein were conducted with an SDF constructed with an angular resolution of 5^0.

Figure 4.6 presents the results of simulations with this resolution and with A varied in the range 0 to 5. The trade-off is between the fall of the intensity in the correlation peak (*PAIR*) and the rise in the SNR_o as A is increased. Two factors combine to cause the rapid fall seen in the *PAIR*: the optical efficiency of the filter is reduced and the breadth of the correlation peak is greatly increased when the contribution made to the correlation by low spatial frequency components is raised.

The SNR_o impacts strongly on the degree to which the different classes of images are distinguished by the correlator. As was discovered in Chapter 3, the response of a filter to a noisy image is sensitive to the level to which amplitude modulation is permitted in its spectrum.

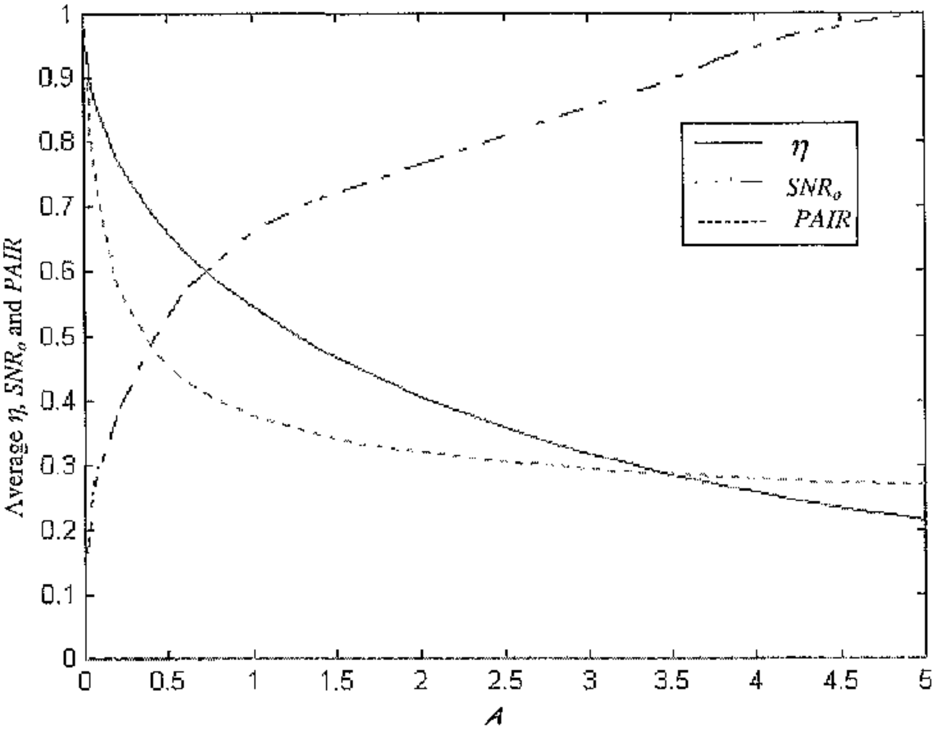

Figure 4.6. Averages of the Horner efficiency (η), the *PAIR* and the SNR_o, varying with the amplitude weighting parameter A.

Figure 4.6 shows that the correlation output is most sensitive to variations of A in the range from 0 to 0.6, depending upon the extent to which the input image is degraded by noise. On exploring this range on A, a filter constructed on a training set modulated with $A = 0.4$ was found to offer a good compromise between the several assessment criteria. This filter is characterised in Figure 4.7; the components of the vector ζ on which the SDF is synthesised are listed in Table 4.1.

A comparison of the performance of the optimum amplitude weighted SDF with a phase-encoded SDF, synthesised from the same images, is given in Table 4.2. Noise present in the input image is strongly suppressed in the correlation formed with the weighted amplitude SDF. This property is illustrated in Figures 4.8 and 4.9, which plot intensity distributions in the correlation plane obtained with the phase-modulated and weighted amplitude filters when presented with noise free and noisy images.

Table 4.1. Components of ζ for an weighted amplitude SDF with $A = 0.4$.

ζ_0	ζ_1	ζ_2	ζ_3	ζ_4	ζ_5	ζ_6
0.7243	0.1922	0.2647	0.4014	0.3286	0.3742	0.2059
ζ_7	ζ_8	ζ_9	ζ_{10}	ζ_{11}	ζ_{12}	
0.2720	0.5140	0.2566	0.3375	0.1514	0.7255	

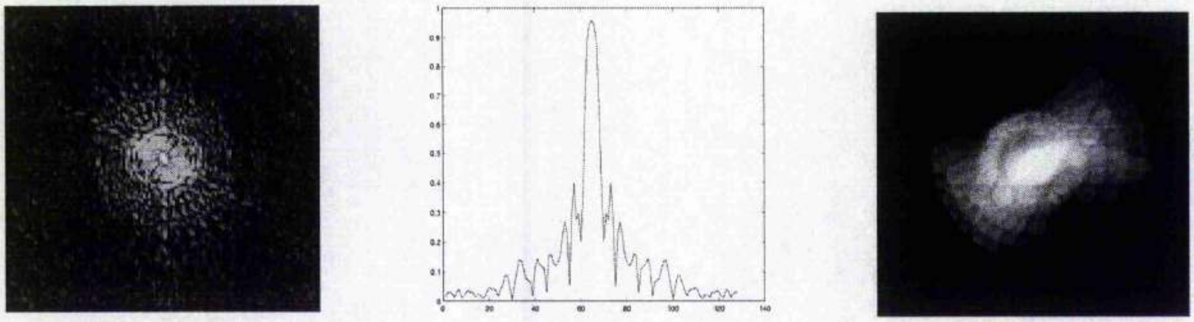

(a) (b) (c)

Figure 4.7. (a) Fourier spectrum of an weighted amplitude SDF with $A = 0.4$; (b) a cross-section taken through the spectrum in (a); (c) the impulse response of the filter.

Table 4.2. Comparison of an weighted amplitude SDF with $A = 0.4$ and a phase-encoded SDF.

Filter	η_{ave}%	$PAIR_{ave}$	SNR_o	DR	$CPI_{\max}$	GV%
Amplitude modulated SDF	68.27	13.38	35.6	1.31	1.14	16.74
Phase-encoded SDF	100	28.54	9.4	0.91	11.5	75.1

[$PAIR_{\max} \times 10^{-3}$ and $CPI_{\max} \times 10^{-3}$].

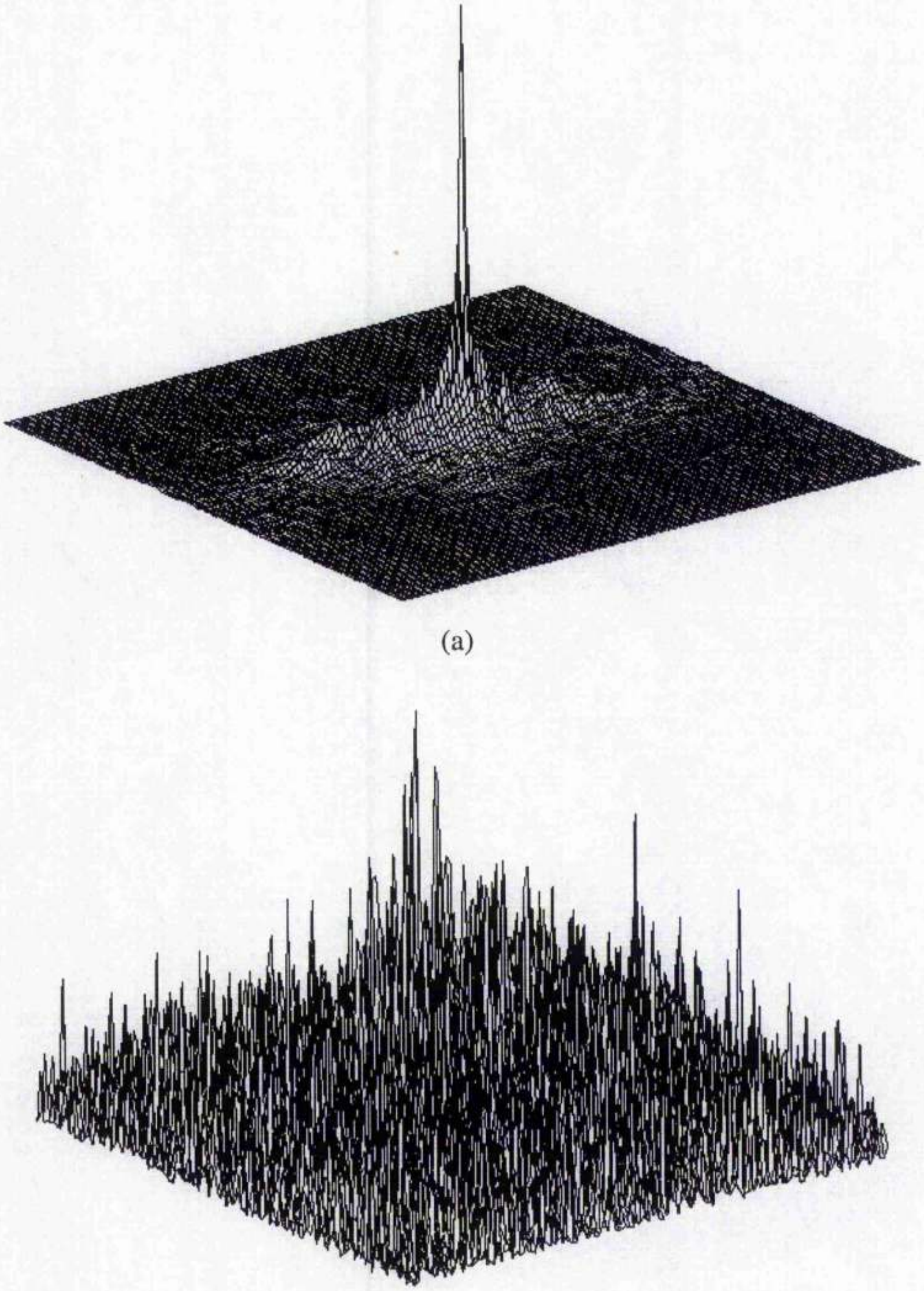

(a)

(b)

Figure 4.8. Cross-correlations obtained with the phase-encoded SDF when presented with (a) noise free and (b) noise corrupted images of the in-class Bradley APC.

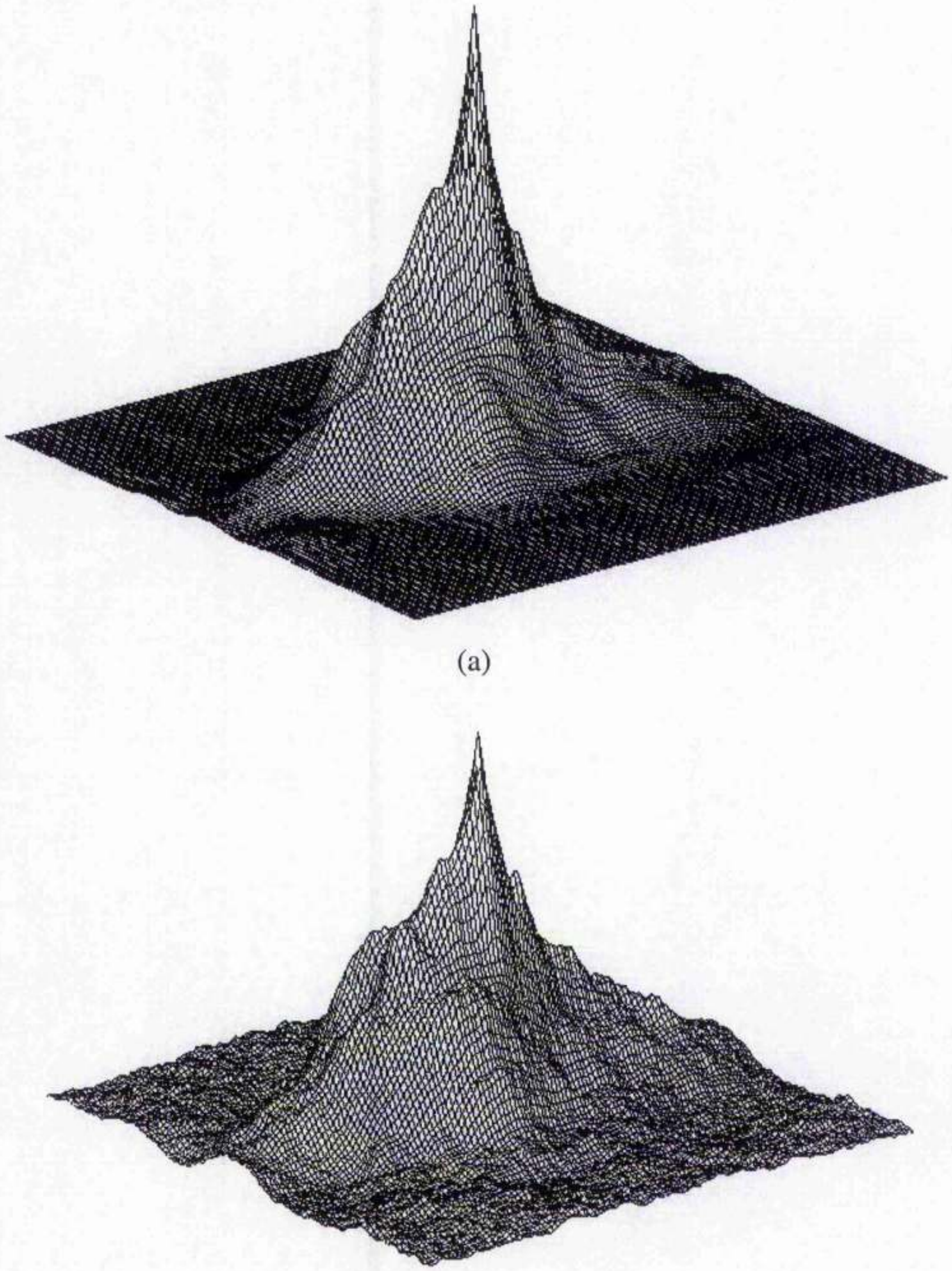

(a)

(b)

Figure 4.9. Cross-correlations obtained with the optimum weighted amplitude SDF (A = 0.4) when presented with (a) noise free and (b) noise corrupted images of the in-class Bradley APC.

The weighted amplitude SDF discriminates the in-class and out-of-class images unequivocally when these images are corrupted by noise to an SNR_I of 0.5. Figure 4.10 demonstrates that a clear separation is maintained between these classes of image and illustrates the regularity of the in-class response across the operational range of the SDF.

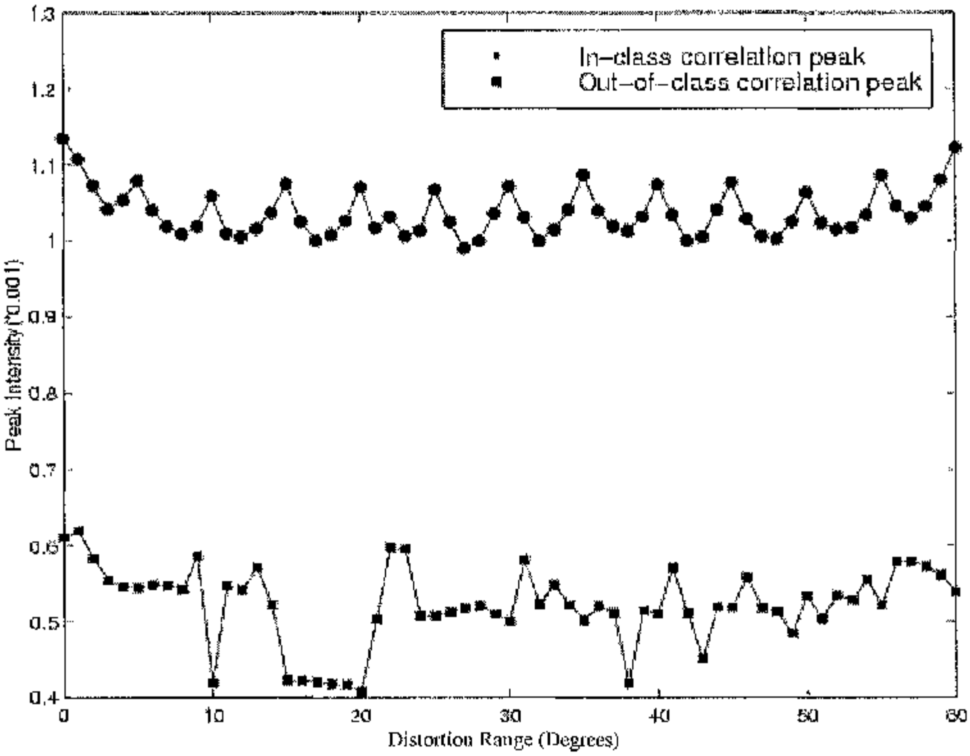

Figure 4.10. Correlations of in-class and out-of-class images obtained with an weighted amplitude SDF (*A*=0.4) and with the input corrupted by noise to a SNR_I of 0.5.

The weighted amplitude synthetic discriminant function filter rely on the appropriate spatial light modulator (SLM) technology for real-time implementation. An optically controlled ferroelectric liquid crystal SLM may be used to control the amounts of magnitude and phase modulation independently[5] [6]. Alternatively, a pair of liquid crystal televisions may be used to obtain a complex modulation with independently controllable phase and amplitude[7]. This particular optical architecture using two LCTVs polarises and lenses can be used.

4.4 CONCLUSIONS

A method has been devised for the design of synthetic discriminant functions that ensures that the response by an optical correlator employing them shall discriminate, unequivocally, between distorted and noisy images of different classes of object that might be submitted at its input.

The principal elucidated in Chapter 3 was adopted: a weighting was applied which attenuated the amplitude of low frequency terms in the spatial frequency spectra of the component filters. The purpose was to raise and sharpen the peak in the correlation output, whilst avoiding the worst depredations of noise impressed on the input image.

The method requires the variation, coincidentally, of a scalar parameter and a vector that operate on the members of a training set of images from which the SDF is constituted. The scalar differentially weights the spectra; the vector resolves the set of weighted images into the plane of the SDF.

A preliminary simulation discovered the sensitivity of filters, so constructed, to the incremental distortion of successive images in the training set. The capacity of the SDF to detect in-plane rotations of images, this being the chosen mode of distortion, was evaluated. A comparison was drawn with the performance of an SDF synthesised from entirely phase-encoded images. Whereas the weighted amplitude filter maintained its capacity for discrimination, the phase-encoded filter failed to distinguish between classes of objects unambiguously when the angular separation of the training images was raised from 5^0 to 10^0 of rotation. Therefore, training sets were constructed at 5^0 increments of rotation for the purposes of subsequent simulations. The correlator was interrogated with variously noisy images spaced at 1^0 increments of rotation.

The trade-off in design is between a sharpened correlation peak and, with a deteriorating SNR_o in the output, a reduced capacity to distinguish between similar target objects as the weighting progressively favours higher spatial frequencies. Simulations that accounted for this balance of influences and the optical efficiency identified a critical range on the value of the weighting parameter. A good compromise between the assessment criteria was secured with the parameter set to 0.4. A filter designed with this value was able to distinguish the images of an in-class and a near out-of-class object clearly when the input was corrupted by noise to a SNR_I of 0.5. When interrogated with in-class images spaced at 1^0 intervals, the maximum variation of the intensity of the correlation peak recorded was less than 18% across a 60^0 span of rotational distortion.

Though the spatial location of the correlation peak was never in doubt, the peaks observed in this work were much broadened when compared with those achieved using the weighting scheme developed in Chapter 3. The weighting profile adopted in this optimisation may not, therefore, be ideal. An examination is required of the prospects for an SDF constructed on images that have been amplitude weighted by a low-cut filter.

4.5 REFERENCES

---

[1] A. A. S. Awwal, M. A. Karim and S. R. Jahan, "Improved correlation discrimination using an amplitude-modulated phase-only filter," *Appl.Opt.* **29**, 233-236 (1990).

[2] G. F. Schils and D. W. Sweeney, "Iterative technique for the synthetic of optical correlator filters," *J.Opt.Soc.Am.A* **3**, 1433-1442 (1986).

[3] D. Casasent, "Unified synthetic discriminant function computational formulation," *Appl.Opt.* **19**, 2343-2350 (1986).

[4] D. Jared and D. Ennis, "Inclusion of filter modulation in the synthetic discriminant function construction," *Appl.Opt.* **28**, 4335-4339 (1989).

[5] J. D. Downe, "Optical binary phase and amplitude correlation filters for polarization rotating spatial light modulators," *Opt.Eng.* **32**, 1886-1896 (1993).

[6] M. O. Freeman, T. A. Brown and D. M. Walba, "Quantized complex ferroelectric liquid crystal spatial light modulators," *Appl.Opt.* **31**, 3917-3929 (1992).

[7] D. A. Gregory, J. C. Kirsch and E. C. Tam "Full complex modulation using liquid crystal televisions," *Appl.Opt.* **31**, 163-165 (1992).

CHAPTER 5

A SDF Filter Synthesised from Phase-Encoded Images and Correlating Phase-Encoded Images

The prospects are explored for an optical correlator that employs a SDF constructed from phase-encoded images and which is presented with phase-encoded images at its input. Noise impressed on the input images will seriously degrade the performance of this correlation. Nonetheless, the availability of phase-modulating spatial light modulators makes real-time correlation a practical proposition, using the scheme proposed.

5.1 INTRODUCTION

Horner and Gianino[1] and Jared and Ennis[2] have designed "phase only" SDF filters. The second of these designs satisfies the condition that correlation peaks formed with member images of the training set shall be of equal amplitude. Wang *et al*[3] found that the discrimination of classes of images was more acute when the SDF filter was, *ab initio*, constructed from phase-encoded images.

The proposition that the discrimination will be yet more acute if the correlation is made with a phase-encoded version of the input image is explored herein. An initial study examines the sensitivity of this form of correlation to the angular spacing of the training set images for the case of in-plane rotation of the images. With the resolution so determined, the capacity of a correlator to distinguish classes of objects is then evaluated by a simulation of its performance.

5.2 THE SIMULATION

5.2.1 Background

Chapter 4 describes the design of synthetic discriminant functions. The substitution of Equation 4.3 into Equation 4.4 yields a result for the output of a SDF filter correlating members of the training set of images with which it was synthesised, viz.

$$t_n(x,y) \otimes h'(x,y) = t_n(x,y) \otimes \boldsymbol{F}^{-1}\boldsymbol{M}\boldsymbol{F}\{\sum_{n=0}^{k} \zeta_n t_n(x,y)\} = c_n . \tag{5.1}$$

In the modification being examined the "weighting function" $\boldsymbol{M}$ does no more than to extract the phase of the signals to which it is applied. Therefore, the summation in Equation 5.1 is of phase-encoded rather than of weighted-amplitude real images. The result is

$$t_{\boldsymbol{M}[n]}(x,y) \otimes h'_{\boldsymbol{M}}(x,y) = t_{\boldsymbol{M}[n]}(x,y) \otimes \boldsymbol{F}^{-1}\boldsymbol{M}\boldsymbol{F}[\sum_{n=0}^{k} \zeta_n t_{\boldsymbol{M}[n]}(x,y)] , \tag{5.2}$$

with

$$t_{\boldsymbol{M}[n]}(x,y) = \boldsymbol{F}^{-1}\boldsymbol{M}\boldsymbol{F}[t_n(x,y)] . \tag{5.3}$$

In aid of clarity, Figure 5.1 sets out the order of the evaluation of Equation 5.2.

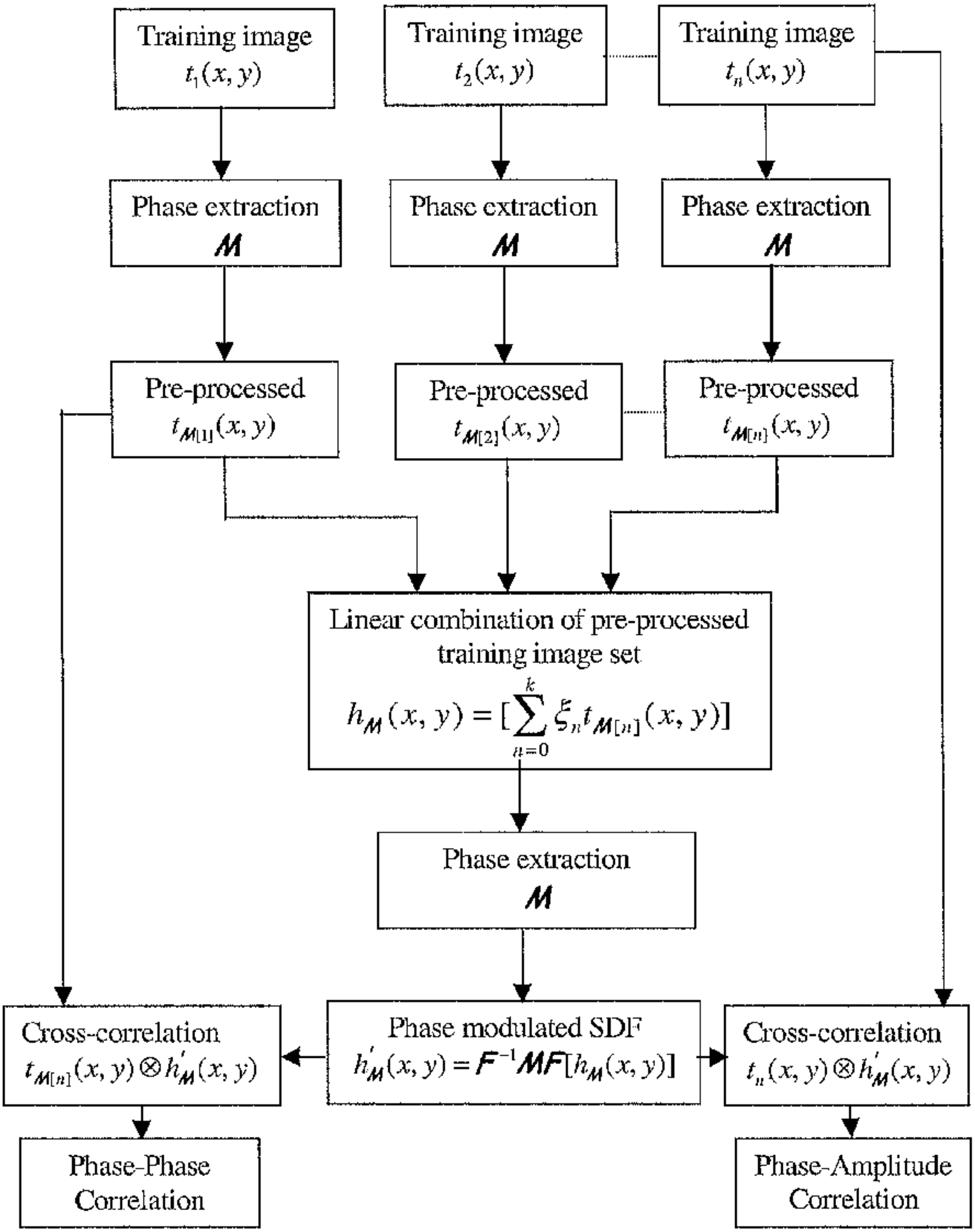

Figure 5.1. Correlation of a phase-encoded SDF with phase-encoded and real images.

5.2.2 The Training Set of Images

Chapter 3 has introduced the images employed in the simulation. Figure 5.2 demonstrates the result of phase extraction applied to images of the Bradley APC and M1 Tank vehicles. One hundred and six images of these vehicles were captured to cover a range of in-plane rotation of 0^0 to 105^0, taken at 1^0 increments.

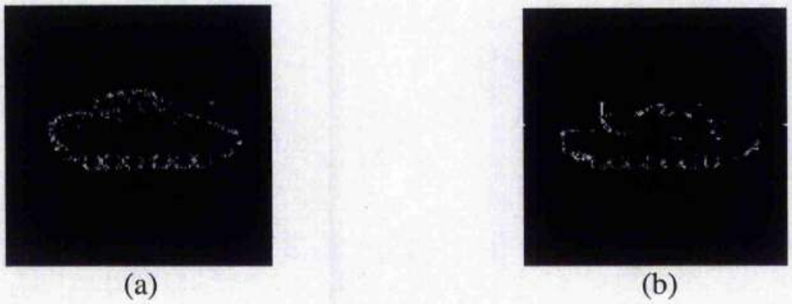

Figure 5.2. Phase-encoded images of the (a) in-class Bradley APC and (b) out-of-class M1 tank.

5.3 RESULTS OF SIMULATIONS

5.3.1 Angular Resolution of the SDF

The sensitivity of phase-phase correlation to the angular resolution of the SDF is illustrated in Figure 5.3. The SDF filters were synthesised from images separated by 3^0 and 5^0 of in-plane rotation. Correlations were simulated with the in-class image rotated by increments of 1^0 over the range from 0^0 to 30^0. The SDF that resolved images rotated by 5^0 was unsatisfactory; the envelope containing the secondary peaks detected in the output intruded upon that enclosing the responses to in-class images. There being no ambiguity in the discrimination when the angular spacing was reduced to 3^0, this resolution was retained in all subsequent simulations. That this was a safe choice is demonstrated in Figure 5.4, which compares the outcomes of phase-amplitude (PAC) and phase-phase (PPC) correlations.

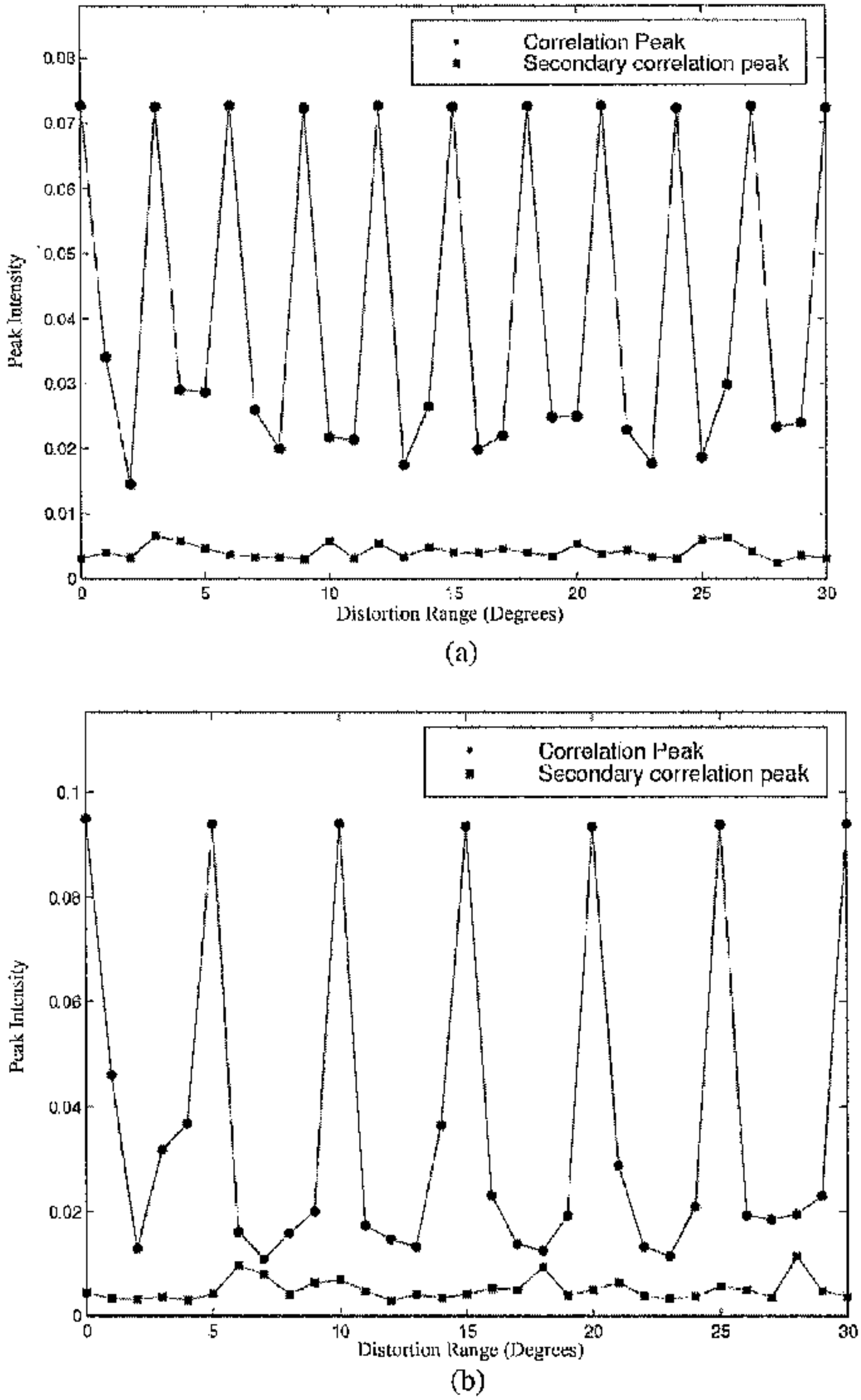

Figure 5.3. Primary and secondary peaks detected in the outputs of phase-phase correlations made with SDF filters constructed with images spaced by (a) 3^0 and (b) 5^0 increments of rotation, when interrogated by the basic training set image rotated successively through intervals of 1^0.

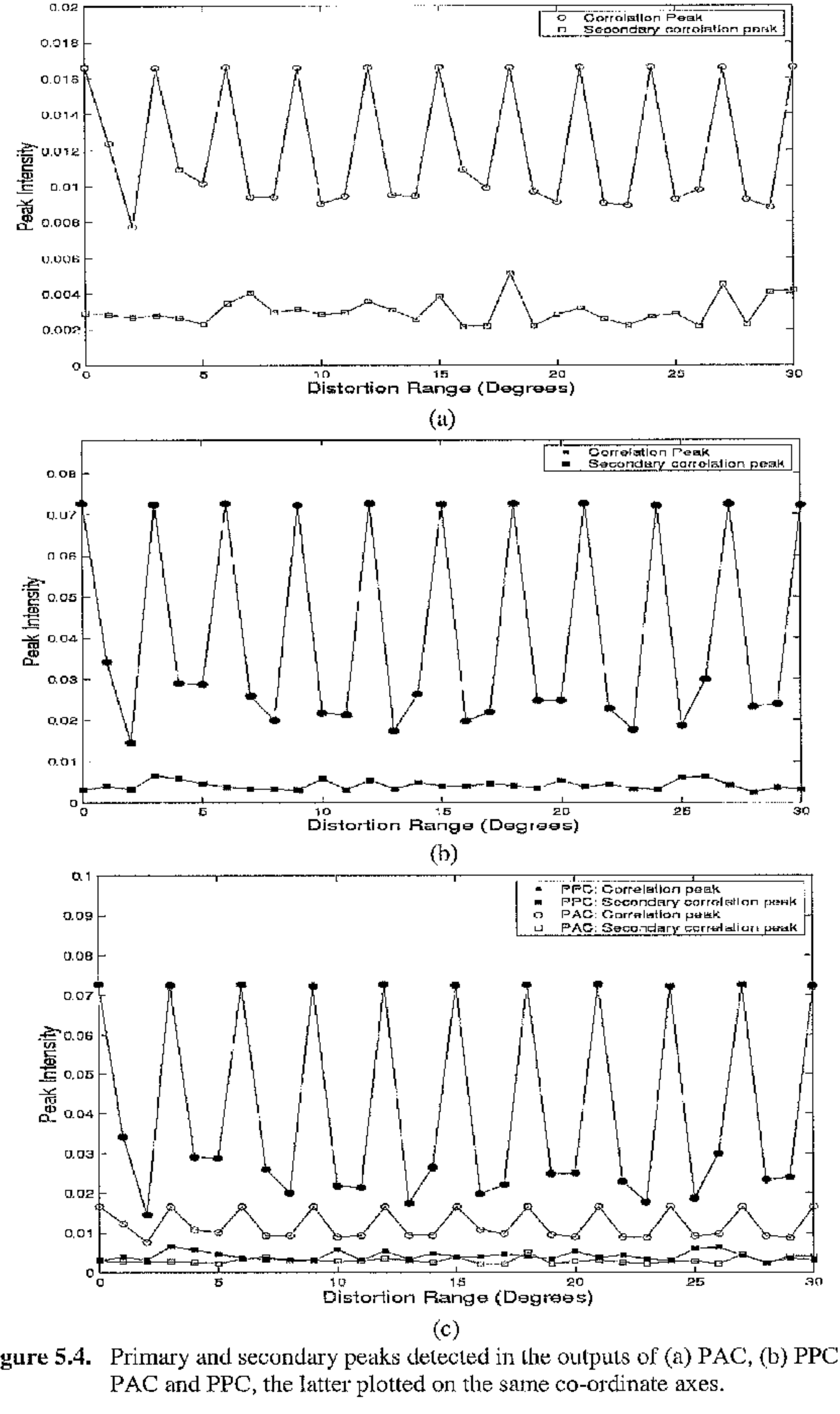

Figure 5.4. Primary and secondary peaks detected in the outputs of (a) PAC, (b) PPC and (c) PAC and PPC, the latter plotted on the same co-ordinate axes.

Amplitude modulation of the input image in the phase-amplitude case reduces the optical efficiency of the correlator and the intensities of the correlation peaks fall. A satisfactory separation of the envelopes containing the primary and secondary correlation peaks is maintained, however. The ratios of the intensities of these peaks for the worst case (the PSR_w, defined in article 2.5.5) were 2.19 and 1.53 for correlations of the phase-encoded SDF with the phase and amplitude encoded images, respectively.

5.3.2 Distortion Range

An increase in the range of the distortion encompassed by an SDF multiplies the volume of information that it must store. The effect on the performance in a correlator of the depth to which the SDF is encoded is examined herein.

Correlations of SDFs constructed with images at 3^0 intervals and interrogated with images spaced by 1^0 of rotation were simulated, with the range of the SDF being varied from 3^0 to 114^0 in 3^0 steps. The sequence started with the construction of an SDF with 0^0 and 3^0 rotated images. This was interrogated with in-class images presented successively to the correlator at distortion angles of 1^0, 2^0 and 3^0; the mean intensity of the correlation peaks detected was recorded. Successive calculations extended the distortion range by the addition to the training set of an image rotated by an additional 3^0.

Figure 5.5 plots the variation of the average intensity of correlation peaks with the range of distortion for phase-phase and phase-amplitude correlations. The ascendancy of PPC, measured in these terms, when the distortion range is less than 30^0 is confirmed; but the mean intensity is very sensitive to growth in the range and is not greatly differentiated from that of PAC as the range rises above 30^0. This is so because of the sensitivity of the high frequencies in the spectrum to rotation of the input image. The explanation is given in article 2.2.

This sensitivity to the span of distortion covered by the SDF constitutes a significant constraint on the utility of phase-phase correlation.

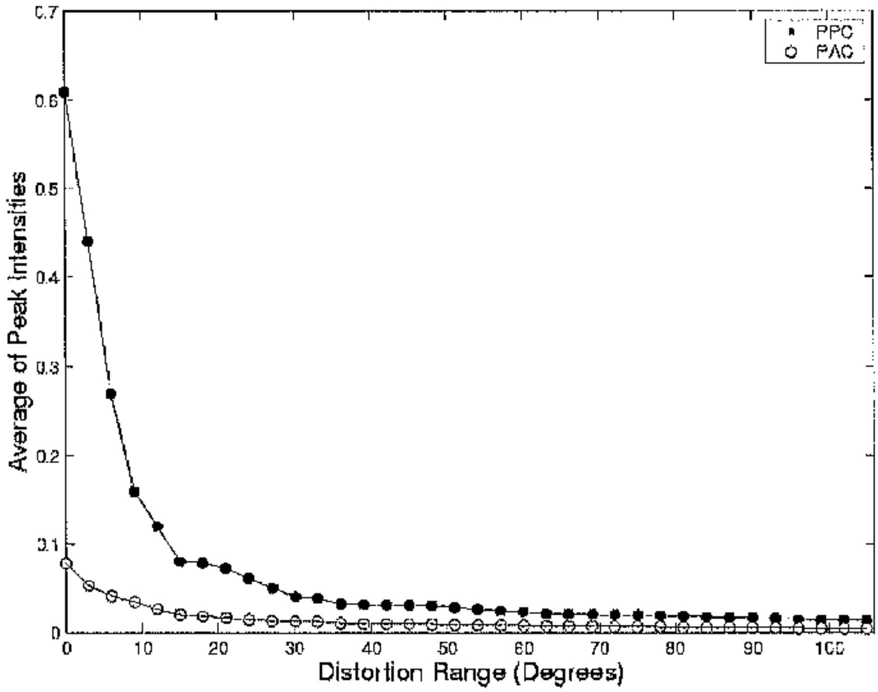

Figure 5.5. Variation of the average intensity of the correlation peak for PPC and PAC as the range of distortion increases from 3^0 to 105^0.

5.3.3 Discrimination of In-Class and Out-of-Class Objects

A figure of merit (*DC*) has been defined in article 2.5.4, which expresses the capacity for discrimination of an SDF filter. SDFs were synthesised from images of the Bradley APC, the in-class object, and the out-of-class M1 tank for the purpose of this evaluation.

Figure 5.6 demonstrates the generally higher level of discrimination achieved by phase-phase correlation. However, this correlation is the more sensitive of the two to the orientation of the image that interrogates the SDF. The highest *DC* values achieved are those corresponding to phase-phase auto-correlations of the SDF with member images of the in-class training set. The responses by PPC and PAC to images at intermediate distortions are not significantly different. PPC and PAC strongly reject out-of-class images. Figure 5.7 shows that the response of the correlations to out-of-class images is of low intensity and nearly constant amplitude across the entire range of distortion.

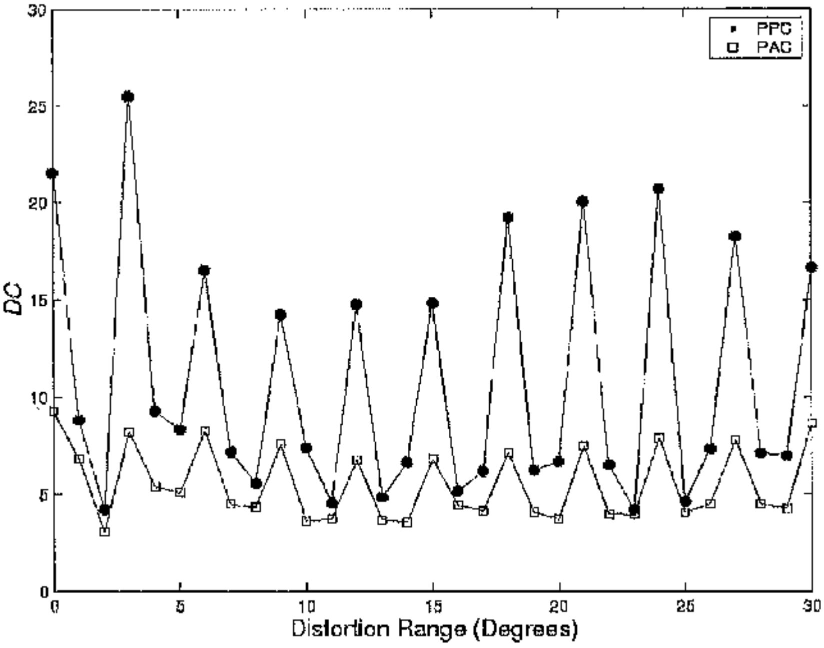

Figure 5.6. Discrimination capability (*DC*) of PPC and PAC with SDFs constructed for a distortion range of 30°.

The intensity fields in the output plane for PPC and PAC are illustrated in Figure 5.8 for in-class images and Figure 5.9 for out-of-class images. The in-class results correspond to auto-correlations with training set members and, therefore, exaggerate the differentiation of PPC and PAC. The average *DC*s are 15.65 for PPC and 5.71 for PAC. A CCD viewing the output field would detect these correlation responses equally well. The correlations are not differentiated by their responses to out-of-class images.

The lower transmittance of the amplitude encoded input image, causing a reduction of the intensity of the output of the correlation, is the primary factor differentiating PAC from PPC. The variation in the response of PAC to changes in the distortion of the input image is notably less than that which occurs in the case of PPC. The separation of the in-class and out-of-class responses, measured by the ratio of the mean values of the intensities of these responses, is around 2.3 for PPC and 1.6 for PAC. These separations are entirely sufficient for the purpose of discrimination of the images.

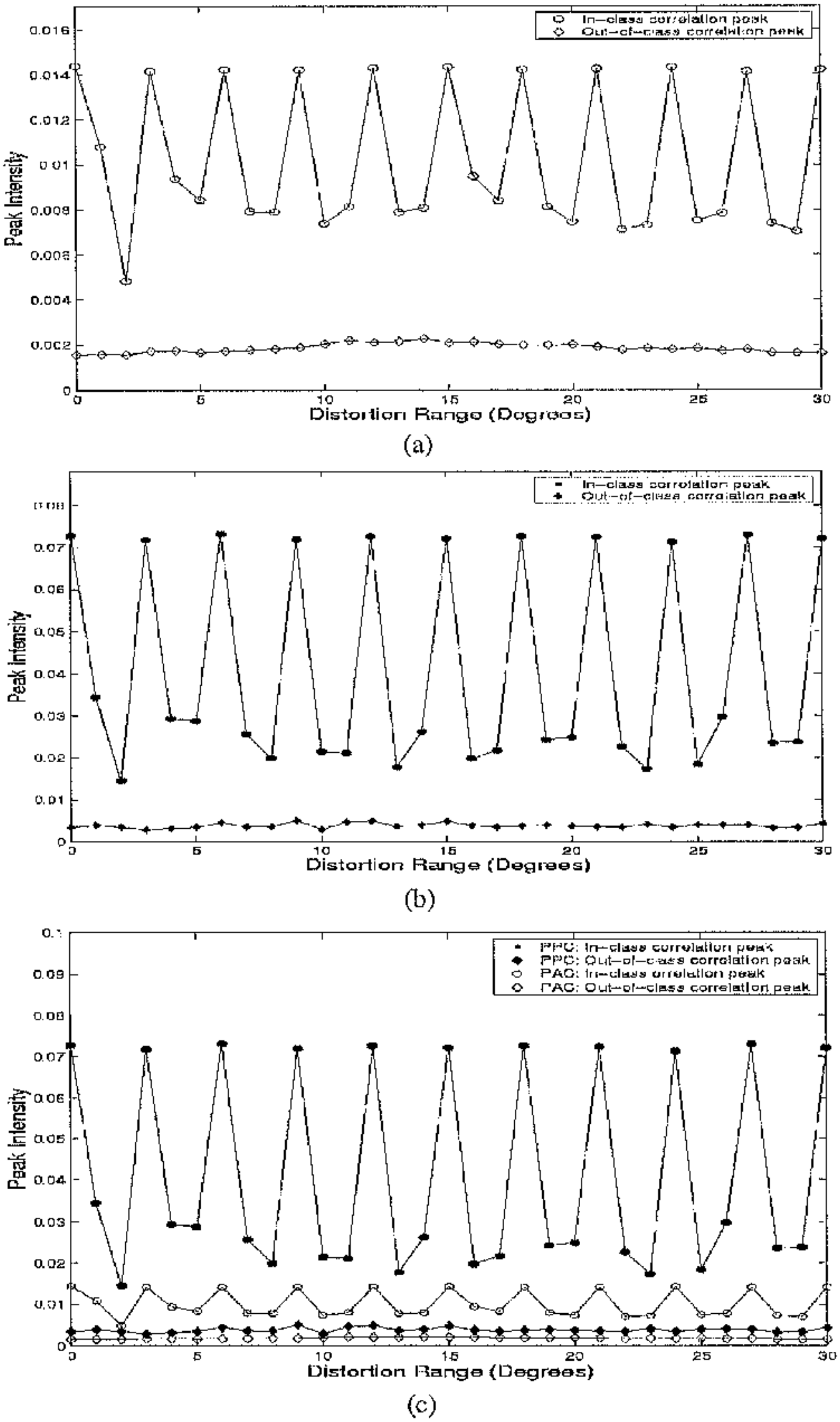

Figure 5.7. Peak intensity of the responses to in-class and out-of-class images by the (a) PAC, (b) PPC and (c) PAC and PPC, the latter plotted on the same coordinate axes.

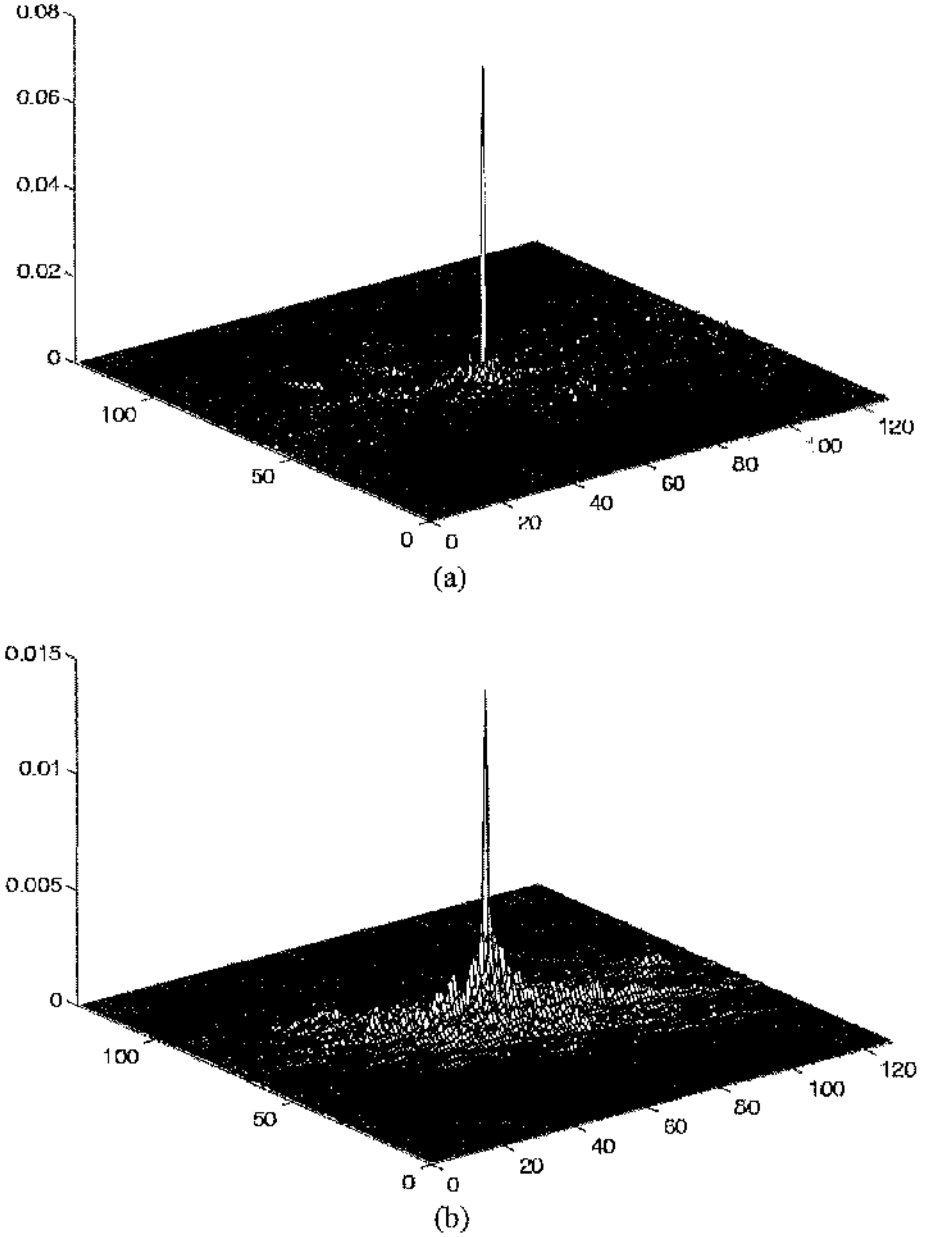

Figure 5.8. Intensity distributions in the correlation plane for (a) PPC and (b) PAC when SDFs constructed for a 30^0distortion range were interrogated by the basic in-class image rotated to a distortion of 15^0.

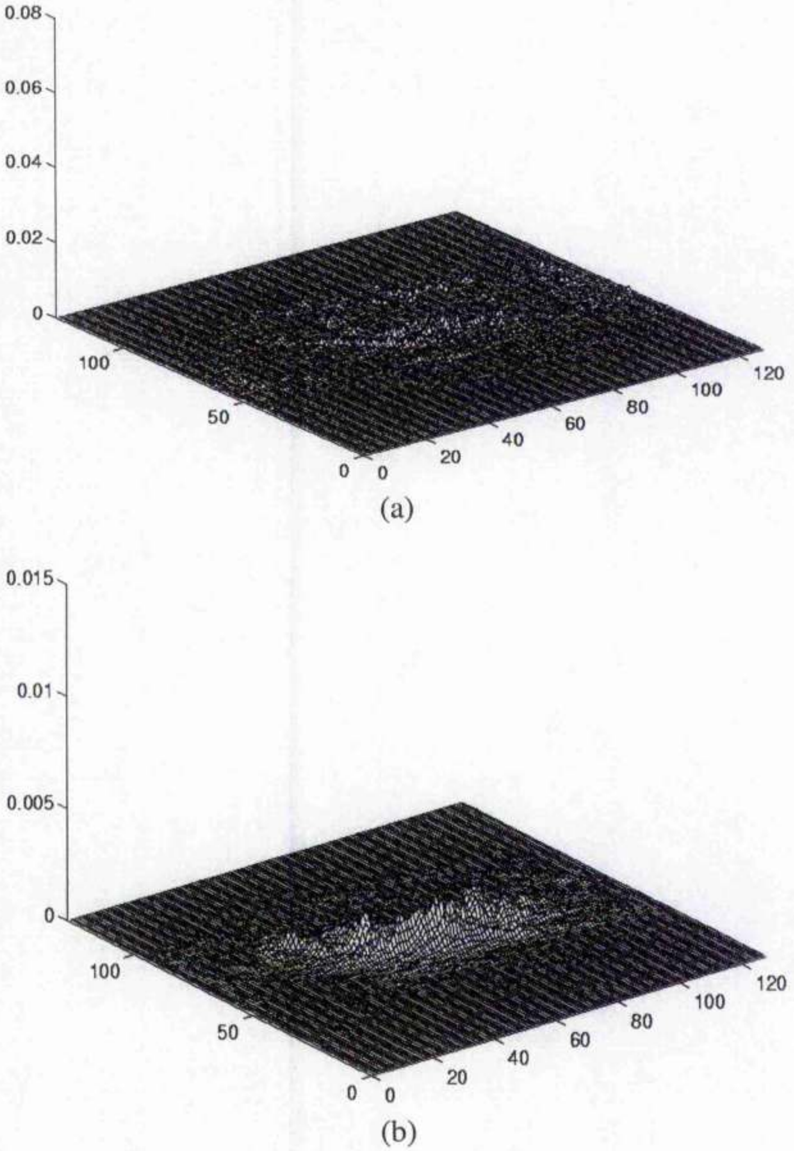

(a)

(b)

Figure 5.9. Intensity distributions in the correlation plane for (a) PPC and (b) PAC when SDFs constructed for a 30^0 distortion range were interrogated by the basic out-of-class image rotated to a distortion of 15^0.

5.4 CONSIDERATION OF REAL-TIME IMPLEMENTATION OF CORRELATING PHASE-ENCODED IMAGES

A liquid crystal television screen may be used as a spatial light modulator. A range of phase modulation exceeding 2π can be achieved[4] with minor attendant amplitude modulation. Figure 5.10 illustrates a real-time correlator using a single phase-modulating SLM[5] [6]. A digital electronic FFT board[7] computes the Fourier transform of the training set images and extracts the phase signature. The CCD camera captures the correlation output.

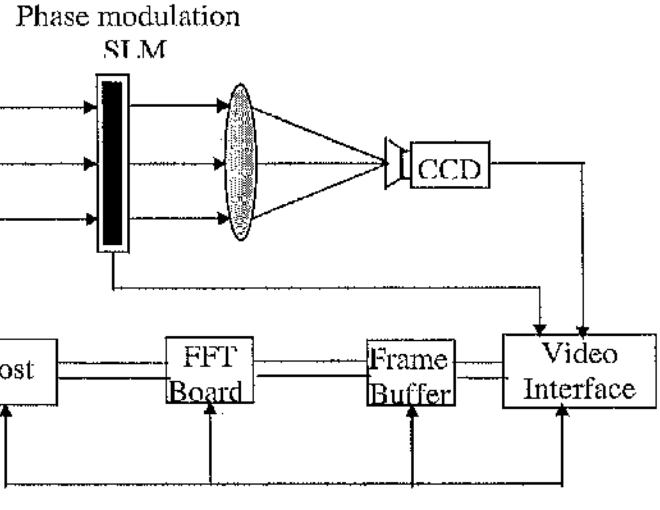

Figure 5.10. Correlation in real-time of phase-encoded images.

The 2-D fast Fourier transform (FFT) board may be hosted from a PC provided a high-bandwidth bus is employed to allow video rate communication between the processor board and frame store. The initial Fourier transform is performed digitally, and the phase-phase addition is calculated by PC.

5.5 CONCLUSIONS

The proposition that phase-phase correlation (PPC) is superior to phase-amplitude correlation (PAC) in correlators employing SDF filters to detect distortion of the input image has been evaluated.

The primary constraint affecting phase-amplitude correlation is the reduction of its optical efficiency, being the consequence of amplitude modulation in the representation of the input image. Otherwise, this correlator is less sensitive than is PPC to the resolution of the images constituting the training set and the range of distortion that is encompassed by the SDF. Furthermore, the variation of the intensity of the correlation peak with the distortion of the input image (the angular rotation in the case simulated) is smallest with PAC.

Phase-phase correlation is more readily adapted to the needs of real-time correlators. However, this case is shadowed by the known sensitivity of phase-encoded filters to noise impressed on the image of the input scene and introduced by elements of the correlator.

The general case for phase-phase correlation is not proved. Advantages might be won with PPC when the distortion range and resolution are restricted and the optical efficiency of the system is at a premium.

5.6 REFERENCES

[1] J. L. Horner and P. D. Gianino, "Applying the phase only filter concept to the synthetic discriminant function correlation filter," *Appl.Opt.* **24**, 851-855 (1985).

[2] D. Jared and D. Ennis, "Inclusion of filter modulation in the synthetic discriminant function construction," *Appl.Opt.* **28**, 232-239 (1989).

[3] R. K. Wang, C. R. Chatwin and M. Y. Huang, "Modified filter synthetic discriminant functions for improved optical correlator performance," *Appl.Opt.* **33**, 7646-7654 (1994).

[4] K. Ohkubo and J. Ohtsubo, "Evaluation of LCTV as a spatial light modulator," Opt.*Comm.* **102**, 116-124 (1993).

[5] R. Young, C. R. Chatwin and B. F. Scott, "High-speed hybrid optical/digital correlator system," *Opt.Eng.* **32**, 2608-2615 (1993).

[6] A. R. Pourzand and N. Collings, Brite EuRam II, Contract No. BRE2-CT93-0592, DR:RY1/TR/NCH/NC&ARP940620, DGXII-CEC-Brussels, 1-10 (1994).

[7] M. Duelli, A. R. Pourzand, N. Collings and R. Dandliker, "Pure phase correlator with photorefractive filter memory," *Optic.Letters.* **22**, 87-89 (1997).

CHAPTER 6

Cosine-Wave, Joint Transform Correlator

A cosine wave, joint transform correlator (CWJTC) is proposed, which responds robustly when the input image is corrupted by noise. This form of joint transform correlator (JTC) is similar to even-function correlation of the phase information in the spatial frequency spectra of the reference and input images. It resembles correlation of the phase information in the input image with a phase-encoded reference image, such as might occur in a Vander Lugt correlator. Simulated correlations demonstrate that the CWJTC is superior to a binary JTC that employs median thresholding when these correlators are presented with multiple targets. Furthermore, this superiority is sustained when the image is noisy and the contrast ratio of the target in the input scene is low. The correlator employs three CCDs to capture the power spectra of the joint input image, the reference image and the input scene. The cosine-wave element of the information contained in the joint power spectrum (JPS) is extracted using elementary subtraction and division operations.

6.1 INTRODUCTION

The JTC produces a strong zero-order peak in the output plane, being the superposition of the auto-correlations of the reference image and the input scene that overlaps the desired correlation signals[1]. In the case of a single noise-free image, the zero-order peak is some four times more intense than are the first order, matched correlation peaks. Noise in the input scene exacerbates this difficulty. Increasing the separation between the target and reference images to widen the separation of the zero and first orders raises the demand for spatial bandwidth placed on spatial light modulators (SLM) and detectors that the correlator might employ.

The binary JTC (BJTC) [2] relies upon a non-linearity in the Fourier plane to effect the transformation of the JPS to binary form. When compared with the classical JTC, the BJTC generates a narrower and more intense correlation peak and discriminates more strongly between similar objects. Furthermore, the spatial bandwidth required of the encoding devices is reduced. Higher harmonic terms may be present in the output plane, however, and cause false alarms. A translation to binary form applied in the Fourier plane is computationally demanding and reduces the processing speed[3]. To circumvent these difficulties a fringe-adjusted technique[5][6] has been designed that modifies the JPS prior to its inversion. Thereby, the higher harmonic terms are removed and the need to compute a thresholding function is avoided. The dynamic range of the modified JPS is increased, however, and exceeds the span of available SLM's. A cosine-wave technique, proposed herein, overcomes this difficulty.

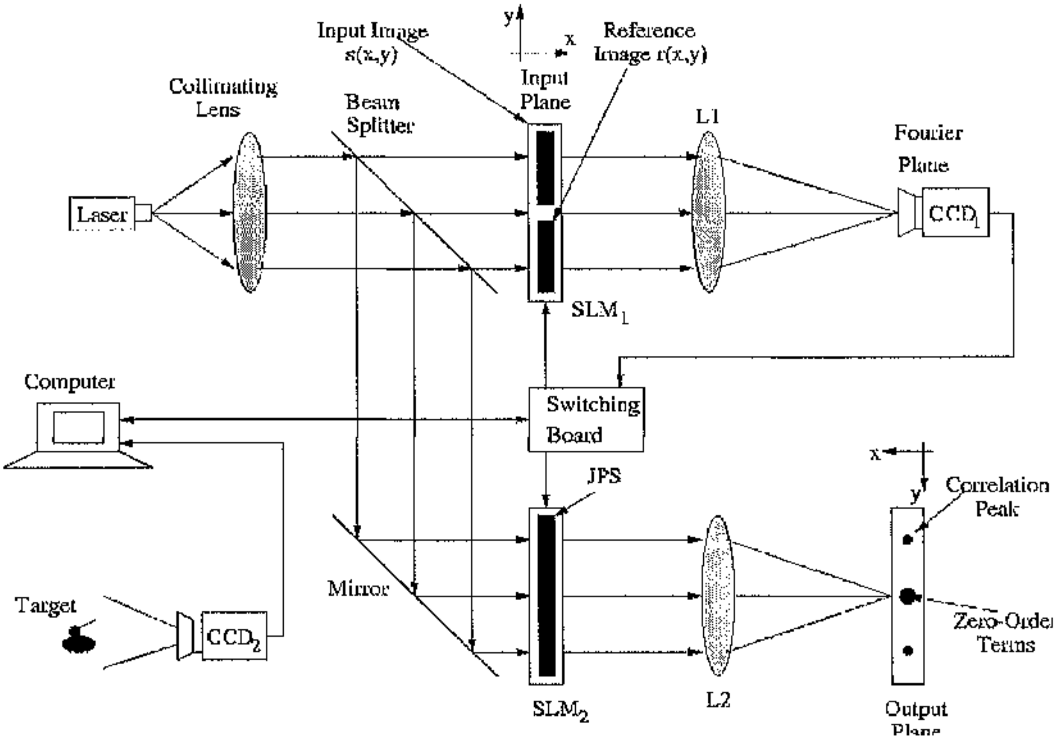

Figure 6.1. Schematic of a real-time JTC.

Simulations are described that present the CWJTC with complex input scenes containing multiple objects. These simulations demonstrate the detection of low contrast ratio objects that are embedded within scenes corrupted with either non-overlapping or additive noise.

6.2 ANALYSIS

A JTC capable of operating in real-time is shown in Figure 6.1. The reference and input images are encoded on single SLM_1 placed in the input plane. This joint image function $f(x,y)$ can be expressed as

$$f(x,y) = r(x+x_o, y+y_o) + s(x-x_s, y-y_s), \tag{6.1}$$

in which $r(x+x_o, y+y_o)$ and $s(x-x_s, y-y_s)$ denote the reference and input functions. Multiple objects $\sum_{i=1}^{k} t_i(x,y)$ may be present in the input scene[2][4] and the image of the scene is often degraded by noise $n(x,y)$. Additive noise may be introduced by image capturing devices or other elements of the system[5]; the scene may be degraded by non-overlapping background noise. When noise is included, the joint input image function is

$$f(x,y) = r(x+x_o, y+y_o) + \sum_{i=1}^{k} t_i(x-x_i, y-y_i) + n(x-x_n, y-y_n). \tag{6.2}$$

The Fourier transform of $f(x,y)$, formed at the back focal plane of lens L_1 (Figure 6.1), is:

$$\begin{aligned} F(u,v) &= R(u,v)exp[j(ux_o+vy_o)] + \sum_{i=1}^{k} T_i(u,v)exp[-j(ux_i+vy_i)] + N(u,v)exp[-j(ux_n+vy_n)] \\ &= R(u,v)exp[j(ux_o+vy_o)] + S(u,v)exp[-j(ux_s+vy_s)] \end{aligned} \tag{6.3}$$

Here, $R(u,v)$, $T_i(u,v)$, $N(u,v)$ and $S(u,v)$ are the Fourier transforms of $r(x,y)$, $t_i(x,y)$, $n(x,y)$ and $s(x,y)$ respectively; u and v are mutually independent spatial frequencies scaled by $2\pi/\lambda f$, λ being the wavelength of the Laser light, and f the focal length of the Fourier lenses L_1 and L_2. The JPS is the intensity of the (complex) light distribution produced in the back focal plane of L_1, viz.

$$\begin{aligned}
|F(u,v)|^2 =& |R(u,v)|^2 + |S(u,v)|^2 + 2|R(u,v)||S(u,v)|\,cos[u(x_0+x_s)+v(y_n+y_s)+\phi_r(u,v)-\phi_s(u,v)] \\
=& |R(u,v)|^2 + \sum_{i=1}^{k}|T_i(u,v)|^2 + |N(u,v)|^2 \\
&+ 2\sum_{i=1}^{k}|T_i(u,v)||R(u,v)|\,cos[u(x_0+x_i)+v(y_o+y_i)+\phi_i(u,v)+\phi_r(u,v)] \\
&+ \sum_{i=1}^{k}\sum_{j=1}^{k}|T_i(u,v)||T_k(u,v)|\,cos[u(x_i-x_k)+v(y_i-y_k)+\phi_i(u,v)-\phi_k(u,v)]\,. \quad (6.4) \\
&+ 2|N(u,v)||R(u,v)|\,cos[u(x_n+x_o)+v(y_n+y_o)+\phi_n(u,v)+\phi_r(u,v)] \\
&+ 2\sum_{i=1}^{k}|N(u,v)||T_i(u,v)|\,cos[u(x_n-x_i)+v(y_n-y_i)+\phi_n(u,v)-\phi_i(u,v)
\end{aligned}$$

The phase terms of the Fourier transforms $R(u,v)$, $T_i(u,v)$, $N(u,v)$ and $S(u,v)$ are $\phi_r(u,v)$, $\phi_i(u,v)$, $\phi_n(u,v)$, and $\phi_s(u,v)$, respectively, (with $i \neq j$). A square law detector, such as a CCD array, might be used to detect the JPS. In the classical JTC the inverse Fourier transform of the JPS is created by lens L_2. This yields: an auto-correlation of the reference image and auto-correlations of the input objects; cross-correlations of the reference image with the input objects, which include the desired signals; and cross-correlations of the different input objects and various noise terms. These last can produce false alarms.

In the median thresholding BJTC[2], the median applied is that of the histogram of intensities recorded in the pixel array upon which the JPS is mapped.

$$V_t = median[|F(u,v)|^2]\,. \tag{6.5}$$

The binary version of the JPS is

$$P_b(u,v) = \begin{cases} +1, & when\,|F(u,v)|^2 > V_t \\ -1, & otherwise \end{cases}. \tag{6.6}$$

The BJTC greatly improves the optical efficiency of the system, for the transmission is unity everywhere in the input plane of the second optical system. However, cross-correlations of images in the input scene remain in the output and may cause false alarms; the zero-order terms persist and continue to mask the desired output signals[5]. Furthermore, the binary transform generates deleterious higher-order harmonics in the output plane. Javidi *et al*[4] developed a thresholding function to control the unwanted correlations. However, the harmonic terms persist in the output.

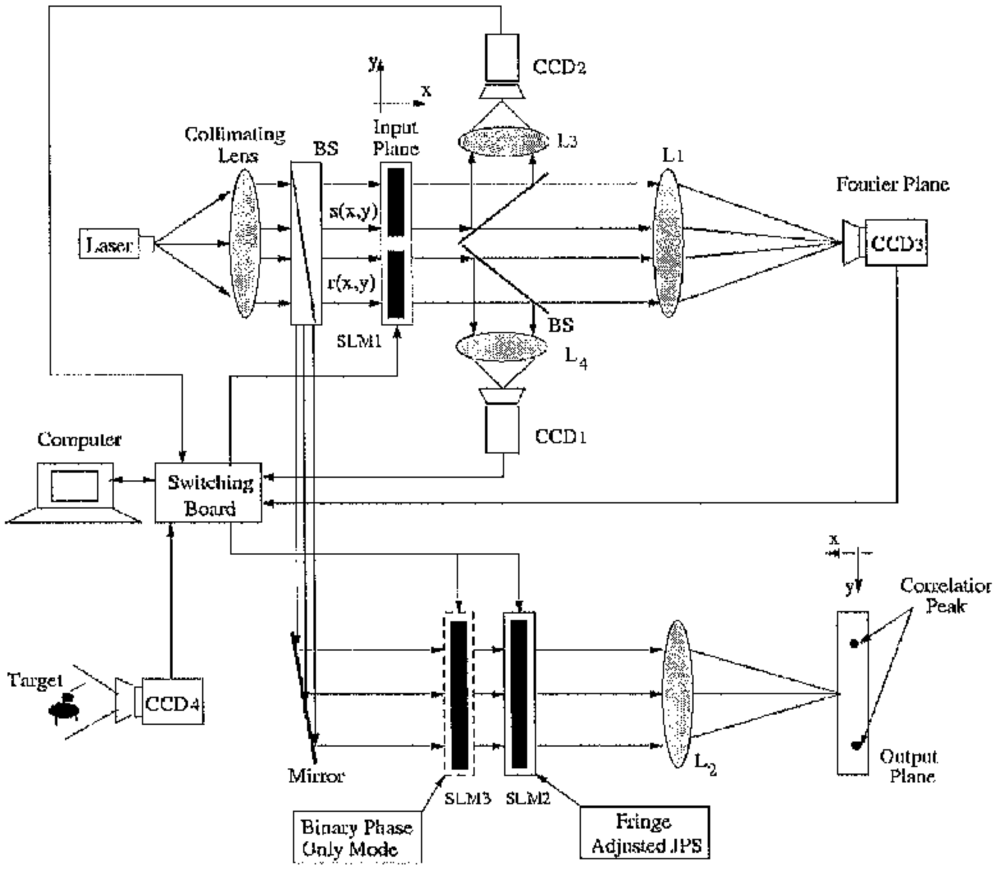

Figure 6.2. An alternative real-time JTC architecture.

The fringe adjusted architecture shown in Figure 6.2 has the capacity to eliminate the zero-order terms, the results of cross-correlations between the different input objects and control the effects of noise. Three separate CCDs are employed to capture the joint transform power spectrum (CCD_3), the power spectrum of the input scene (CCD_2) and the power spectrum of the reference image (CCD_1). The result of subtracting the power spectra of the input scene and the reference image from the JPS is:

$$\begin{aligned}P(u,v) &= |F(u,v)|^2 - |R(u,v)|^2 - |S(u,v)|^2 \\ &= 2\,|R(u,v)||S(u,v)|\,cos[u(x_o + x_s) + v(y_o + y_s) + \phi_r(u,v) - \phi_s(u,v)] \\ &= 2\sum_{i=1}^{k} |T_i(u,v)||R(u,v)|\,cos[u(x_o + x_i) + v(y_o + y_i) + \phi_i(u,v) + \phi_r(u,v)] \\ &\quad + 2\,|N(u,v)||R(u,v)|\,cos[u(x_n + x_o) + v(y_n + y_o) + \phi_n(u,v) + \phi_r(u,v)]\,. \end{aligned} \tag{6.7}$$

This modified power spectrum is recorded on SLM_2, which generates the correlation signal. It can be shown[5] that the zero-order terms and the cross-correlations formed between the different objects are removed from the output and that the deleterious effects of noise may be reduced. This scheme provides for the reference image to be up-dated in real time. However, the broad correlation peaks generated make it difficult to separate the outputs corresponding to similar objects present in the input scene. Neither can the large dynamic range of the modified power spectrum be readily accommodated by available SLM's,

A cosine-wave encoded JTC is proposed to overcome these problems inherent to the fringe-adjusted JTC scheme, The modified power spectrum in the case of the CWJTC is

$$C(u,v) = cos[u(x_o + x_s) + v(y_o + y_s) + \phi_r(u,v) - \phi_s(u,v)]. \tag{6.8}$$

Thus, the cosine terms alone of Equation 6.7 are retained. A division of the modified JPS by the product of the amplitudes of the Fourier spectra of the reference image and the input scene is necessary, i.e.

$$\frac{P(u,v)}{(|R(u,v)| + \varepsilon_1)(|S(u,v)| + \varepsilon_2)} \approx 2C(u,v). \tag{6.9}$$

In this result, ε_1 and ε_2 are introduced to eliminate the occurrence of poles in the evaluation of Equation 6.9. They may be made functions of the spatial frequency and differentially weight the spectra of $R(u,v)$ and $S(u,v)$. The CWJTC can be realised optically, for this function is real-valued and the optical gain is less than unity.

It is evident from Equation 6.7 that the CWJTC is equivalent to an even function correlation the Fourier phase of the reference and input images, for

$$\mathcal{F}\{exp[j(\alpha+\beta)]\} = \mathcal{F}\{cos(\alpha+\beta)\} + j\,\mathcal{F}\{sin(\alpha+\beta)\}, \tag{6.10}$$

in which $\mathcal{F}$ refers to the Fourier transform operation. Nearly 50% of the light incident on the filter is transmitted and, being a real function, the cosine-waveform is implemented more easily than is the "phase-only" filter[7]. The correlation of phase representations of images in a Vander Lugt configuration depends upon digital computation for the extraction of the phase components of the input scene.

When an object in the input scene coincides with the reference image, i.e. when $\phi_s(u,v) = \phi_r(u,v)$, the effect of the CWJTC is to invert the Fourier transform of the cosine- wave, viz. of $cos[u(x_o + x_s) + v(y_o + y_s)]$, which function is determined by the spacing of the reference and input images alone. Two delta functions are generated in the output plane, spaced apart by a distance $2\sqrt{(x_o + x_s)^2 + (y_o + y_s)^2}$. If the input scene contains several objects that match the reference image, these objects will generate a pair of delta functions in the output. These several outputs will appear in the correlation plane, separated by distances proportional to the magnitude of the displacements of the objects in the input scene relatively to the position of the reference image.

When targets matching the reference image are embedded in non-overlapping or additive noise, Equation 6.8 becomes

$$\begin{aligned} C(u,v) &= \cos[u(x_o + x_s) + v(y_o + y_s) + \phi_r(u,v) - \phi_s(u,v)] \\ &= \frac{|T(u,v)|}{|S(u,v)|}\cos[u(x_o + x_t) + v(y_o + y_t)] + \\ &\frac{|N(u,v)|}{|S(u,v)|}\cos[u(x_o + x_n) + v(y_o + y_n) + \phi_n(u,v) + \phi_r(u,v)], \end{aligned} \tag{6.11}$$

(x_i, y_i) are the co-ordinates of the i$^{\text{th}}$ target in the input plane. The first term produces the delta function responses, which identify the object. Since the phases $\phi_n(u,v)$ and $\phi_r(u,v)$ are randomly distributed, the output due to the second term is random. This is so, because the Fourier transform of a random function is itself a random function retaining the energy of the original function. As a result, the power appearing in the output due to noise impressed on the input scene will be of relatively low amplitude, for it is distributed randomly across the entire output field.

The JPS described in Equation 6.11 may contain negative values, which cannot be encoded by SLM_2. To circumvent this difficulty a phase modulating SLM operating in the binary mode, is introduced (SLM_3) to apply the modulation:

$$G(u,v) = \begin{cases} +1, & C(u,v) \geq 0 \\ -1, & \text{otherwise} \end{cases} . \tag{6.12}$$

Amplitude modulation by SLM_2, accords with the conditions:

$$C^{'}(u,v) = \begin{cases} C(u,v), & C(u,v) \geq 0 \\ -C(u,v), & \text{otherwise} \end{cases} . \tag{6.13}$$

Thus, SLM_3 introduces a 180^0 phase shift and guarantees thereby that SLM_2 is always presented with positive inputs.

6.3 RESULTS OF SIMULATIONS

The performance of the cosine-wave encoded JTC was investigated for the case of scenes corrupted with either non-overlapping noise or additive noise and containing a single target object. The ε_i in Equation 6.9 were set equal to 1×10^{-6}. A simulation was conducted with a median thresholding BJTC for the purposes of a comparison.

The intensity of the correlation peak (*CPI*), the ratio of the intensities of the correlation peak and that of the secondary peak detected (*PSR*), the area of the correlation peak evaluated on its half-peak intensity profile (*FWHM*) and the ratio[8] of the intensity of the correlation peak to that of the noise (*PNR*) were the assessment criteria.

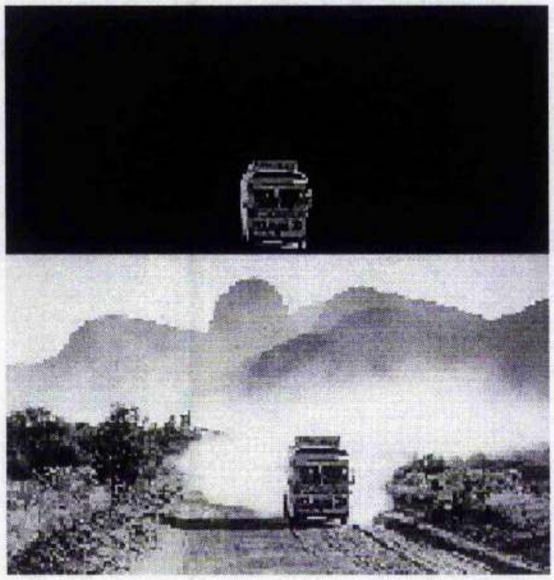

Figure 6.3. An arbitrary scene corrupted with non-overlapping noise. The bus is the target object; the reference image is recorded in the upper half of the frame.

Figure 6.3 shows a bus standing in an arbitrary scene, which is corrupted by non-overlapping noise. The scene is represented in a rectangular array of 128×192 pixels; the reference image occupies 25×32 pixels. The joint image was padded with zeros to fill a frame size of 256×256 pixels. The power transmitted by the image of the bus is 1.2% of the total power transmitted by the scene.

Figure 6.4 represents the output for a classical JTC when presented with this scene. As was forecast, the correlation with the target image is obscured completely by the effects of noise. Results such as this have engendered the search for more satisfactory solutions, such as the BJTC.

In comparing the performances of the median thresholding binary JTC and the cosine-wave JTC, it proved instructive to observe the forms of the modified joint power spectra that these options generated. It is evident from Figure 6.5 that the fringe information is distributed uniformly across the entire field of the JPS in the case of the cosine-wave scheme. Distributions such as this favour the generation of sharp peaks in the correlation plane. In contrast, the loss of information intrinsic to binary correlation is evident in Figure 6.6, which displays the markedly non-uniforms JPS that this method generated. The zero-order term is in evidence.

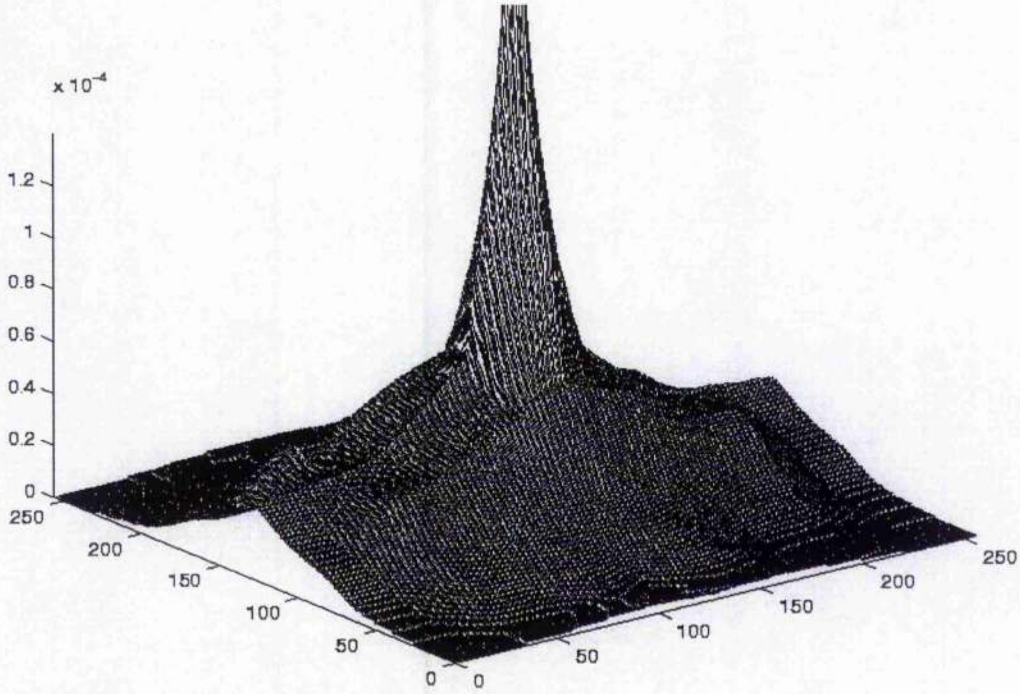

Figure 6.4. Intensity distribution in the output plane of a classical joint-transform correlator presented with the scene recorded in Figure 6.3.

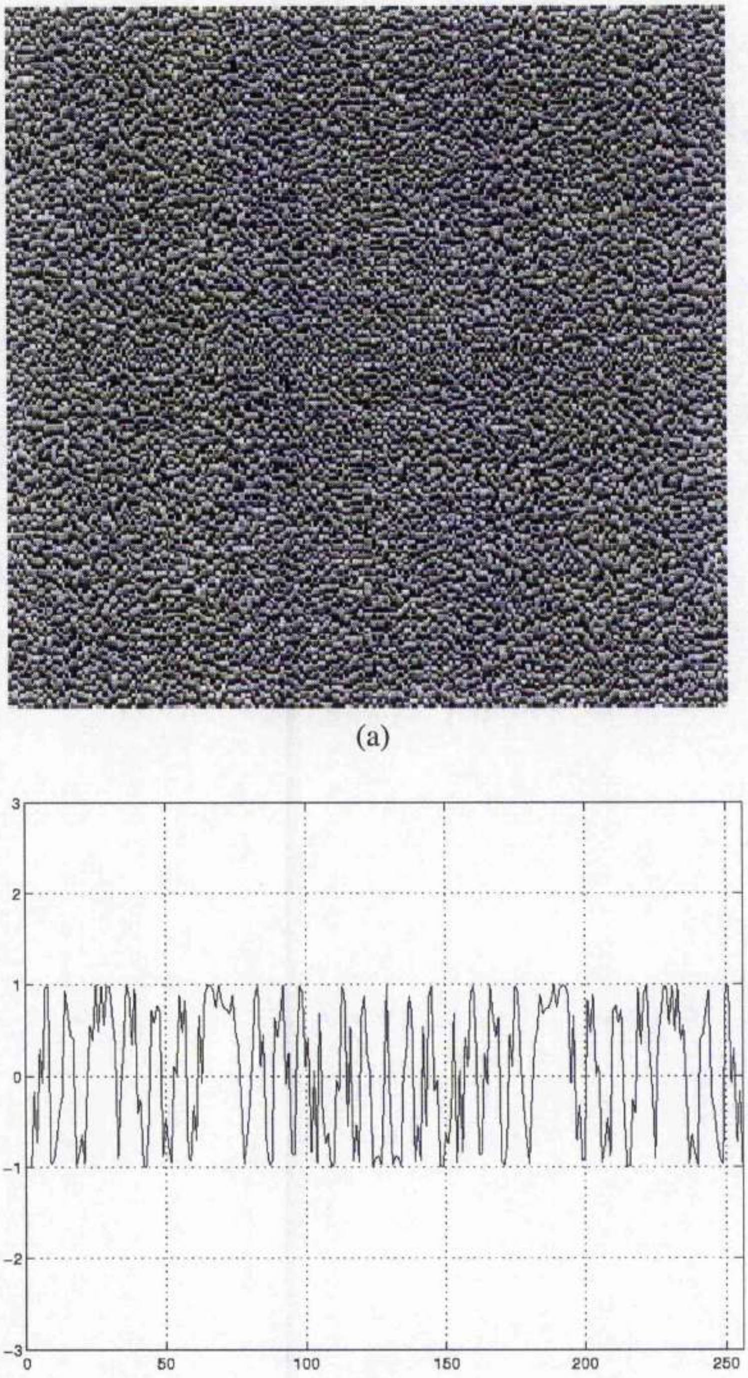
(a)

(b)

Figure 6.5. Joint power spectrum (a) created by a CWJTC and (b) a representative cross-section taken through the spectrum.

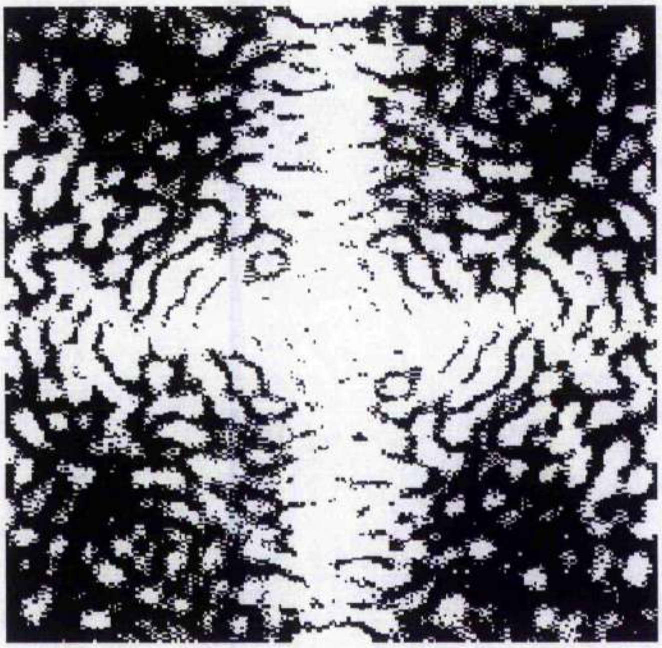

Figure 6.6. Joint power spectrum created by a median thresholding BJTC.

Correlations corresponding to these spectra are illustrated in Figures 6.7(a) and 6.7(b). The target vehicle is identified unequivocally by the cosine-wave scheme, which, as was predicted, provides a pair of sharply defined correlation peaks standing in a low amplitude field of background noise (*PNR* of 10). In representing the binary device, it was necessary first to truncate the high amplitude zero-order peak that this system generates. There being less power available to supply them, the intensities of the correlation peaks were less by nearly an order of magnitude than those generated by the CWJTC. Table 6.1 represents the performance of the correlators in terms of the assessment criteria defined earlier.

Table 6.1. Performances of the cosine-wave and median thresholding binary correlators, detecting the bus in the scene depicted in Figure 6.3.

	CPI	*PSR*	*PNR*	*FWHM*
CWJTC	419.53	15.27	862.55	1
BJTC	64.61	8.05	64.74	1

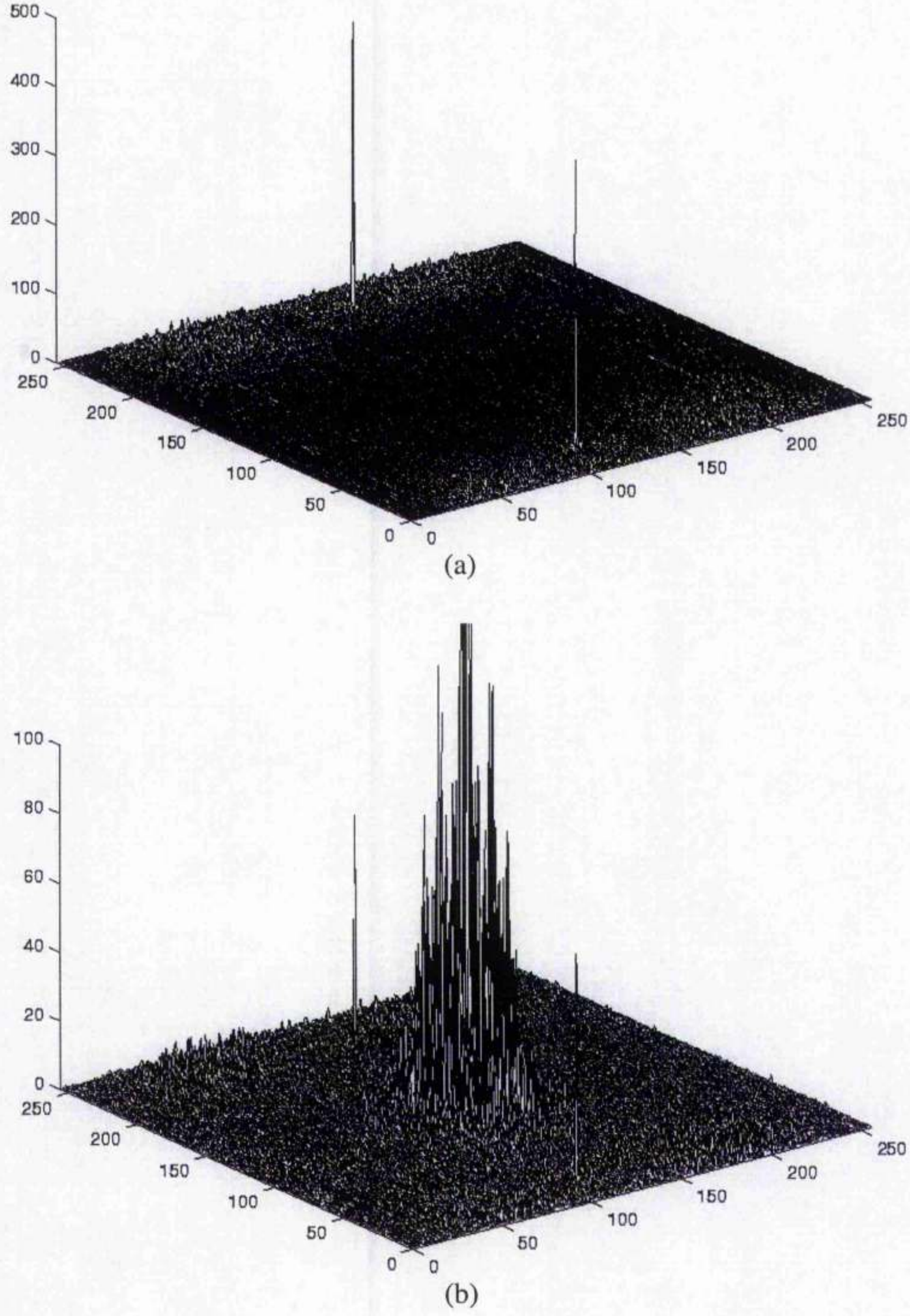

(a)

(b)

Figure 6.7. The CWJTC (a) and the median thresholding BJTC (b), detecting the bus in the scene depicted in Figure 6.3.

Realistic scenes contain multiple objects standing in cluttered or otherwise confused backgrounds. Recorded in Figure 6.8 is one such scene that includes two target aircraft and several non-target objects and is corrupted by non-overlapping noise. The transmission of light by the target images is 0.65% of the transmission by the entire scene.

Correlations of this scene with a reference image of the aircraft made with the CWJTC and median thresholding BJTC are represented in Figure 6.9(a) and (b). The former generates two Pairs of sharply defined correlation peaks, standing in a low noise amplitude floor; the non-target objects have been rejected. The output field generated by the BJTC includes the required correlations peaks, but is cluttered with secondary peaks and dominated by the power in the low-order terms.

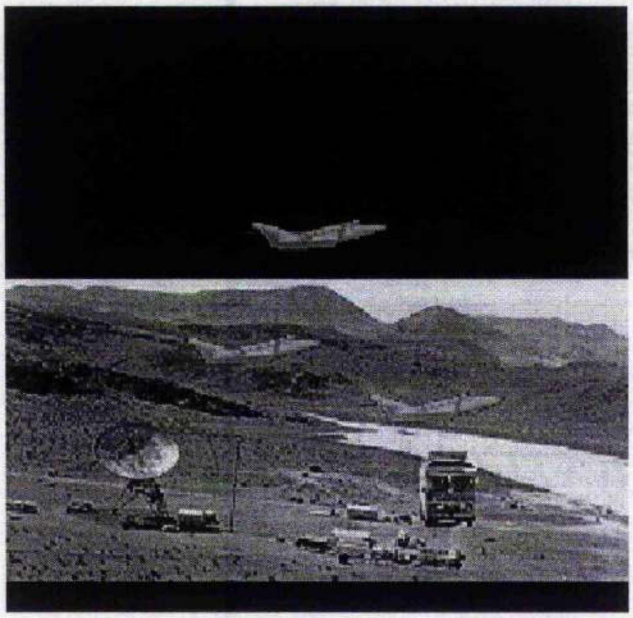

Figure 6.8. A complex scene that includes two target aircraft and other objects and which is corrupted by non-overlapping noise. A reference image of the aircraft is shown in the upper half of the frame.

Table 6.2 represents the performance of the correlators in terms of the assessment criteria. The response by the CWJTC discriminates between the aircraft by allocating a 50% higher peak intensity to the left-hand aircraft. An explanation is to be found in the proximity of the right-hand aircraft to the river and the reduced contrast ratio that this might cause. Nonetheless, the intensity of the correlation peak for this aircraft exceeds that of the worst secondary peak by a factor of two; the corresponding *PNR* is better than two orders of magnitude.

The median thresholding BJTC must be adjudged unsatisfactory in this duty. Whilst the desired correlation peaks are sharply defined, a detector viewing the entire output plane would not readily distinguish them from amongst the greatly more intense peaks that abound in the field.

Table 6.2. Performance of the cosine-wave and median-thresholding binary correlators, detecting the aircraft in the scene depicted in Figure 6.8. (The *MSI* is the maximum of the side-lobe peak intensities.)

	Left-hand aircraft			Right-hand aircraft			
	CPI	*PNR*	*FWHM*	*CPI*	*PNR*	*FWHM*	*MSI*
CWJTC	81.06	162.70	1	54.37	109.13	1	27.18
BJTC	29.23	29.28	1	26.67	26.72	1	16.62

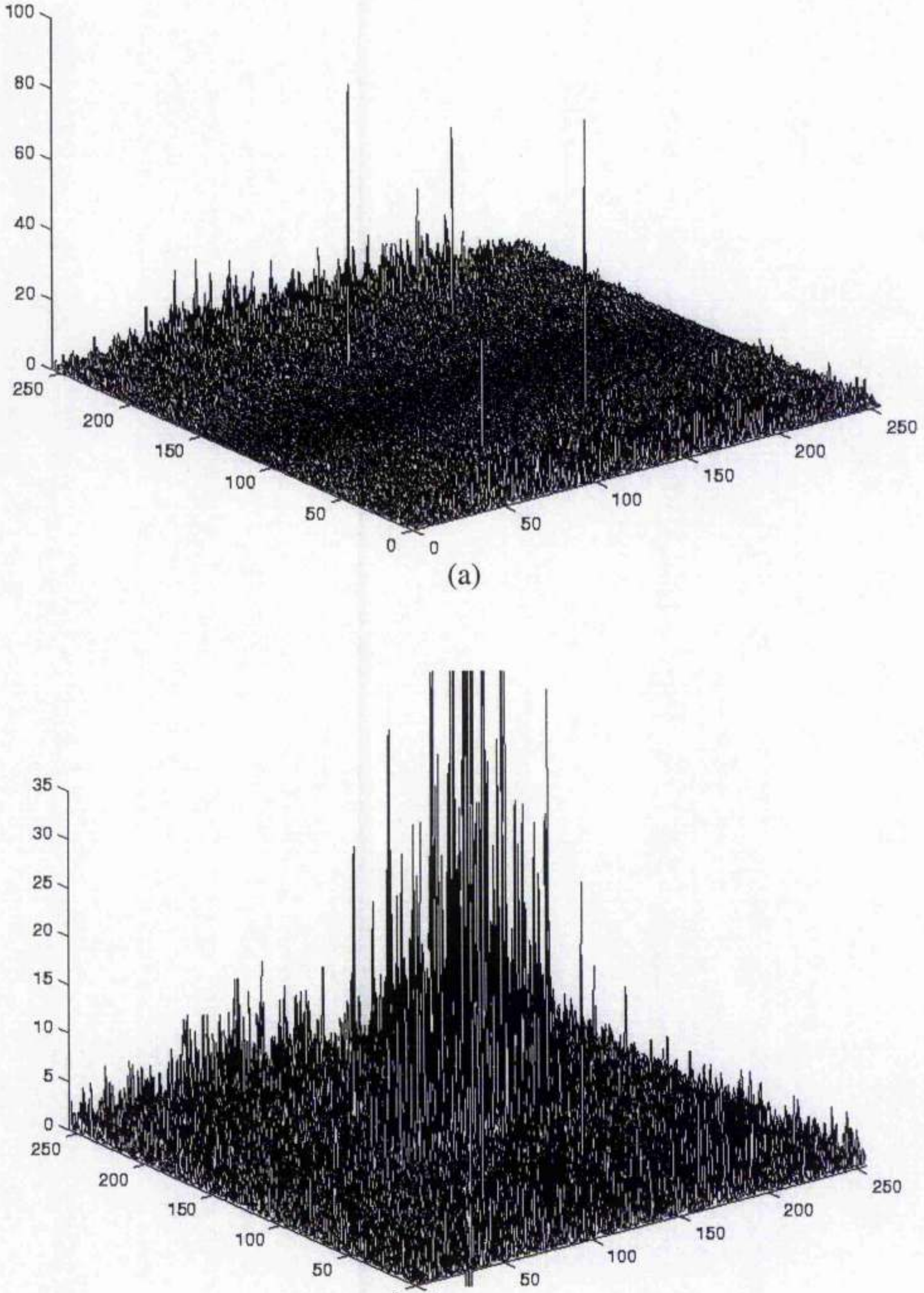

(a)

(b)

Figure 6.9. The CWJTC (a) and the median thresholding BJTC (b), detecting the target aircraft in the scene depicted in Figure 6.8.

Simulations were conducted to assess the impact of additive noise impressed on scenes presented to the correlators. A scene containing three similar objects, depicted in Figure 6.10, was prepared for this purpose. The power transmitted by the target image was 7.7% of that transmitted by the entire scene.

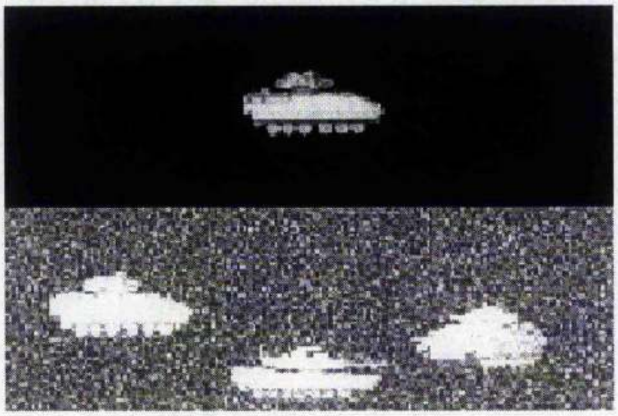

Figure 6.10. A scene including multiple objects and corrupted by additive noise to an SNR_I of 0.21. The target object is identified in the reference image recorded in the upper half of the frame.

Figure 6.11 demonstrates the superiority of the CWJTC in undertaking this task: the correlator rejects the near-class images and accommodates noise excellently, achieving a *PNR* of 500:1. Table 6.3 compares the performances of the correlators in terms of the assessment criteria. The *PSR* of 6.23 allocated to the BJTC takes no account of the low-order peaks in the output and, as Figure 6.11(b) demonstrates, exaggerates the correlator's performance.

Table 6.3. Performance of the cosine-wave and median-thresholding binary correlators, detecting the reference vehicle in the scene depicted in Figure 6.10.

	CPI	*PSR*	*PNR*	*FWHM*
CWJTC	230.50	14.35	467.68	1
BJTC	84.03	6.23	84.27	1

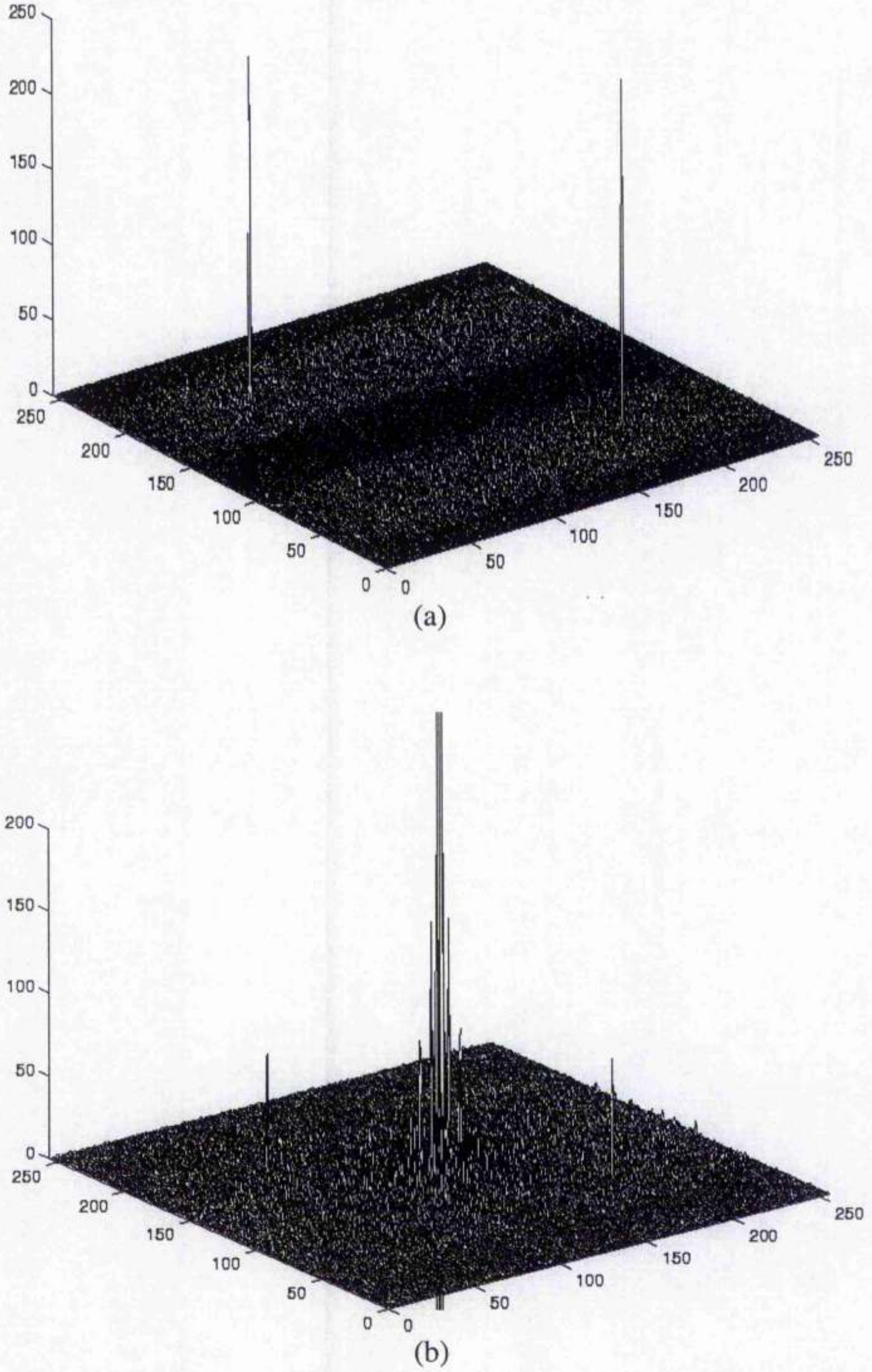

(a)

(b)

Figure 6.11. The CWJTC (a) and the median thresholding BJTC (b), detecting the reference vehicle in the scene depicted in Figure 6.10.

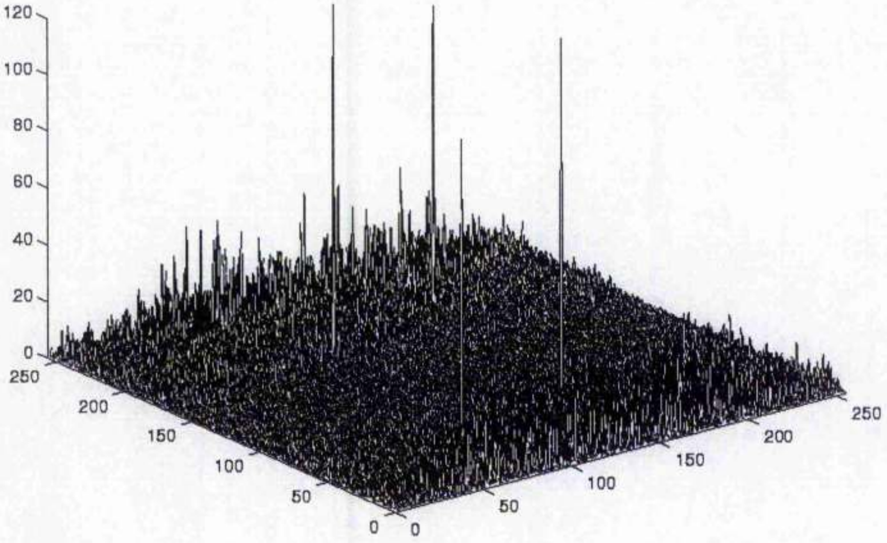

Figure 6.12. The thresholding function BJTC, detecting the target aircraft in the scene depicted in Figure 6.8.

In all of the correlations simulated, the BJTC generated sharply defined correlation peaks that identified the target objects. The difficulty encountered was that these peaks were overwhelmed by low-order peaks and could not be discriminated readily by a detector viewing the entire output field. The thresholding function[4] that has been developed provide for the elimination of this peak. Therefore, the response of a thresholding function BJTC correlating the image depicted in Figure 6.8 was simulated. The result recorded in Figure 6.12 is to be compared directly with the correlations illustrated in Figure 6.9. Binary transformation by the application of a thresholding function signally improves the performance of the binary JTC. The near 100% optical efficiency of the BJTC produces a high proportion of the incident power into the correlation peaks. The intensities of the peaks corresponding to the left-hand and right-hand aircraft are 125 and 107, respectively, and greatly exceed the intensities achieved by the cosine-wave scheme. The ratios of the intensities of the primary and secondary peaks are comparable for both schemes, as are the worst-case *PNR*s of 109 and 108 achieved by the CWJTC and BJTC respectively.

The action of the thresholding function is equivalent to a binary transformation of the cosine-wave modified JPS with respect to the zero level. This form of BJTC does not therefore utilise the entire fringe information of the unmodified JPS and may be made the more susceptible to noise. The simulation reported here is insufficient and, therefore, is inconclusive in this matter.

Thresholding function is frequency dependent, the thresholding process rely on the auto-correlation of reference image and joint scene. It certainly has flexible advantage over the median-thresholding JTC, which the thresholding value is fixed on obtained joint power spectrum.

6.4 CONCLUSIONS

A scheme has been devised that extracts the cosine-wave element of the joint power spectrum generated in a JTC and returns this element alone to the correlator for inversion. The gains in prospect were that the cosine-wave JTC (CWJTC) might detect target images with greater finesse than does the binary JTC (BJTC) and be less affected by noise in the input scene. The method adopted subtracts the power spectra of the reference image and the input scene from the joint power spectrum and normalises the result with respect to the product of these spectra. The outcome is a cosine-wave of which the argument is proportional to the displacement of the target with respect to the reference in the joint input image.

A pair of delta functions, standing displaced from the origin in the correlation plane, signals the detection of a target object. Noise affecting the input image is returned, randomly distributed across the entire correlation plane.

Simulations were conducted to assess the performance of the CWJTC. The input scenes employed contained multiple instances of target and other objects represented in realistic backgrounds. These scenes were corrupted by additive or non-overlapping noise, appropriately.

Sharply defined correlation peaks were generated in all of the simulations performed. The ratio of the intensity of the correlation peak to that of the worst secondary peak detected always exceed 10^1. Depending upon the number of target images detected, the ratio of the intensity of the correlation peak to the mean intensity of noise in the correlation plane (*PNR*) varied in the range 10^2 to 10^3. The cosine-wave, joint transform correlator detected multiple targets, standing with low contrast ratios in confused scenes, unequivocally and demonstrated its capacity to discriminate against near-target objects.

These simulations were repeated with a median thresholding, binary JTC. This scheme does not remove the zero-order peak that dominates the output of the classical JTC. The presence of this peak confuses the detection of the desired correlation signals i.e., of the first-order terms. Nonetheless, though the *PNR* never exceeded 10^2, clear correlation peaks were evident in all simulations.

In light of this result, a single simulation was conducted with a thresholding function BJTC. The input scene contained two target objects standing in a complex background and was corrupted by non-overlapping noise. The performance of this variant BJTC matched that achieved by the CWJTC. That the binary correlator might be the more sensitive to noise requires investigation.

6.5 REFERENCES

[1] F. T. S. Yu, Q. W. Song, Y. S. Cheng, and D. A. Gregory, "Comparison of detection efficiencies for VanderLugt and joint transform correlators," *Appl.Opt.* **29**, 225-232 (1990).

[2] B. Javidi, and J. Wang, "Binary joint transform correlation with median and sub-median thresholding," *Appl.Opt.* **30**, 967-976 (1991).

[3] J. A. Davis, E. A. Merrill, D. M. Cotrell and R. M. Bunch, "Effects of sampling and binarization in the output of the joint transform correlation," *Opt.Eng.* **29**, 1094-1100 (1990).

[4] B. Javidi, J. Wang, and Q. Tang, "Multi-object binary joint transform correlation using multiple-level thresholding crossing," *Appl.Opt.* **30**, 4234-4244 (1991).

[5] R. K. Wang, L. Shang, and C. R. Chatwin, "Modified fringe-adjusted joint transform correlation to accommodate noise in the input scene," *Appl.Opt.* **35**, 286-296 (1996).

[6] M. S. Alam, and M. A. Karim, "Fringe-adjusted joint transform correlation," *Appl.Opt.* **32**, 4344-4350 (1993).

[7] J. L. Horner, and P. D. Gianino, "Phase-only matched filtering," *Appl.Opt.* **23**, 812-816 (1984).

[8] J. L. Horner, "Metrics for assessing pattern recognition performance," *Appl.Opt.* **31**, 165-166 (1992).

CHAPTER 7

Conclusions

Simulations of optical correlators locating target objects in noisy scenes and recognising them have informed the design of the spatial frequency filters that they employ to represent the reference image.

Band pass and spatial frequency dependent weighting functions have been applied to the amplitude component of the spatial frequency spectra of matched reference filters. The aim was to raise the acuity of the discrimination achieved between closely similar objects and the finesse with which target objects may be located in the input scene. The challenge is to sustain the quality of the correlation when optical noise degrades the input scene.

A filter was constructed on a superposition of Gaussian form, high band-pass and low band-pass filters with which the susceptibility of the quality of the correlation to modulations impressed on the frequency spectrum of the reference filter could be explored. The criterion defining quality included measures of the correlation peak and its intensity, the signal to noise ratio and optical efficiency. A numerical scheme was devised which maximised the quality of the correlation by varying the four parameters which characterised the filter. The primary effect of the optimal filter, so determined, was to cut a narrow band of frequencies centred on the zero order. Most physical bodies and manufactured artefacts generate spatial frequency spectra with very large amplitudes at and around the zero order. Therefore, the effect of this sharp cut was to magnify the amplitude of the higher frequency spectrum substantially and, equivalently, to emphasise the contribution by phase modulation to the correlation output. However, the filter's susceptibility to noise was sensitive to the width of the zero order cut; the response of an entirely phase modulated representation of the filter was greatly affected by noise.

That the low frequency cut profile might be represented by a single parameter was evident. With this simplification a practical scheme for optimising synthetic discriminant function (SDF) filters was brought within reasonable reach.

When adapted to the synthesis of SDF filters the optimisation procedure required the coincident variation of a scalar parameter, weighting the amplitude of the spectra, and a vector that resolved the set of weighted images into the plane of the SDF. The simulation undertaken evaluated the capacity of the SDF to detect in-plane rotations of images, this being the chosen mode of distortion. The trade-off in design is between a sharpened correlation peak and, with a deteriorating signal to noise ratio, a reduced capacity to distinguish between similar targets. It was found that a reduction of the angular spacing of the training set of images was necessary if the capacities of the SDF to resolve distorted images were to be preserved. When interrogated with in-class images corrupted to a signal to noise ratio of 0.5 and spaced at 1^0 intervals the maximum variation of the intensity of the correlation peak recorded with the optimal filter was less than 18% across a span of 60^0 of rotational distortion. Near, out-of-class images were strongly rejected.

A scheme has been proposed that extracts the cosine-wave element of the joint power spectrum (JPS) generated in a joint transform correlator (JTC) and returns this element alone for inversion. In this case, the design task is to extract information from the JPS rather than to modulate the spectrum of the reference image. When a target image is detected a pair of delta functions appears in the correlation plane standing displaced from the origin by a distance proportional to the separation of the target in the image from the reference image. Noise affecting the input image is returned randomly distributed across the entire correlation plane. This characteristic constitutes a strength of the system. In simulations of performance the intensity of the correlation peak exceeded the mean intensity of noise in the correlation plane by two to three orders when the signal to noise ratio in the input image was 0.5.

The cosine-wave JTC detected multiple targets represented at low contrast ratios in confused scenes unequivocally and discriminated strongly against near-target objects. In prospect is a JTC capable of real time correlation.

CHAPTER 8

Future Work

The target objects employed in the simulations shared similar characteristics, being vehicles of one kind or another; they generated broadly similar spectra in the Fourier plane. Whilst the schemes introduced to design optimal filters are of general utility, their application in the research has been to this restricted range of objects. Real-time operation of optical correlators may depend upon near real-time design of filters. Therefore, the influence of the peculiar spectral characteristics of targets on the design rules that real time evaluations might employ is in need of research.

The weighting function used in the optimisation of SDF filters described in Chapter 4, though it was satisfactory for purpose, was not regarded as ideal. The application of a low-cut filter as in the work of Chapter 3 should be explored.

The tolerance of noise displayed by the cosine-wave JTC should be investigated in yet greater depth.

APPENDIX

Fourier Transform Properties

A.1 LINEAR THEOREM

Given that C_1 and C_2 are two arbitrary constants. If $f_1(x,y)$ and $f_2(x,y)$ are Fourier transformable, i.e., if

$$\mathcal{F}\left[f_1(x,y)\right]=F_1(u,v) \qquad \text{and} \tag{A-1}$$

$$\mathcal{F}\left[f_2(x,y)\right]=F_2(u,v)\,, \tag{A-2}$$

then

$$\mathcal{F}\left[C_1 f_1(x,y)+C_2 f_2(x,y)\right]=C_1 F_1(u,v)+C_2 F_2(u,v)\,. \tag{A-3}$$

A.2 SIMILARITY THEOREM

If $f(x,y)$ is Fourier transformable, so that $\mathcal{F}\left[f(x,y)\right]=F(u,v)$, then

$$\mathcal{F}\left[f(ax,by)\right]=\frac{1}{ab}F(\frac{u}{a},\frac{v}{b})\,, \tag{A-4}$$

where a and b are arbitrary constants. This theorem shows that a magnification of the spatial domain results in demagnification in the spatial frequency domain, and an overall reduction in the amplitude spectrum.

A.3 SHIFT THEOREM

If $f(x,y)$ is Fourier transformable, so that $\mathcal{F}[f(x,y)] = F(u,v)$, then

$$\mathcal{F}[f(x-a, y-b)] = F(u,v)\exp[-j2\pi(ua+vb)]. \tag{A-5}$$

The translation of a function in the spatial domain causes a linear phase shift in the spatial frequency domain.

A.4 RAYLEIGH'S THEOREM

If $f(x,y)$ is Fourier transformable, so that $\mathcal{F}[f(x,y)] = F(u,v)$, then

$$\int_{-\infty}^{\infty}\int_{-\infty}^{\infty}|f(x,y)|^2\,dxdy = \int_{-\infty}^{\infty}\int_{-\infty}^{\infty}|F(u,v)|^2\,dudv. \tag{A-6}$$

It could be clear that Rayleigh's theorem implies the conservation of energy.

A.5 CONVOLUTION THEOREM

If $f_1(x,y)$ and $f_2(x,y)$ are Fourier transformable, so that

$$\mathcal{F}[f_1(x,y)] = F_1(u,v) \qquad \text{and} \tag{A-7}$$

$$\mathcal{F}[f_2(x,y)] = F_2(u,v), \tag{A-8}$$

then

$$\mathcal{F}[f_1(x,y)\Theta f_2(x,y)] = F_1(u,v)F_2(u,v), \tag{A-9}$$

where Θ denotes the convolution operation.

REFERENCES

J.W.Goodman, "Introduction to Fourier Optics," New York, McGraw-Hill, 1995.

List of Publications

1. Design of Synthetic Discriminate Functions for use in a Hybrid Optical-Digital Correlator, Lin Shang, B.F.Scott and J.H.Sharp. (3073-02). *AeroSense'97*, Florida USA, 20-25 April. 1997.
2. Frequency Multiplexed DOG filter, Lin Shang, C.R.Chatwin and R.K.Wang, *Optics and Lasers in Engineering*, Vol.27. 161-177(1997).
3. Modified fringe-adjusted joint transform correlation to accommodate noise in the input scene. R.K.Wang, Lin Shang and C.R.Chatwin, *Applied Optics*. Vol. 35. 286-296(1996).
4. Fringe phase encoded joint transform correlator, R.K.Wang, Lin Shang, Ian A. Watson and B.F.Scott. *CLEO/EUROPE'96*, Hamburg Germany, 8-14 Sept 1996.
5. Cosine wave encoded joint transform correlation, R.K.Wang, Lin Shang, Ian A. Watson and C.R.Chatwin, *Optical Engineering*, Vol 35, 1901-1910(1996).
6. Synthetic Discriminate function fringe-adjusted joint transform correlator, R.K.Wang, C.R.Chatwin and Lin Shang, *Optical Engineering*, Vol 34, 2935-2944(1995).